Analysis of SCF^{+} cardiac cells in mice

Dissertation

zur

Erlangung des Doktorgrades (Dr. rer. nat.)

der

Mathematisch-Naturwissenschaftlichen Fakultät

der

Rheinischen Friedrich-Wilhelms-Universität Bonn

vorgelegt von

Tianyuan Hu

aus

Shanghai, China

Bonn, 30. November 2017

Angefertigt mit Genehmigung der Mathematisch-Naturwissenschaftlichen
Fakultät der Rheinischen Friedrich-Wilhelms-Universität Bonn

Erstgutachter: Prof. Dr. Bernd K. Fleischmann
Zweitgutachter: Prof. Dr. Dieter O. Fürst

Tag der mündlichen Prüfung: 6. Juli 2018
Erscheinungsjahr: 2018

Die vorliegende Arbeit wurde von Dezember 2013 bis Dezember 2017 am Institut für Physiologie I der Rheinischen Friedrich-Wilhelms-Universität Bonn unter Anleitung von Prof. Dr. Bernd K. Fleischmann erstellt.

Erklärung

Hiermit versichere ich, dass ich die vorliegende Arbeit selbstständig und ohne jede unerlaubte Hilfe angefertigt habe. Alle von mir verwendeten Hilfsmittel und Quellen sind als solche gekennzeichnet. Des Weiteren hat die Arbeit keiner anderen Prüfungskommission zur Begutachtung vorgelegen.

_____

Tianyuan Hu Bonn, den

TABLE OF CONTENTS

1. INTRODUCTION

1.1 The role of c-kit$^+$ cells in the heart

According to the World Health Organization, cardiovascular diseases are the number 1 cause of death globally. [1] Coronary artery disease can lead to the constriction of blood supply to the heart which in turn can cause a severe loss of cardiomyocytes, e.g. after myocardial infarction. The mammalian heart has a very limited regenerative capacity to replenish the lost cardiomyocytes, which result in a persistent scar in the ischemic area. Surgical procedures aimed to revascularize the heart, such as percutaneous coronary intervention and coronary artery bypass surgery, are clinically used to restore blood supply to the myocardium. On the other hand, the recently successful applications of stem cell therapies in other fields [2] have spurred enthusiasm in developing cell-based regenerative therapies to repair the injured heart.

However, the long-held view that the adult mammalian heart is a postmitotic, terminally differentiated organ that has minimal regenerative capacity has been actively debated for over 150 years. [3] New approaches such as isotope dating [4], genetic fate mapping [5]–[7] and identification of supposedly resident cardiac stem cells have accumulated contradictory data over the years. The regenerative capacity of the adult heart was denoted from almost not existing to significant. [3] In the early 2000s, potential cardiac stem cells were identified as c-kit$^+$ cells with properties such as self-renewal, clonogenicity, and ability to differentiate into adult cardiac lineages. [8]–[12] However, subsequent independent studies were unable to confirm the ability of adult c-kit$^+$ cells to differentiate into cardiomyocytes. [13][14] One of the main reasons for such contradictive results is the lack of proper methods to identify cardiac c-kit$^+$ cells *in vivo*, due to technical challenges concerning the specificity of c-kit antibodies especially in the adult heart. More recently, the roles of c-kit$^+$ cells in heart development and regeneration were directly examined by adopting the Cre-lox based genetic fate mapping method to trace the fate of adult c-kit$^+$ cells. [15]–[17] These studies have reported 8 independently designed gene-targeted mouse models in total to carefully and exhaustively assess the identity of c-kit$^+$ cells in the heart and essentially disproved previously claimed roles of cardiac c-kit$^+$ cells. In light of these new evidences, a general consensus about the current controversy over the function of c-kit$^+$ cells emerged in the field of heart regeneration in 2017, which stated the

contribution of bone marrow derived c-kit$^+$ cells and other types of resident stem/progenitor cells to cardiomyocytes to be minimal in adulthood. [18]

1.2 SCF/c-kit signalling

Although the controversy over the role of cardiac c-kit$^+$ cells in cardiac regeneration mostly settled, whether c-kit signalling plays important roles during repair after myocardial infarction is largely unclear. The two main components of SCF/c-kit signalling are the cytokine ligand, stem cell factor (SCF) and the receptor tyrosine kinase, c-kit. In mice, SCF is encoded by nine exons and two main mRNA transcripts are expressed, that are translated into a soluble- and a membrane-bound form of SCF by alternative splicing (Fig. 1.1A). [19] The soluble form contains exon 6 which encodes a 28-amino acid proteolytic cleavage site and which is spliced out in the membrane-bound form. Cleavage at this site generates soluble SCF without a transmembrane domain (Fig. 1.1B). [20] However, the regulation of SCF expression on the gene level is currently unclear. Both forms of SCF can bind to c-kit and trigger downstream signalling. [21] Well-established downstream signalling proteins of c-kit include phosphatidylinositol 3'-kinases, tyrosine kinases of the Src family, mitogen-activated protein kinases, and phospholipases. [22]

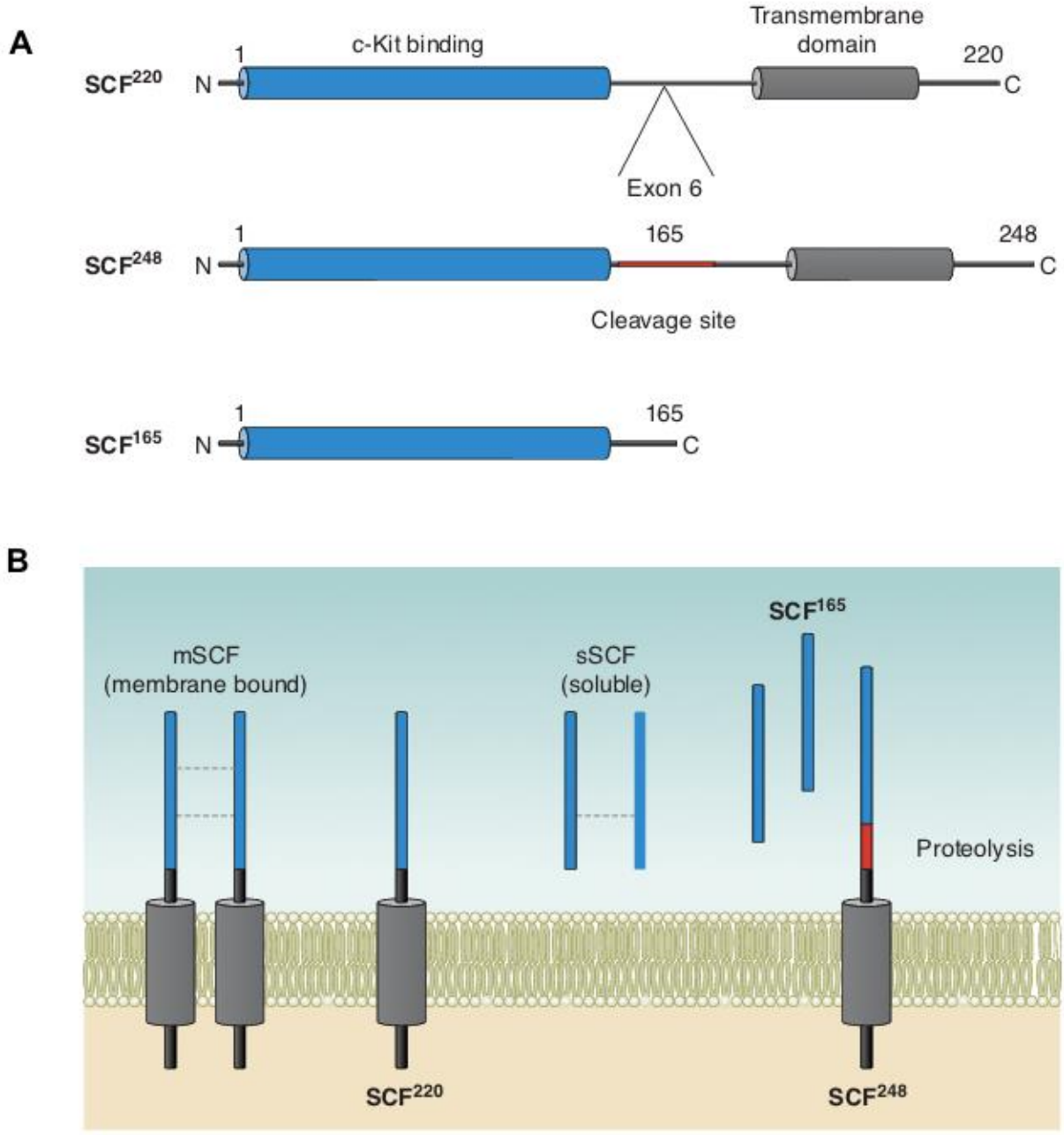

Fig. 1.1 Schematic representation of SCF splice isoforms (modified from Lennartsson et. al. 2012 [22]):

A) SCF protein is produced as two transmembrane isoforms due to alternative splicing of exon 6: SCF220, and SCF248. In SCF248, exon 6 is present and encodes a proteolytic cleavage site, generating the soluble SCF165. **B)** SCF220, lacking the cleavage site, is translated to the membrane-bound SCF, and SCF248 is processed to SCF165 that is translated to soluble SCF.

1.3 Biological functions of SCF and c-kit

Many naturally occurring mutants of SCF and c-kit discovered in early studies, known as steel locus mutations (*sl*) [22][23] and white spotting locus mutations (*W*) [25][26] respectively, provided much information about the main function of SCF/c-kit

signalling *in vivo*. These loss-of-function mutations in SCF or c-kit produce many allelic phenotypes in the hematopoietic system, germ cell development and skin pigmentation. [24], [27]–[30] Many mutations in *sl* and *W* loci severely diminish primordial germ cells and result in infertility. [28] Heterozygous mutations of SCF and c-kit adversely affect melanogenesis and create white spots in the fur on the trunk. [31] Targeted gene deletions of SCF and c-kit are perinatal lethal due to severe anaemia. [32] Recently, several studies applied Cre-loxP based conditional knockout mouse models to advance the understanding of SCF/c-kit function in adulthood. [33][34] The advantages of these loxP based knockouts is that it can avoid perinatal lethality and interferences from developmental defects and made it possible to test the hypothesis, that SCF^+ cells serve as stem cell niches in various organs. Stem cell niches are specialized micro-environments that regulate the maintenance of their associated stem cells via intercellular interactions. The concept of stem cell niches and/or their function(s) in health and disease is still somewhat controversial and their molecular characterization is for most of the systems incomplete. [35] Most information is currently available from the bone marrow. For instance SCF^+ bone marrow endothelial cells and reticular perivascular stromal cells are thought to be vital for maintaining hematopoietic stem cells (HSCs). [33] This was demonstrated by a conditional deletion of c-kit in HSCs, which resulted in adhesion failure between HSCs and SCF^+-niche cells and eventually depletion of HSCs. [34] A relatively well characterized niche in the bone marrow is the osteogenic niche, in which SCF production by bone marrow cells is necessary to maintain homeostasis of niche cells such as osteoblasts, bone marrow stromal cells and sinusoids. [36]–[40] In addition, SCF^+ vascular endothelial cells (VECs) in thymus were found to serve as a vital niche for the earliest thymocyte progenitors [41] and SCF^+ progenitor cells in the hair shaft provide an important niche for the maintenance of differentiated melanocytes. [42] Furthermore, c-kit^+ crypt base secretory cells in the colon serve as niches for intestinal stem cells in a SCF-c-kit dependent manner. [43] These recent studies have provided experimental evidence that SCF/c-kit signalling constitutes an important signalling pathway for cellular communication between stem cells and their niches.

1.4 Functions of SCF in the cardiovascular system

The functions of SCF are well characterized in the hematopoietic system. [33] However, the roles of SCF in the cardiovascular system during physiological and

pathological conditions are poorly understood. A study using a closed chest model of murine cardiac infarction/reperfusion showed that releasing soluble SCF by bone marrow cells was necessary to activate c-kit$^+$ cells in the bone marrow which induced bone marrow progenitor cell mobilization after ischemic cardiac injury. [44] It was also shown that mice carrying loss-of-function mutations in either SCF or c-kit developed cardiac failure after myocardial infarction and that this striking phenotype could be rescued by bone marrow transplantation from wild type mouse donors. [44] However, these results have not been reproduced by other laboratories and therefore need to be taken with caution. In addition, cardiomyocyte-specific overexpression of human SCF using a genetic mouse model was shown to improve myocardial function and survival after myocardial infarction in mice. [45] Mechanistically it was proposed to be the result of increased neovascularization and recruitment of endothelial progenitor cells by SCF action. Adenovirus based gene transfer of SCF into cardiomyocytes was reported to improve cardiac function and repair in rats and swine, but the underlying mechanism(s) of this effect is/are not clear. [46][47] Besides basic mechanistic studies, a recent clinical survey also showed that decreased plasma SCF levels in patients are associated with higher risks of cardiovascular disease and death. [48] The study further showed that lower SCF levels were associated with more severe carotid disease, less fibrous atherosclerotic plaques and an increased incidence of heart failure. [49] Furthermore, inhibition of SCF/c-kit signalling by tyrosine kinase inhibitors, such as Nilotinib, which is used in the treatment of chronic myeloid leukemia, has been shown to cause coronary artery diseases in some of the patients. [50]–[52] These clinical studies collectively indicate that SCF plays an important role for cardiovascular functional integrity, but lacked mechanistic insights.

Despite these very interesting correlations to the relevance of SCF function for the cardiovascular system relatively little information is currently available about SCF's expression pattern and its cell specific functions during development, postnatal growth and disease. Early studies in the 1990s used *in situ* hybridisation to analyse SCF expression during embryonic development and revealed high SCF expression in the developing brain, lung, guts, liver and gonads. However, due to technical shortcomings at the time, such as insufficient resolution, the cellular expression pattern of SCF in the cardiovascular system could not be revealed in detail. [53]–[55] These studies consistently showed very low to no expression of SCF in the entire

embryonic heart from e9.5 to e13.5. There was only one study suggesting high SCF expression in the developing valves of e11.5 hearts. [53] Unfortunately there are currently no additional tools such as highly specific antibodies against SCF and/or its splice variants available so that genetic tools need to be used in order to gain detailed information on the expression pattern and potential function(s) of this important molecule/pathway. In recent years, genetic mouse models expressing reporter genes under SCF promoter control were generated and led to the discovery of SCF expressing cell populations in bone marrow [33] and thymus [41]. These new mouse models provide new opportunities to systematically characterize the SCF^+ cells in the heart during embryonic development, postnatal growth and pathological remodeling.

1.5 Embryonic development of the heart.

Proper heart development is critical to embryogenesis, because a pumping heart is vital for the survival of the embryo. Understanding the developmental programs of heart formation can deepen the understanding of congenital heart disease and provide valuable insights into heart diseases. [56] As an example, characterization of c-kit^+ cells in the developing heart has provided valuable clues about the controversial role of cardiac c-kit+ cells in adult. During embryonic development c-kit^+ cardiac cells have bipotential differentiation capacity for cardiomyocytes and smooth muscle cells. [57] However these embryonic c-kit^+ cardiac cells, which originate from neural crest, have very limited cardiomyogenic capacity due to the nonpermissive milieu in the embryonic heart. [57][58] These studies directly challenged the notion that c-kit^+ cardiac cells contribute to the formation of new cardiomyocytes after myocardial infarction in the adult heart (see 1.1). Since embryonic cells are generally more potent in terms of differentiation and lineage transition than their adult derivatives, understanding the phenotypic properties of embryonic cells could provide much information about the biological functions of their adult lineages. According to this, the identification of SCF^+ cells in the embryonic heart could provide important insights into their potential roles in the adult heart during physiological and pathological conditions.

The heart is the first organ to form shortly after gastrulation and a functional cardiovascular system is, together with a working placenta, vital for the survival of the embryo. [59][60] Gastrulation of the mouse embryo happens approximately at day

6.25 of embryonic development (e6.25), which is the major morphogenetic event that leads to the formation of the three germ layers: endoderm, ectoderm and mesoderm. [61] At e6.5-7.0, the newly formed pre-cardiac mesodermal cells, which are located at the anterior part of the primitive streak, migrate towards the future anterior part of the embryo (splanchnic/visceral mesoderm) to form the cardiac crescent (Fig.1.2A). [62] The cardiac crescent consists of two distinct territories of cardiac progenitor cells which form the first and secondary heart fields (FHF and SHF). [63] At about e8.0, the cardiac crescent fuses at the ventral midline to form the primitive heart tube (Fig.1.2B). Cells that initially contribute to the primary heart tube arise to form the FHF. The FHF occupies a distinct anterior-lateral territory within the cardiac crescent and can be identified by the expression of HCN4. [63][64] Multipotent cardiac progenitors originating from the SHF and locating to the medial and posterior part of the cardiac crescent also contribute to heart tube formation. [65] These cardiac progenitors gradually add cardiomyocytes to the primary heart tube which acts as a scaffold for heart tube elongation from both the arterial and venous pole (Fig. 1.2C). [66] SHF cells are marked by the persistent expression of ISL1 and constitute a reservoir of undifferentiated cardiac progenitors within the pharyngeal mesoderm. [67] The FHF will give rise to the left ventricle and parts of the atria, while the SHF will give rise to the right ventricle, the sinus venosus and parts of the atria. After initial contributions of cardiac progenitors from FHF and SHF, heart growth is driven by the proliferation of cardiomyocytes and endocardial cells until the perinatal stage. [66] Concurrent with its elongation, the primitive heart tube starts to loop rightward at e8.25-9.0 (Fig. 1.2D). The looped heart at e9.5-10.5 is segmented into the atrium and ventricle, separated by the atrioventricular canal (AVC) and the outflow tract (OT) at the arterial end (Fig. 1.2E). [59] Endocardial cushions are formed in the lumen of the AVC and in the proximal OFT by the accumulation of abundant extracellular matrix (cardiac jelly) between the endocardial and myocardial layer. The endocardial cells undergo epithelial-to-mesenchymal transition (EMT) and migrate into the endocardial cushions to populate the cardiac jelly. [68] The lumen of the distal OT undergoes a similar swelling process but its endocardial cushion is populated by mesenchymal cells originating from the neural crest. [69] During development of these cushions, the proepicardial organ near the sinus venosus starts to gradually spread out and grows over the heart surface to form the epicardium. [70] The AVC endocardial cushions develop into the mitral and tricuspid valves, whereas the OT endocardial

cushions develop into the aortic and pulmonary valves. [71] By the end of e13.5, the septation of the atrial and ventricular chambers is complete. At e14.5, the four-chambered heart looks very similar to the adult heart with the exception of the trabeculae carneae in the ventricles (Fig. 1.2.F). The trabeculae carneae consist of myocardial protrusions which extend on the luminal side of the free ventricular walls and are covered by endocardial cells. These structures will disappear to form compact ventricular walls shortly after birth.

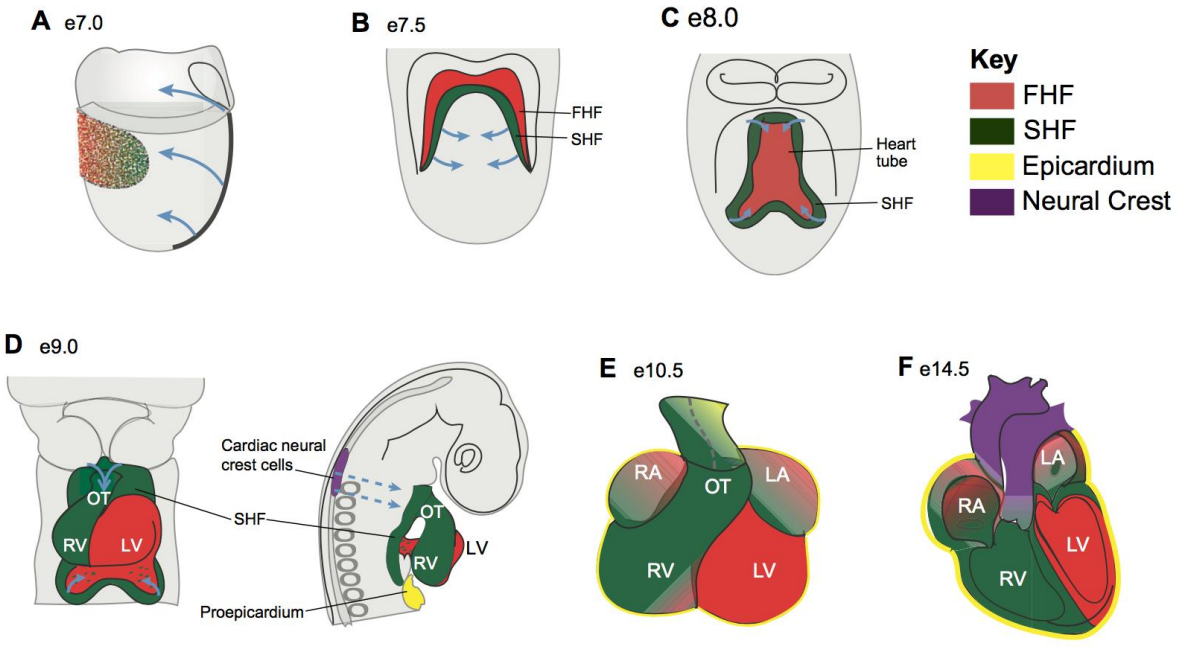

Fig. 1.2. Embryonic development of the mouse heart (adapted from Santini et. al. 2016 [72]):

A) During gastrulation at about e7.0, mesodermal cells, including heart progenitors from FHF (red) and SHF (green), undergo lateral migration (blue arrows) away from the primitive streak (black line). **B)** During the cardiac crescent stage at e7.5, the location of FHF and SHF are shown in red and green. **C)** During the formation of the early heart tube at e8.0, FHF descendants first differentiate into primitive heart tube and some of the SHF descendants start to contribute to the primitive heart tube from arterial and venous poles of the heart tube (blue arrows). **D)** Frontal and lateral views of the heart region at e9.0 showing the looped heart tube. Dashed arrows indicate migration of cardiac neural crest cells into the heart. **E)** The chambered heart at e10.5; the contributions of FHF and SHF cells are shown in red and green. **F)** The chambered heart at e14.5; the contributions of FHF and SHF cells are shown in red and green. Another major event during the formation of the heart is the development of the coronary vessels. Cardiac cells, in particular cardiac muscle cells are critically depending on an appropriate blood supply which is provided by the coronary vessels. Understanding the developmental program of the coronary arteries can possibly provide new insights into the treatment of coronary vessel diseases in adulthood. Given the potential correlation between SCF and coronary artery diseases, it is also important to analyse if SCF is involved in the developmental progression of coronary arteries.

1.6 Formation of the coronary vessels during development

In adult mouse heart, the left and right major coronary arteries branch from the aorta and transport oxygenated blood to the heart. They give rise to small muscular arteries that penetrate the myocardium and are termed intramural arteries. These intramural arteries eventually branch into arterioles and capillaries that surround the cardiomyocytes. The veins on the backside of the heart transport the deoxygenated blood into the right atrium. In contrast to the adult heart, the early embryonic mouse heart lacks its own vessel network. During the early stages of development, when the ventricular walls are very thin, nutrients supply the heart by diffusion (Fig. 1.3A). However, as the ventricular wall grows thicker over time, VECs start to appear sporadically on the surface of the heart. Initial sprouting of VECs, which are precursors of the future coronary vasculature, starts at e11.0 when the heart tube has finished looping and forms atria and ventricles (Fig. 1.3B). [73][74] These VECs are dedifferentiated venous cells from the SV posterior to the common ventricle that spreads onto the dorsal side of heart surface beneath the epicardium and are called subepicardial endothelial cells (SECs). [74][75] The SECs can either differentiate into both arterial and venous VECs, or maintain in an undifferentiated state by staying in a subepicardial position. As SECs sprouts continue to extend, some of them invade the compact myocardium. At e12.5 to e13.5 a small part of the endocardial cells also starts to invade the compact myocardium and forms blood islands budding on the central ventral surface of the heart (Fig. 1.3C). [73][74] At the same time, the ventricles undergo septation and the ventricular septum is formed, which results in lineage transition of endocardium to coronary VECs during trabecular coalescence (Fig. 1.3D). [73] These VECs form an immature coronary plexus that consist of sprouting VECs that have not connected to the circulation, yet. Blood flow is established around e14.5, once the immature coronary plexuses in the left anterior and right posterior region connect to the aorta (Fig. 1.3E). [76][77] Subsequently, the blood flow from the aorta provides a physical stimulus to transform the plexus into a mature vascular network in which large coronary arteries and veins start to be established at e14.5-15.5. Further, during the perinatal stage, ventricles of mouse hearts undergo rapid compaction by trabecular coalescence, which also results in lineage transition of endocardium to coronary VECs in the inner layer of the free ventricles (Fig. 1.3F). [78]

In summary, coronary vessel development in mice is highly compartmentalized. SV-derived vessels contribute to a large number of arteries, capillaries, and veins on the dorsal and lateral sides of the heart at e11.0 to e12.5. Blood island budding contributes to a relatively small number of vessels in the central part of the ventral side of the heart at e12.5-e13.5. Ventricular septation via trabecular coalescence contributes to the coronary vessels in the ventricular septum at e11.5-14.5. And finally, neonatal myocardium compaction by trabecular coalescence contributes to coronary vessels in the inner side of the myocardium around P0-P3.

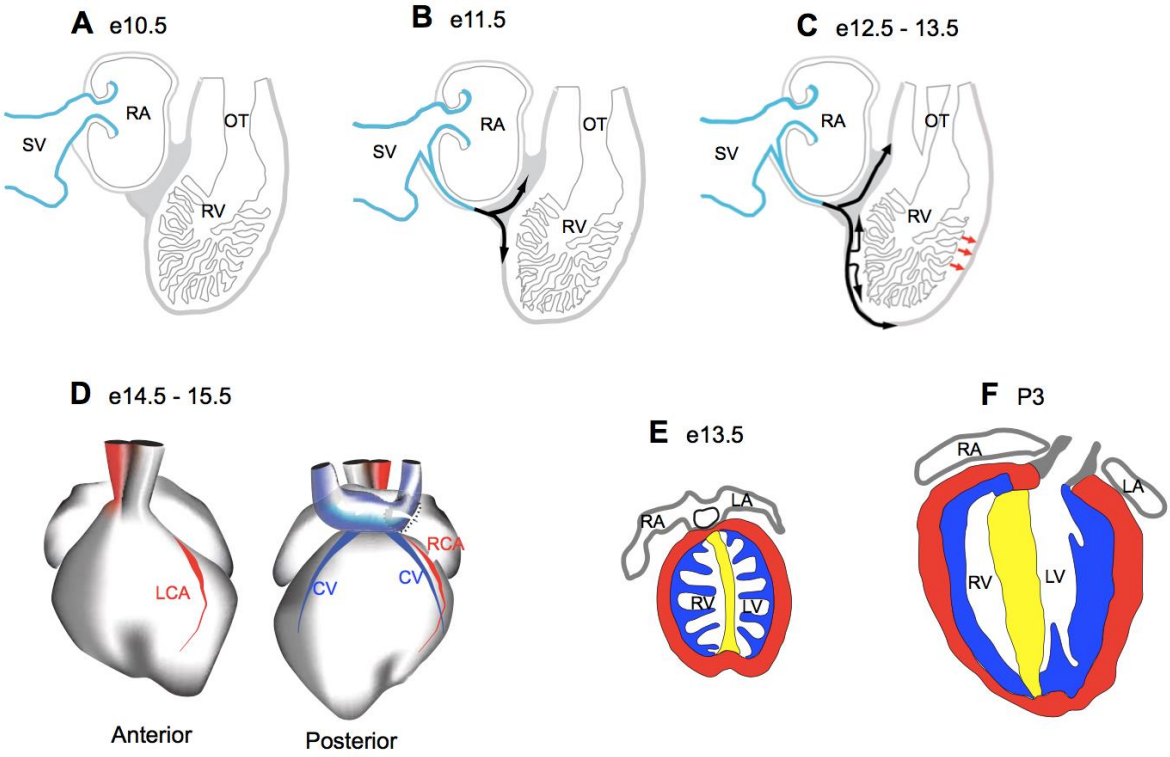

Fig. 1.3 Coronary vessel development in mice (adapted from Kristy et. al. 2010 [74] and Burns et. al. 2014 [79]):

A) Schematic sagittal section of an e10.5 heart. Coronary vessels have not formed yet. **B)** Schematic sagittal section of an e11.5 heart. Endothelial cells of the SV (blue) sprout towards the heart ventricle (black arrows). **C)** Schematic sagittal section of an e12.5-13.5 heart. SECs spread beneath the epicardium and invade the myocardium (black arrows). Endocardium in the frontal side of the ventricle lumen sprouts into the central anterior region of the heart (Red arrows). **D)** Schematic of the newly formed LCA (anterior view, red), RCA (posterior view, red) and CV (posterior view, blue) at e14.5-15.5. **E)** Schematic transverse section of an e13.5 heart. The VECs of the ventricular septum (yellow) originate from endocardium via trabecular coalescence. **F)** Schematic coronal section of the P3 heart. The VECs of the inner layer of the free ventricles (blue) originate from endocardium by trabecular coalescence.

These different developmental origins of coronary arteries suggest a high level of plasticity in early embryonic VECs. However, as soon as coronary circulation is

established, the primitive coronary plexus starts to specify into different types of vessels, such as arteries, capillaries and veins. As a result, VECs form different subpopulations by adopting different phenotypes to accustom their particular physiological functions, including the control of vasomotor tone, blood cell trafficking, hemostatic balance, permeability, proliferation, quiescence and immunity. This differential regulation of VEC phenotypes in different environments causes the phenomenon of "VEC heterogeneity." [80] Such diversity is critical to the physiological functions of the entire vascular tree under physiological and pathological conditions. Given the potential importance of SCF in the functional integrity of the coronary circulation, the correlation between SCF expression and various subpopulations of VECs needs to be analysed.

1.7 Subpopulations of VECs in the heart

In a prototypic vascular bed, different types of vessels are categorized based on their distinct properties. By definition, arteries are vessels that transport blood from the heart to different parts of the body. Veins are vessels that transport blood back to the heart. Capillaries transport blood from arterioles (vessels connecting arteries and capillaries) to venules (vessels connecting capillaries and veins). The VECs of arteries and veins display different phenotypes in correlation to their physiological functions. Furthermore, the formation of arteries and veins initiates from VECs by genetically predetermined mechanisms, including signalling pathways like VEGF, Notch and EphrinB2. [81]–[83] Many key components of these signal pathways have been used as markers for arterial and venous identities of VECs. Arterial VECs express specific markers such as Dll4 [84], EphrinB2 [85], Hey1 and Hey2 [86], and neuropilin 1 [86], while venous VECs express markers such as EphB4 [87], neuropilin 2 [88], and COUP-TFII [89]. However, these markers cannot be used to determine the arterial and venous identities of VECs in the adult mouse heart due to a lack of specific antibodies for these markers in the heart. Instead, the arterial and venous identities of coronary vessels in adult mice are determined by their anatomic features. The major coronary arteries of the mouse heart locate beneath the surface of the myocardium in the left anterior area and right posterior area of the ventricles. The intramyocardial arteries and arterioles can be distinguished from veins and capillaries by the smooth muscle layer of these vessels. The major coronary veins can be found on the surface of the backside of the heart. However, the VECs of

coronary venules and intramyocardial veins are largely unknown in adult mouse heart due to the inability to label them. [90]

Functionally, arterial and venous VECs maintain a certain level of plasticity, activated by hypoxia and hemodynamics. Recent study using Cre-loxP mediated genetic lineage tracing demonstrated that almost all revascularization after myocardial infarction originated from pre-existing VECs. [91] Cre-LoxP based genetic mouse models also played important roles in resolving the controversy over c-kit^{+} cardiac cells. They can be useful tools to investigate the SCF lineage in early embryos.

1.8 The Cre-LoxP system

The Cre recombinase from P1 bacteriophage is widely used in nearly all fields of biological research. The function of Cre (Causes recombination) is to catalyze the recombination between two of its recognitions sites, called LoxP-sites (locus of crossing over in phage P1). [92] The LoxP site is a 34 bp DNA sequence that consists of two 13 bp palindromic sequences at the 5' and 3' ends, and an 8 bp sequence in the middle. The DNA sequence between two LoxP sites is excised when they are oriented in the same 5' to 3' direction. One great advantage of the Cre-LoxP system is its simplicity, as there is no additional requirement of co-elements or specific cell types. Furthermore, LoxP is 34 bp in length, which makes it almost impossible to have off-target effects of Cre-activity in the mammalian genome. The first indication that the phage enzyme would be functional in mice was demonstrated by Orban and colleagues in 1992. [93] This study demonstrated the current main method for deletion of a gene of interest in a specific cell type, which is to use an established transgenic line that expresses Cre under the control of a cell type-specific promoter and to cross it with a mouse line harboring a target gene flanked by two loxP. In such a compound transgenic mouse line Cre excises the gene of interest only in the specific cell type. However, many targeted genes are essential for embryonic development and a homozygous deletion will result in non-viable embryos which make it impossible to study the function of the gene in adulthood. To circumvent this problem, many laboratories developed inducible Cre-loxP systems by taking advantage of the nuclear translocation of steroid hormone receptors in the presence of their ligands. Among them, CreER^{T2} was most widely used until today due to its highest score in ligand dependent Cre activity. [94][95] CreER^{T2} is a fusion protein consisting of a n-terminal Cre recombinase and a c-terminal ER^{T2}, a mutated

ligand-binding domain of the estrogen receptor with impaired ability to bind endogenous estrogen but binding affinity to the drug tamoxifen. In general, CreER^{T2} is placed under transcriptional control of a gene which is selectively expressed in the cell population of interest. The Cre-activated reporters usually contain a ubiquitous promoter, a loxP-flanked transcriptional stop cassette and a reporter gene. In the absence of tamoxifen, CreER^{T2} stays in the cytosol and the loxP-flanked (floxed) stop cassette blocks the expression of the reporter gene (Fig.1.4A). Tamoxifen administration leads to nuclear translocation of CreER^{T2} and subsequent excision of the floxed stop cassette (Fig.1.4B), which allows the expression of the reporter gene (Fig.1.4C). Because the genetic labelling is irreversible and therefore heritable, the cells of interest and all of their descendants will express the reporter gene.

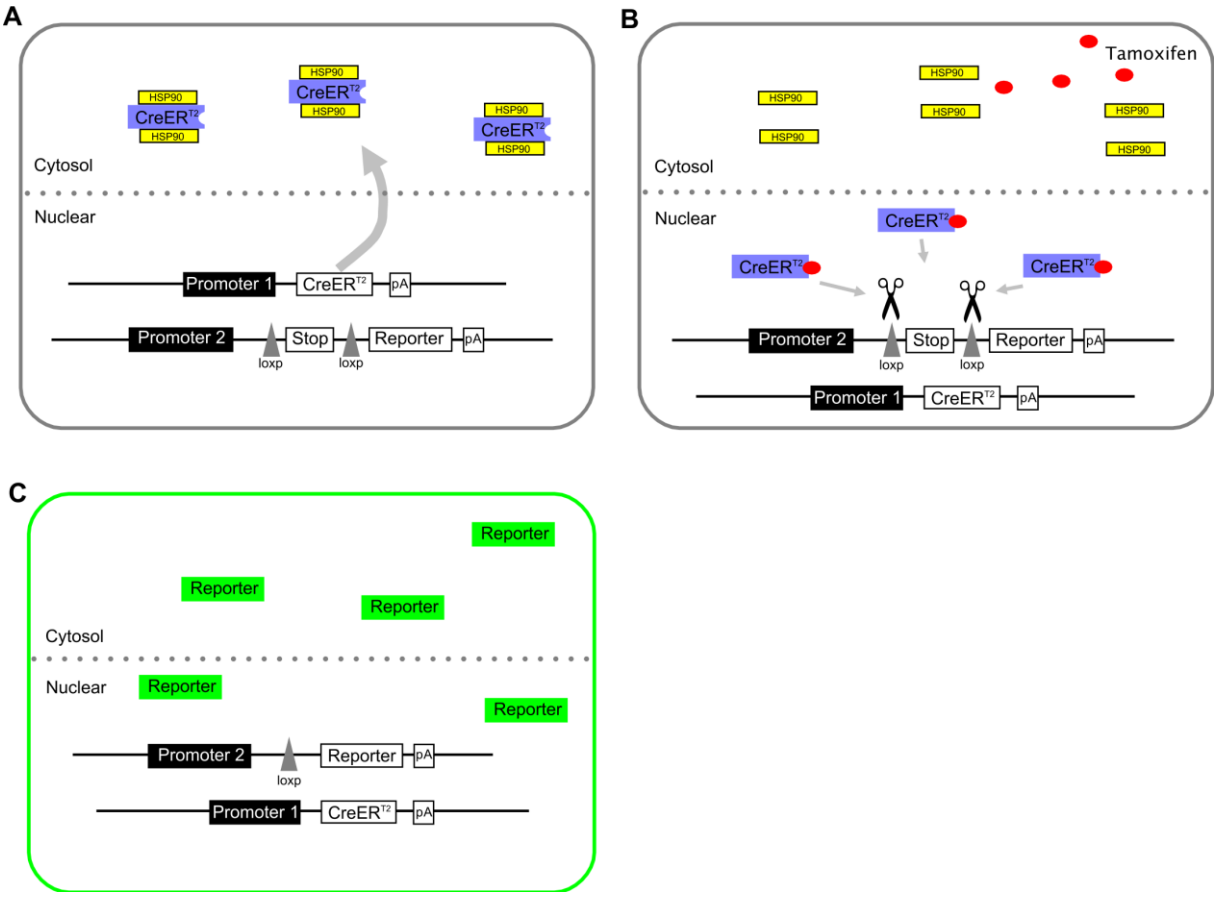

Fig. 1.4 CreER^{T2} mediated genetic cell labelling:

A) Without tamoxifen, CreER^{T2} fusion protein binds to HSP90 (a heat shock protein subtype acting as a chaperone) and localizes to the cytosol. **B)** After tamoxifen administration, CreER^{T2} is activated by ligand binding and translocates into the nucleus with the loxP flanked stop cassette. **C)** After Cre excision of the loxP flanked stop cassette, the reporter gene is expressed, regardless of CreER^{T2} is expression.

2. MATERIALS AND METHODS

2.1 Materials

2.1.1 Reagents

Product Name	Company
Acetic acid	Sigma Aldrich, Steinheim, Germany
Agarose	Carl Roth, Karlsruhe, Germany
Boric Acid	Sigma Aldrich, Steinheim, Germany
Corn oil	Sigma-Aldrich, Steinheim, Germany
Dimethyl Sulfoxide (DMSO)	Sigma-Aldrich, Steinheim, Germany
DNA Gel Loading Dye (6X)	Thermo Fisher Scientific, Waltham, MA, USA
Donkey Serum (DS)	Jackson ImmunoResearch, Suffolk, England
Dulbecco's Phosphate-buffered saline (DPBS)	Invitrogen/Life Technologies, Darmstadt, Germany
Ethidium Bromide	Fluka/Sigma-Aldrich, Steinheim, Germany
	Carl Roth, Karlsruhe, Germany
Ethanol	Carl Roth, Karlsruhe, Germany
Ethylenediaminetetraacetic Acid, EDTA	Sigma-Aldrich, Steinheim, Germany
Gentra Puregene Mouse Tail Kit	Qiagen, Hilden, Germany
GoTaq® Green Master Mix	Promega, Medison, USA
Heparin	Rotexmedica, Trittau, Germany
Horse serum	Sigma-Aldrich, Steinheim, Germany
Hydrochloric Acid (HCl)	Sigma-Aldrich, Steinheim, Germany
Hydrogen Peroxide (H_2O_2, 30%)	Sigma-Aldrich, Steinheim, Germany
Isopropanol	VWR, Darmstadt, Germany
β-Mercaptoethanol	Sigma-Aldrich, Steinheim, Germany
2-Methylbutan (Isopentanol)	Carl Roth, Karlsruhe, Germany
O'GeneRuler 1 kb DNA Ladder, ready-to-use	ThermoFisher Scientific, Waltham, MA, USA
Paraformaldehyde (PFA)	Sigma-Aldrich, Steinheim, Germany
Phosphate-Buffered Saline (PBS)	Invitrogen/Life Technologies,

	Darmstadt, Germany
PBS Tablets	Invitrogen/Life Technologies, Darmstadt, Germany
Potassium Chloride (KCl)	Sigma-Aldrich, Steinheim, Germany
Sodium Chloride (NaCl)	Sigma-Aldrich, Steinheim, Germany
Sodium Dodecyl Sulfate (SDS)	Sigma-Aldrich, Steinheim, Germany
Sodium Hydroxide (NaOH)	
Sucrose	Sigma-Aldrich, Steinheim, Germany
Tamoxifen	Sigma-Aldrich, Steinheim, Germany
Tissue-Tek® O.C.T.™ Compound	Sakura Finetek Europe B.V., Zoeterwoude, Netherlands
Tris-base	Sigma Aldrich, Steinheim, Germany
Tris-HCl	Sigma Aldrich, Steinheim, Germany
TritonX-100	Sigma Aldrich, Steinheim, Germany
TSA® Plus Cy3	PerkinElmer, US
TSA® Plus Cy5	PerkinElmer, US
TSA® Plus Fluorescein	PerkinElmer, US

2.1.2 Primers for genotyping of transgenic mice

All primers were used as described in the publications ([41], [96]–[100]) of the transgenic mouse lines and supplied by ThermoFisher /Life Technologies:

Mouse line	**Sequence (5'-3')**
CAG-mTmG	Forward: CTCTGCTGCCTCCTGGCTTCT
	Reverse wild type: CGAGGCGGATCACAAGCAATA
	Reverse mutant: TCAATGGGCGGGGGTCGTT
	Mutant fragment = 284 bp
	Heterozygote fragments = 284 bp and 297 bp
	Wild type fragment = 297 bp
SCF-CreER^{T2}	Forward mutant: CACCTCCCACAACGAGGACTA
	Forward wild type: GGGCTTCATTTGCTGTCTGTC
	Reverse: TCTCACACCACGCCTGTCTCT
	Wild type fragment = 400 bp
	Mutant fragments = 400 bp and 590 bp

Tie2-Cre	Forward: CGCATAACCAGTGAAACAGCATGGC
	Reverse: GGCAAATTTTGGTGTACGGTC
	Mutant fragment = 220 bp
$SCF^{\Delta Ex7}$	Forward: GGGCCTCAAAGAAATTCAAA
	Reverse: TCATCATGATTTGGCACCTT
	Wild type fragment = 265 bp
	Mutant fragment = 382 bp
c-kit^{BAC}-eGFP	Forward: GCAGGTGGAGAAACTGAGCATG
	Reverse: CCCAGGATGTTGCCGTCCTCCT
	Mutant fragment = 1095 bp
Ai9	Forward: AAGGGAGCTGCAGTGGAGTA
	Reverse wild type: CCGAAAATCTGTGGGAAGTC
	Reverse mutant: GGCATTAAAGCAGCGTATCC
	Mutant fragment = 196 bp
	Heterozygote fragments = 297 bp and 196 bp
	Wild type fragment = 297 bp
VECad-$CreER^{T2}$	Forward: CGAAAAGAAAACGTTGA
	Reverse: ATCCAGGTTACGGATATAGT
	Mutant fragment = 970 bp
Anillin-eGFP	Forward: GGCACAAGCTGGAGTACAAC
	Reverse: TGGCACTGGTGCAAAGTATG
	Mutant fragment = 850 bp

2.1.3 Solutions and Buffers

Name	**Composition**
Borate Solution	0.01% Hydrogen Peroxide (30%)
	0.1 M Boric Acid
	NaOH (adjust PH to 8.5)
H_2O_2 Blocking Solution 1	3% Hydrogen Peroxide (30% stock solution) in PBS
H_2O_2 Blocking Solution 2	10% Hydrogen Peroxide (30% stock solution) in PBS
2ME/SDS Solution (50ml)	10 ml 10% (M/V) SDS

	6.25 ml 0.5 M Tris-HCl PH 6.8 38.75 water 0.4 ml β-Mercaptoethanol (2-ME) add fresh
PBS Washing Solution	Made directly by dissolving PBS tablets
5% PBSST	5% (v/v) Donkey Serum in PBST
2.5% PBSST	2.5% (v/v) Donkey Serum in PBST
PBST	0.1% (v/v) TritonX-100 in DPBS
PBS-Heparin	500 I.U. Heparin in 50 ml PBS
PFA Fixing Solution	4% PFA (w/v) in PBS
Sucrose Solution	30% Sucrose (w/v) in PBS
TAE Buffer	40 mM Tris-base 2 mM EDTA 20 mM Acetic acid dissolve in water set pH = 8.5
Tamoxifen Solution	20 mg/ml Tamoxifen in corn oil
TSA Cy3 Stock solution	TSA® Plus Cy3 dissolved in DMSO
TSA Cy5 Stock solution	TSA® Plus Cy5 dissolved in DMSO
TSA Fluorescein Stock solution	TSA® Plus Fluorescein dissolved in DMSO

2.1.4 Equipments and Materials

Name	**Company**
Analytical Balance XS205	Mettler Toledo, Columbus, OH, USA
Balance 440-45	KERN, Balingen, Germany
Cell Culture Dishes (10 cm)	Greiner Bio-One, Frickenhausen, Germany
Centrifuge 5415D	Eppendorf, Wesseling-Berzdorf, Germany
Colibri Illumination System	Carl Zeiss, Jena, Germany
Coverslips	Fisher Scientific, US.
Cryostat Microtome (Kryotom CM 3050S)	Leica, Solms, Germany

15 ml Reaction Tubes	Falcon, Gräfeling-Lochnam, Germany
50 mL Reaction Tubes	Falcon, Gräfeling-Lochnam, Germany
Gel Electrophoresis Chamber	BioRAD, Munich, Germany
Gel Documentation System	NeoTech, San Diego, US
Haraeus® Heating and Drying Oven	Heraeus, Hanau, Germany
ImmEdge Hydrophobic Barrier PAP Pen	Vector Laboratories, Burlingame, US
Laser Scanning Microscope Eclipse Ti	Nikon instruments, Düsseldorf, Germany
Microcentrifuge Tubes 1.5 ml	Eppendorf, Hamburg, Germany Sarstedt, Nuembrecht, Germany
Macroscope AXIO Zoom V16	Carl Zeiss, Jena, Germany
Microscope Axiovert40CFL	Carl Zeiss, Jena, Germany
Microscope Axiovert200	Carl Zeiss, Jena, Germany
Microscope Observer Z1 with Apotome	Carl Zeiss, Jena, Germany
NanoDrop 100 Spectrophotometer	Peqlab, Erlangen, Germany
Peel-A-Way embedding Mold	Sigma/Merck, US
Pipet “Pipettor”	Eppendorf, Wesseling-Berzdorf, Germany
Microscopic Slides	Menzel-Gläser/VWR, Darmstadt, Germany
laminar flow HERAsafe	Heraeus, Hanau, Germany
Stereomicroscope AxioZoom V16	Carl Zeiss, Oberkochen, Germany
Thermocycler TProfessional TRIO	Biometra, Göttingen, Germany
Tissue-Tek® Mold	Sakura Finetek Europe B.V., Zoeterwoude, Netherlands
Vortex Mixer	VWR International

2.1.5 Mouse Lines

Name	Source
SCF-CreER^{T2}	Prof. Claus Nerlov, University of Oxford, UK.[41]
SCF$^{\Delta Ex7}$	Prof. Claus Nerlov, University of Oxford, UK.[41]
Tie2-Cre	Prof. Claus Nerlov, University of Oxford, UK.[100]

CAG-mTmG	Stock# 007576, Jackson Laboratory, US.[98]
eGFP-anillin	Dr. Michael Hesse. Institute of Physiology I. Bonn.[99]
c-kit^{BAC}-eGFP	Prof. Michael Kotlikoff, Cornell University, US.[96]
VECad-CreER^{T2}	Prof. Michael Kotlikoff, Cornell University, US.[101]
Ai9	Prof. Michael Kotlikoff, Cornell University, US.[97]

2.1.6 Primary Antibodies

Primary Antibody (Company, Cat#)	**Note (Working Dilution)**
Anti-α-Actinin (Sigma; A7811)	(1:400)
Anti-α-Smooth Muscle Actin (Sigma; A5228)	(1:800)
Anti-Human Estrogen Receptor (Abcam; ab27595)	(1:1)
Anti-CD31 (BD; 550274)	(1:500)
Anti-CD45 (Millipore; CBL1326)	(1:1000)
Anti-GFP-FITC Conjugated (Abcam, ab6662)	(1:400)
Anti-PDGFRβ (eBioscience; 14-1402)	(1:500)
Anti-RFP (Rockland; 600-401-379)	(1:400)
Anti-VECadherin (R&D; AF1002)	(1:100)

2.1.7 Secondary antibodies

All fluorochrome conjugated secondary antibodies were ordered from Jackson ImmunoResearch:

Secondary antibodies conjugated with Fluorochromes (Species, Working Dilution)

Anti-goat IgG-Cy2 (Donkey, 1:400)

Anti-goat IgG-Cy5 (Donkey, 1:400)

Anti-mouse IgG1-Cy5 (Goat, 1:400)

Anti-mouse IgG2a-Cy5 (Goat, 1:400)

Anti-rabbit-Cy3 (Donkey, 1:400)

Anti-rat-Cy5 (Goat, 1:400)

For signal enhancement, peroxidase conjugated secondary antibodies were ordered from Vector laboratories:

Secondary antibodies conjugated with peroxidases (Species, Working Dilution)

Immpress™ HRP Anti Rabbit (Horse, 1:1)

Immpress™ HRP Anti Rat (Goat, 1:1)

2.2 Molecular Biology Methods

2.2.1 Genomic DNA purification from mouse tail

Tail tip biopsies were collected from individual mice for genotyping. The procedure complies to the guidelines of international and domestic animal welfare laws and was approved by the institutional committee for experimental animal use of the University of Bonn. The Gentra Puregene Mouse Tail Kit was used for DNA purification by following the manufactures protocol with minor modifications. About 3-5 mm mouse tail tip was cut and transferred into a 1.5 ml reaction tube with 300 µl Cell Lysis Solution and 1.5 µl proteinase K. The sample was incubated overnight at 56 °C until the tissue was completely lysed. 100 µl Protein Precipitation Solution was added to each sample. The samples were subsequently mixed vigorously for 20 s and centrifuged for 3 min. at 16000 x g. Supernatants containing the genomic DNA were transferred into a clean 1.5 ml reaction tube containing 300 µl 2-methylbutane. The samples were mixed by inverting gently for 50 times and centrifuged for 1 min. at 16000 x g. After removing the supernatant, 300 µl of 70% ethanol was added per sample to wash the DNA pellet. The 70% ethanol was removed after very short washing by centrifugation at 16000 x g. The DNA pellet was rehydrated in 500 µl water for 1 hour at 56 ℃ and stored at 4°C.

2.2.2 Genotyping by PCR

The polymerase chain reaction (PCR) was used to detect the foreign transgenes in the genomic engineered mouse lines as described by previous studies. [102] The DNA fragments of the genes of interest were amplified by hot-start PCR and analyzed by agarose gel electrophoresis. Oligonucleotide primers were used as described in 2.1.2. The PCR reaction mix was prepared for each sample as indicated in Table 2.1. The PCR was run in a Thermocycler using the protocol from Table 2.2.

Table 2.1 PCR reaction mix

Component	Volume (10 µl)
Genomic DNA	1 µl (ca. 200 pg)
GoTaq® Green Master Mix	5 µl
Primer Mix:	1 µl (10 µM)
Water	3 µl

Table 2.2 PCR protocol

Mouse line	Step	Temperature	Time
SCF-CreER^{T2}	Initial denaturation	95°C	4 min
36x	Denaturation	94°C	30 s
	Annealing	62°C	30 s
	Extension	72°C	1 min
	Final Extension	72°C	10 min
		4°C	hold
CAG-mTmG	Initial denaturation	95°C	4 min
36x	Denaturation	94°C	30 s
	Annealing	62°C	30 s
	Extension	72°C	1 min
	Final Extension	72°C	10 min
		4°C	hold
c-kit^{BAC}-eGFP	Initial denaturation	95°C	4 min
17x decrease 0.5 °C per cycle	Denaturation	94°C	30 s
	Annealing	68-60°C	30s
	Extension	72°C	1.5 min
16x	Denaturation	94°C	30 s
	Annealing	60°C	30 s
	Extension	72°C	1.5 min
	Final Extension	72°C	10 min
		4°C	hold
SCF$^{\Delta Ex7}$	Initial denaturation	95°C	4 min
	Denaturation	94°C	30 s

17x decrease 0.5 °C per cycle	Annealing	63-55°C	30s
	Extension	72°C	1.5 min
	Denaturation	94°C	30 s
16x	Annealing	55°C	30 s
	Extension	72°C	1.5 min
	Final Extension	72°C	10 min
		4°C	hold
Tie2-Cre	Initial denaturation	95°C	4 min
36x	Denaturation	94°C	30 s
	Annealing	59°C	30 s
	Extension	72°C	1 min
	Final Extension	72°C	10 min
		4°C	hold
eGFP-anillin	Initial denaturation	95°C	4 min
36x	Denaturation	94°C	30 s
	Annealing	60°C	30 s
	Extension	72°C	1 min
	Final Extension	72°C	10 min
		4°C	hold

2.2.3 Analysis of PCR products by gel electrophoresis

Genotyping was performed by gel electrophoresis of the PCR fragments obtained from each mouse line. Gel electrophoresis is a basic method that allows separation of nucleic acids based on their size, which migrate through a pre-casted agarose gel in an electrical field. The gel was prepared by dissolving 5 µl of ethidium bromide and 1-2 mg agarose in 100 ml TAE-buffer while heating and subsequently casting in a specific casting mold to cool down to room temperature (RT). The gel was submerged in an electrophoresis chamber containing TAE-buffer. The PCR reactions (approximately 10 µl each) were loaded directly into the small wells formed by the casting mold. The gel was run for 45-60 min. at 100-120 Volts (5-8 V per cm of gel). Since the DNA nucleotides have negative charges, they move towards the positive charged anode and the smallest fragments migrate the fastest. Afterward, the gel was analyzed under UV light to visualize DNA bands marked by ethidium bromide.

To identify the different sizes of PCR products, 5 µl of O'GeneRuler 1 kb DNA Ladder was loaded onto the gel along with the PCR products.

2.3 Immunohistochemistry Methods

2.3.1 Tissue process and sectioning

Embryos and embryonic hearts from euthanized mice were dissected under a macroscope and briefly washed in PBS for 3 times. Postnatal hearts were washed in PBS-Heparin Solution for 3 times and then submerged into 1% (w/v) KCl cardioplegic solution for 3-5 min. All samples were fixed in 4% PFA solution for 1h at 4 °C. Subsequently, samples were washed for 3 x 5 min. in PBS and then stored in 30% sucrose solution at 4°C for at least 14 h. Cryosectioning blocks were prepared by embedding the samples after sucrose solution into plastic molds of appropriate sizes containing Tissue-Tek® O.C.T.™ compound. Hearts were positioned coronally, sagittal or transversely before freezing depending on the experimental purpose. The samples were frozen on top of dry ice and stored at - 80°C. 10 µm sections were cut with a Cryostat microtome and collected on microscopic slides and stored at - 20°C.

2.3.2 Immunostaining protocols

Microscopic slides containing tissue sections were taken from the -20°C refrigerator and thawed at RT. Remnants of Tissue-Tek® O.C.T.™ compound were teared away manually with fine forceps. An ImmEdge Hydrophobic Barrier PAP pen was used to draw a circle around each tissue section. The tissue sections were sequentially rehydrated in PBS for 5 min., post-fixed with PFA fixing solution for 10 min. and washed in PBS for 3 x 5 min. In cases that the peroxidase conjugated secondary antibodies were needed, H_2O_2 blocking solution 1 was applied to the tissue sections for 2 x 15 min. at RT. After that, tissue sections were permeabilized and blocked with 5% PBSST for 30 min. at RT. After blocking, primary antibodies (see working dilutions 2.1.11) were diluted in 2.5% PBSST and added onto the tissue sections. The slides were then incubated in the dark at 4°C overnight. Afterwards, the slides were washed for 3 x 5 min. in PBS before applying the secondary antibodies. The secondary antibodies were diluted in PBS and applied to the tissue sections for 1 h at RT. In case of using peroxidase conjugated secondary antibodies, the Tyramide Signal Amplification (TSA) reagents were used as substrates by dissolving TSA stock

solution in Borate solution (1:1000) to add fluorochromes onto the binding sites of secondary antibodies for 5 min. at RT. If two peroxidase conjugated secondary antibodies from different species were used, two antibodies and their corresponding TSA reactions were applied separately with an additional blocking step in between (H_2O_2 blocking solution 2 for 2 x 15 min. at RT). After a short wash with distilled water, sections were mounted with Vectashield mounting media (including DAPI nuclear stain) and coverslips. The slides were stored at RT to let them dry overnight and stored at 4°C in the dark. The edges of the coverslips were fortified by nail polish.

In the case of two primary antibodies from the same species were required for immunostaining, the staining was applied sequentially by using the peroxidase TSA system as described above. Additionally in between the two stainings antibodies were eluted as follows: [103] After finishing the TSA reaction for the first antigen, the section was submerged in preheated 2-ME/SDS solution and incubate at 56°C for 30 min. The section was then washed in distilled water for at least 1 h with water change every 15 min. to get rid of residual β-mercaptoethanol. Then the second antigen was stained following the protocol described above starting with encircling the section with an ImmEdge Hydrophobic Barrier PAP pen.

2.3.2 Imaging of sections and post-processing protocols

Whole mount fluorescent pictures of embryos and hearts were taken by a Stereomicroscope AxioZoom V16. The tissues were briefly fixed with PFA solution to stop the movement of the hearts. A cell culture dish containing a 5 mm thick layer of 2% agarose gel and PBS was used to position the tissues under the stereomicroscope. The positions of the tissues were adjusted to the experimental needs by manually digging a hole with fine forceps on the agarose gel layer. Pictures of entire tissue section were taken by an Observer Z1 microscope with Apotome system with a 20x objective with disabled Apotome function. For overview pictures, individually acquired pictures were stitched together by the ZEN software. More detailed pictures were taken by either Observer Z1 microscope with Apotome system equipped with a 40x objective with Apotome function or by a Laser Scanning Microscope Eclipse Ti with 40x or 60x objectives. All the images were adjusted for brightness and contrast with the manufacturer's software and ImageJ. Quantification of different types of cells was done with the help of ImageJ's "cell counter" plugin and

the statistics program Graph Pad Prism v.5.0. The marks used on the pictures (e.g. scale bar, arrowheads, sketches, etc.) were made with Photoline v. 19.50, Computerinsel GmbH.

2.4 Animal experiments

2.4.1 Mouse lines used in the current study

All animal procedures in the current study complied with the guidelines of international and domestic animal welfare laws and were approved by the institutional committee for experimental animal use of the University of Bonn. All transgenic mouse lines used in this thesis have been previously published (listed in 2.1.5). To study the SCF expression maps at various developmental stages, the SCF-CreER^{T2} mouse line was used. To study the fate map of SCF^{+} cells during heart development, the SCF-CreER^{T2} line was crossbred to the CAG-mTmG mouse line. To study the loss of function of SCF in VECs, a Tie2-Cre mouse line was crossbred to the SCF$^{\Delta Ex7}$ mouse line. To study the roles of c-kit during revascularisation of injured heart, the VECad-CreER^{T2}, Ai9, c-kit^{BAC}-eGFP mouse lines were crossbred together to create a triple transgenic mouse model. To study cell cycle activity and the role of SCF during repair of a neonatal injury, the SCF-CreER^{T2} mouse line was crossbred to the eGFP-Anillin mouse line.

2.4.1.1 The SCF-CreER^{T2} mouse line

The SCF-CreER^{T2} mouse line was generated by Buono and colleagues. [41] It contains a transgene co-expressing CreER^{T2} and tdTomato [104], a red fluorescent protein, knocked into the SCF promoter on a bacterial artificial chromosome (BAC) (Fig. 2.1). With the help of this mouse line, SCF^{+} cells were identified in the thymus which consisted of two sub-populations of cortex-specific VECs and cortical thymic epithelial cells. The latter provide a stem cell niche for early thymocyte progenitors. In this study, only the tdTomato signal was used to identify SCF expressing cells in the thymus. To verify the faithful representation of endogenous SCF expression by the tdTomato signal, the authors purified tdTomato^{+} and tdTomato^{-} cell populations by flow cytometry and examined the expression of SCF in both populations by quantitative Polymerase Chain Reaction (qPCR), 2nd generation RNA sequencing, and 2nd generation RNA sequencing of single sorted cells. Data analysis demonstrated consistent expression patterns of SCF and tdTomato. Thus, the SCF-

CreER^{T2} mouse line is an ideal genetic tool to study the expression pattern of SCF in the heart.

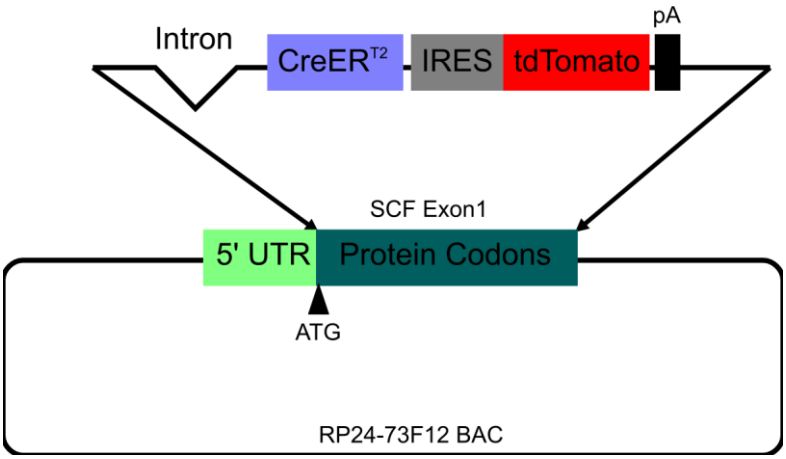

Fig. 2.1. Schematic representation of the SCF-CreER^{T2} BAC transgene (Adapted from Buono et. al. 2015 [41]):

The SCF-CreER^{T2} BAC transgene was generated by replacing the endogenous exon 1 of SCF with a cassette consisting of a hybrid intron (to ensure a controlled splicing event), a Kozak–ATG–CreER^{T2} moiety, an IRES followed by tdTomato and a SV40 polyA site on The RP24–73F12 BAC backbone (BacPac Resources, CHORI).

2.4.1.2 The SCF$^{\Delta Ex7}$ mouse line

The SCF$^{\Delta Ex7}$ mouse line was generated by Buono and colleagues. [41] Exon 7 of the SCF gene, encoding the transmembrane domain, was flanked by two loxP sites (Fig. 2.2). The expression of soluble SCF was confirmed by ELISA *in vitro*. Complete knockout of the SCF$^{\Delta Ex7}$ allele in homozygous mice displayed perinatal lethality due to severe developmental and hematopoietic abnormalities, similar to mutants of Steel alleles [32] and SCF complete knockout lines for both soluble and membrane bound SCF [33]. The strong phenotype of SCF exon 7 knockout mice supported a critical physiological role of membrane bound SCF.

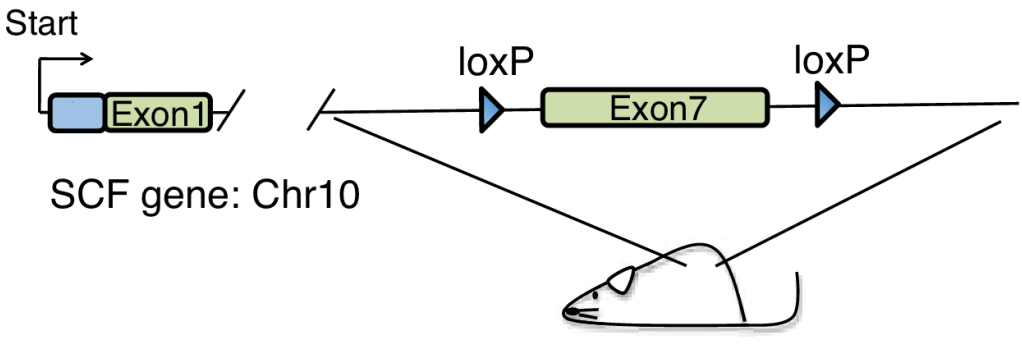

Fig. 2.2 Schematic representation of the SCF$^{\Delta Ex7}$ mouse line (Adapted from Buono et. al. 2015 [41]):

Two loxP sites were introduced into intron 6 and intron 7 respectively by homologous recombination, thereby flanking exon 7. Under the presence of Cre recombinase, exon 7 of the SCF gene, which encodes the transmembrane domain of SCF, will be excised. Homozygous knockout mice of the SCF$^{\Delta Ex7}$ line only produce the soluble form of SCF.

2.4.1.3 The C-kit^{BAC}-eGFP mouse line

The c-kit^{BAC}-eGFP mouse line was generated by Tallini and colleagues. [96] It was one of the first mouse lines generated to identify the c-kit^{+} cardiac cells. An EGFP coding sequence was inserted at the start codon of c-kit on a BAC (Fig. 2.3). To verify faithful representation of endogenous c-kit expression by eGFP, the authors compared eGFP expression with previously well characterized c-kit^{+} cell populations such as melanocytes, interstitial cells of the intestines and stomach, muscle layer of the uterus and testis, basket and stellate cells in cerebellum, and hippocampus. [27][32][103][104] Thus, the c-kit^{BAC}-eGFP mouse line faithfully recapitulates the endogenous c-kit expression.

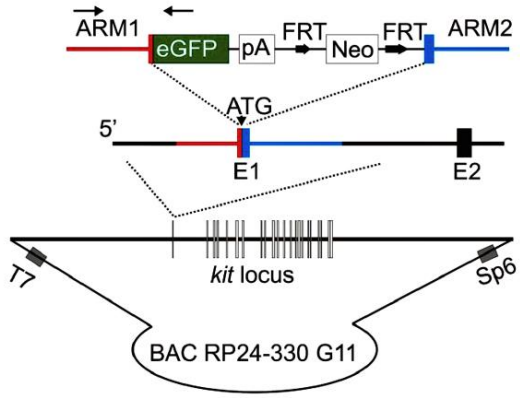

Fig. 2.3 Schematic representation of the c-kit^{BAC}-eGFP transgene (Adapted from Tallini et. al. 2009):

The c-kit^{BAC}-eGFP transgene was generated by inserting an eGFP-pA cassette into the BAC clone RP24-330G11 at the initiation codon of c-kit by homologous recombination.

2.4.1.4 The VECad-CreER^{T2} mouse line

The VECad-CreER^{T2} mouse line was generated by Monvoisin and colleagues. [101] In this mouse line CreER^{T2} is driven by the endothelial specific promoter, VECad (vascular endothelial cadherin, [107]).(Fig. 2.4) To verify EC specific CreER^{T2} expression, the VECad-CreER^{T2} mouse line was crossbred with the Rosa26R

reporter mouse line [108] that expresses β-galactosidase after Cre-mediated deletion of a stop cassette. Tamoxifen injections were shown to induce β-galactosidase expression in different types of ECs in both embryos and adult mice. Furthermore, injection of tamoxifen in adult mice resulted in negligible recombination in the hematopoietic lineage. However, even after a long period of Cre induction β-galactosidase^{+} ECs only make up less than 50% of total ECs, which substantially limits the usage of this line. Applying new Cre-reporter mouse lines that are more sensitive to low levels of Cre expression may improve the percentage of Cre recombination in ECs.

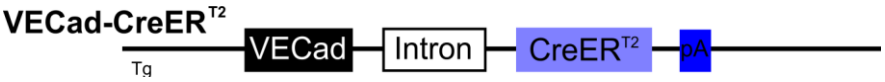

Fig. 2.4 Schematic representation of the VeCad-CreER^{T2} transgene:

The CreER^{T2} coding sequence was inserted downstream of a 2.5 kb VECad minimal promoter [107] which contained a synthetic intron composed of sequences from the rabbit β-globin locus. The construct was randomly integrated into the mouse genome by pronuclear injection.

2.4.1.5 The Tie2-Cre mouse line

The Tie2-Cre mouse line was generated by Kisanuki and colleagues. [100] The Cre recombinase is driven by the endothelial specific promoter, Tie2 (angiopoietin receptor, [109]). (Fig.2.5) To verify the EC specificity of Cre expression, the Tie2-Cre mouse line was crossbred with the Rosa26R reporter mouse line [108]. The authors demonstrated that virtually all vessels in e11.5 embryos are labelled by the Tie2-Cre line, indicating high levels of Cre expression at least in early embryonic stages.

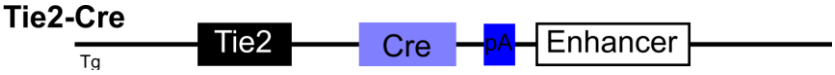

Fig. 2.5 Schematic representation of the Tie2-Cre transgene:

The Cre coding sequence was cloned behind the murine 2.1-kb Tie2 promoter, pg50H1-2. A 10 kb murine Tie2 enhancer fragment derived from pg50-2.11 [109], was inserted downstream of the polyA signal sequence. The construct was randomly integrated into the mouse genome by pronuclear injection.

2.4.1.6 The CAG-mTmG mouse line

The CAG-mTmG mouse line was generated by Muzumdar and colleagues. [98] It was one of the first reporter mouse lines for Cre activity with robust and ubiquitous expression of fluorescent proteins. It is a double-fluorescent Cre reporter mouse that expresses membrane-targeted tandem dimer Tomato (mT) prior to Cre-mediated excision of the loxP flanked mT and membrane-targeted green fluorescent protein (mG) after excision. By examining all major organs in the mouse, the authors demonstrated that both mT and mG signals were highly ubiquitously expressed which allowed their visualization *in vivo* and *in vitro*. Both membrane-targeted markers outline cell morphology and highlight membrane structures.

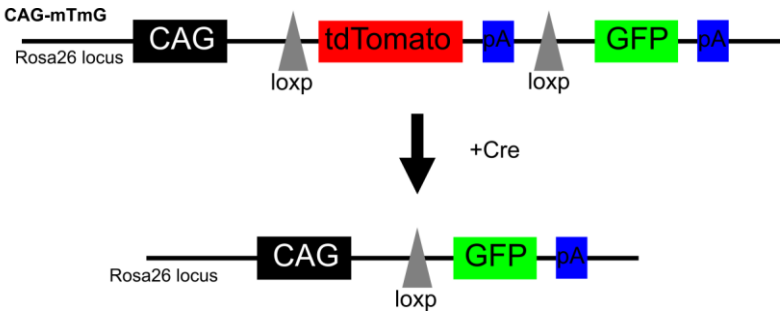

Fig. 2.6 Schematic representation of the CAG-mTmG transgene before and after recombination by Cre:

The targeting vector for the CAG-mTmG mouse line was generated by inserting a cassette consisting of a tdTomato-polyA moiety flanked by two loxP sites, followed by GFP and SV40 polyA into a pCAG (a CMV/β-actin enhancer-promoter) expression vector. The construct was subsequently integrated into the Rosa26 locus of the mouse genome by homologous recombination. After Cre recombination, the mT sequence is excised, allowing the expression of mG.

2.4.1.7 The Ai9 mouse line

The Ai9 mouse line is one of a series of universal Cre-reporter mouse lines generated by Madisen and colleagues. [97] In the Ai9 transgenic mouse line a construct containing the CAG promoter, followed by a loxP-flanked stop cassette and tdTomato-polyA sequence was inserted into the Rosa26 locus (Fig. 2.7). This mouse line was characterized by using a large amount of available Cre-driver lines to test the signal intensity and Cre-dependent reporter gene expression. As a result, Ai9 displayed excellent signal intensity and Cre sensitivity. Thus, the Ai9 mouse line is ideal to bred to mouse lines with weak Cre expression.

Fig. 2.7 Schematic representation of the Ai9 transgene (Adapted from Madisen et. al. 2010 [97]):

The targeting vector of the Ai9 mouse line consist of the CAG promoter, followed by a loxP flanked stop cassette, tdTomato coding sequence and SV40 polyA signal. The construct was recombined into the Rosa26 locus of the mouse genome. After Cre recombination, the stop sequence is excised, allowing the expression of tdTomato.

2.4.1.8 eGFP-anillin mouse line

The eGFP-anillin mouse line was generated by Hesse and colleagues. [99] Before the generation of the eGFP-Anillin mouse line, cell proliferation was mostly determined by bromodexyuridine or thymidine incorporation assays and/or immunostaining with cell cycle specific antibodies. However, these methods cannot differentiate authentic cell division from cell cycle variants such as endoreduplication (DNA replication without karyokinesis or cytokinesis), or acytokinetic mitosis (karyokinesis without cytokinesis). This is particularly important in cardiomyocytes, which are known to undergo these cell cycle variants. The eGFP-anillin mouse line expresses a fusion protein consisting of eGFP fused to the N-terminus of the scaffolding protein anillin, a component of the contractile ring. eGFP-anillin is absent in quiescent cells due to its ubiquitination by anaphase-promoting complex and degradation by the proteasome. eGFP-anillin is localized in the nucleus during late G1-, S-, and G2-phases of the cell cycle, in the cytoplasm during early M-phase, and in the contractile ring and midbody during late M-phase (Fig. 2.8). Thus, the eGFP-Anillin mouse line enables direct visualization of M-phase events, cytokinesis and cell separation by detection of cytokinetic structures, such as the contractile ring and midbody.

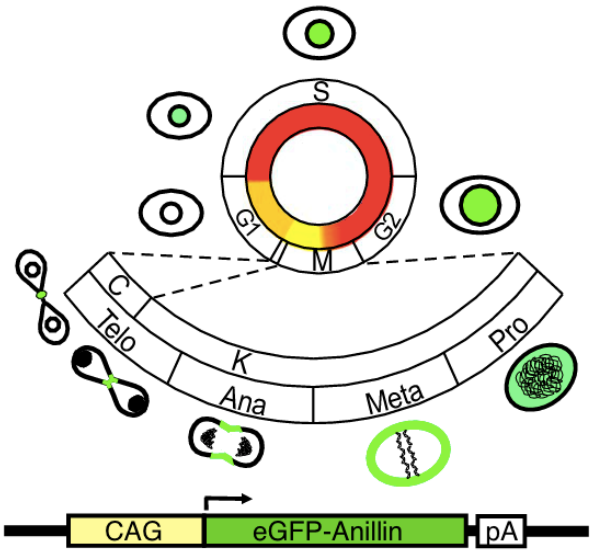

Fig. 2.8 Schematic representation of the subcellular localization of the eGFP-anillin fusion protein during the cell cycle and the expression construct of the eGFP-Anillin mouse line (adapted from Hesse, et. al. 2012 [99]):

The mouse anillin coding sequence was ligated to the c-terminus of eGFP. The CAG promoter was used to drive the expression of the eGFP-anillin fusion protein. C, cytokinesis; K, karyokinesis.

2.4.2 Tamoxifen administration to transgenic mice

The most common approach to apply tamoxifen is by intraperitoneal injection. However, a recent study demonstrated that using the oral gavage method provides more precise and reliable control of Cre activation. [73] To understand changes of SCF expression in hearts during embryonic development, we applied tamoxifen by oral gavage to SCF-CreER^{T2} x CAG-mTmG compound transgenic mice. Tamoxifen was dissolved in corn oil at a concentration of 20 mg/ml by shaking overnight at RT. Embryonic stages were determined by checking for vaginal plugs every day after setting up a mating (occurrence of plug counted as day 0.5 of embryonic development, e0.5). 1 mg of Tamoxifen were given to each pregnant mouse once by oral gavage using a blunt end reusable Feeding Needle (FST, 18060-20) (Fig. 2.9A). In VECad-CreER^{T2} x Ai9 x c-kit^{BAC}-eGFP triple transgenic mice, 2 mg of tamoxifen were given to each mouse via intraperitoneal injection for three times in a week to ensure high recombination frequency of CreER^{T2} (performed by the lab of M. Kotlikoff, Pen University, USA). Mice were then kept in stock for 1 week to clean out residual tamoxifen in their system before going to the next step of experiment (Fig. 2.9B). Tamoxifen binds to the ER^{T2} and induces relocation of CreER^{T2} protein into the nucleus. As a result, the CreER^{T2} signal becomes concentrated in the nucleus, which eases the visualization of cells with weak SCF expression by immunostaining. In SCF-CreER^{T2} x eGFP-anillin double transgenic mice, 0.2 mg of tamoxifen were injected intraperitoneally 2 days before there were sacrificed to improve CreER^{T2} signals in cardiomyocytes (Fig. 2.9C).

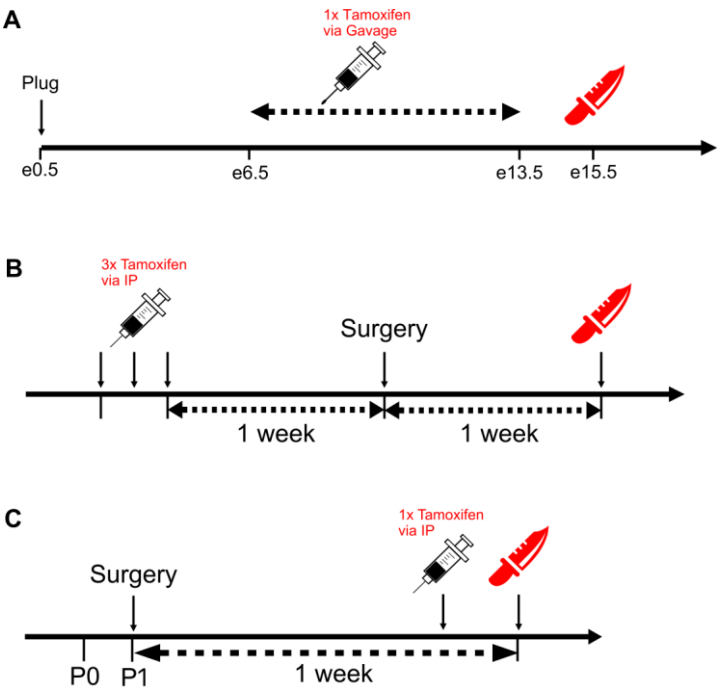

Fig. 2.9 Schematic representation of tamoxifen administration strategies for different mouse lines:

A) SCF-CreER^{T2} x CAG-mTmG mouse line. **B)** VECad-CreERT2 x Ai9 x c-kit^{BAC}-eGFP mouse line. **C)** SCF-CreER^{T2} x eGFP-anillin mouse line.

2.4.3 Adult Myocardial Infarction models

To study the possible roles of SCF in infarcted heart, SCF-CreER^{T2} and Tie2-Cre x SCF$^{\Delta Ex7}$ mouse lines were subjected to acute a myocardial infarction model by ligation of the left anterior descending coronary artery. This model was performed by Dr. Annika Ottersbach (Institute of Physiology I, Bonn). The experimental procedure was described in a previous study by Roell and colleagues [110] and applied with minor modifications. Mice were sedated by narcotic gas (50% O_2, 50% N_2O, and 3 to 4 vol% of isoflurane) in a gas chamber. The mouse was quickly intubated with a Braun Vasofix® safety cannula (22G) and put on a self-made temperature-controlled heating plate at 37°C. A mechanical ventilation device (MiniVent type 845, Harvard Apparatus, March, Germany) was connected to the mice at a breathing rate of 100/min. (tidal volume of 0.5 mL). Mice were kept under narcotic gas with isoflurane concentrations between 0.8 and 1.3 vol %. Then, the chest wall was shaven and disinfected with 70% ethanol. After cutting a small skin incision, the superficial muscle layers were transected to expose the fourth intercostal space (Fig. 2.10A). After opening of the chest by cutting the intercostal muscles, a self-made chest

retractor was placed, the pericardium was opened, and the apex of the heart was exposed (Fig. 2.10B). A self-made elliptical spoon was used to push up and to immobilize the heart outside the chest wall. To directly visualize the LAD coronary artery, a Leica M651 surgical microscope was used with strong illumination. An 8-0 prolene suture (Ethicon) was used to make a tight ligation on the stem of the LAD coronary artery (Fig. 2.10D). Before closing the chest, a 22-G blunt end needle was inserted into the chest cavity. At this point N_2O supply was stopped, and the thorax was closed by 6-0 prolene sutures (Ethicon). The pneumothorax was drained by applying negative pressure through the blunt needle, which was removed afterwards (Fig. 2.10E). The incision on the skin was subsequently closed using the same suture for the thorax (Fig. 2.10F). Postoperatively, the mice were placed into cages with heating lamps and monitored several hours before transferring them to their cages in the animal facility. The first 3 days after operation, metamizol (100 mg/kg) as analgesic and cefuroxime (100 mg/kg) as antibiotic were administered intramuscular twice a day, respectively.

The VECad-CreER^{T2} x Ai9 x c-kit^{BAC}-eGFP mouse line underwent a similar procedure except occlusion of the LAD artery (sham control). To evoke a reproducible size of myocardial lesions, cryo-injury was performed by pushing a liquid nitrogen cooled probe (3-mm diameter, cooled in liquid nitrogen for 2 min) against the free left ventricular wall for 3 x 20 sec (Fig. 2.10C). These operations were performed in the laboratory of M. Kotlikoff, Cornell University, USA.

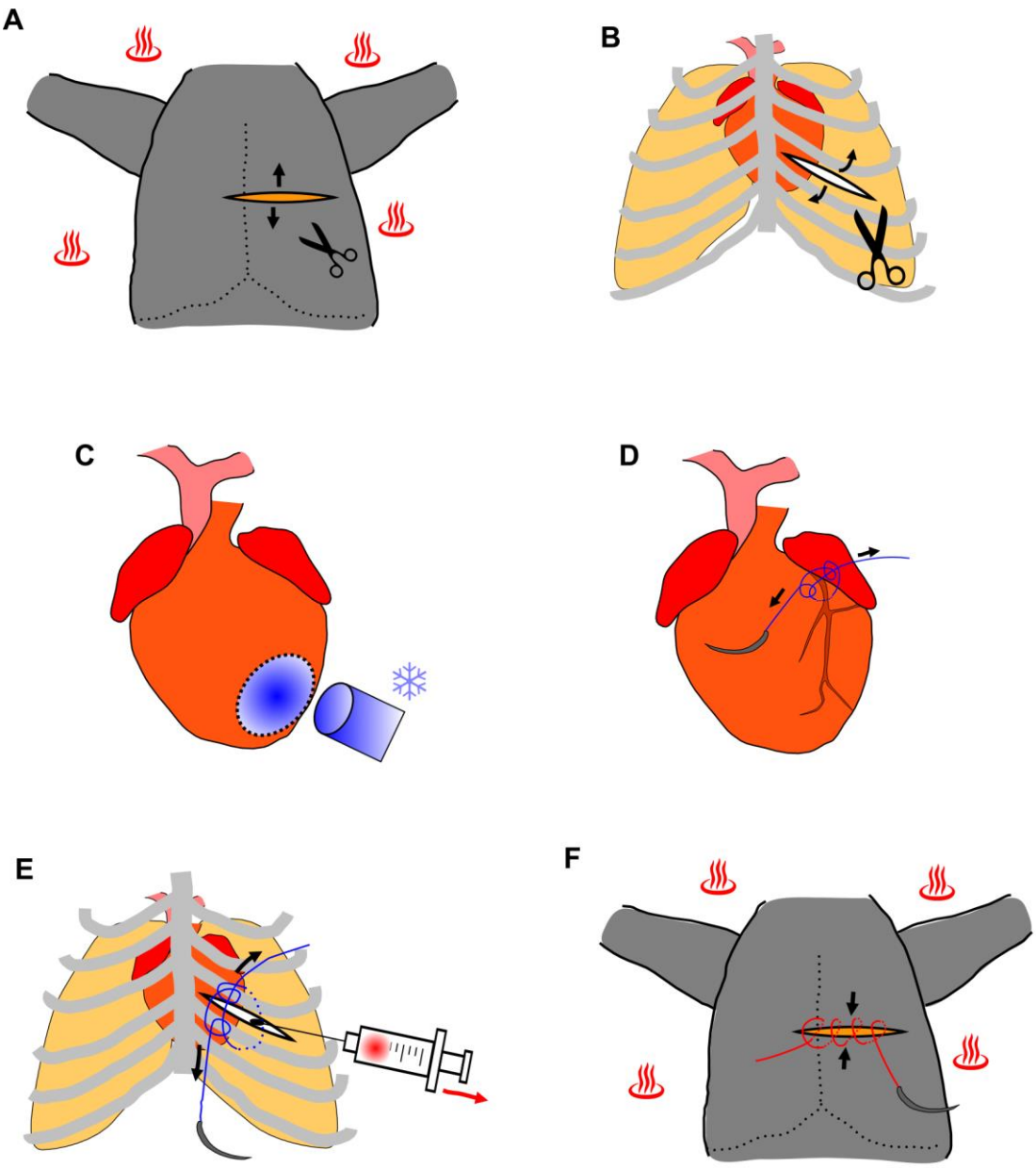

Fig. 2.10 Myocardial infarction models of the adult mouse heart:

A) After anesthesia, mouse is immobilized in the supine potions on a 37 °C heating plate. Skin incision is performed transversely along the chest cavity. **B)** Heart is accessed through intercostal muscle separation at the fourth intercostal space. **C)** Cryo-injury model: Free left ventricle is injured by a liquid nitrogen cooled probe (3 mm diameter) for 3 x 20 seconds. This part of the experiments was performed at Cornell University. **D)** LAD coronary artery ligation model: an 8-0 Prolene suture is used to make a tight ligation on the stem of the LAD coronary artery. **E)** Pneumothorax is drained by a 22-G blunt end needle before closing the chest. **F)** The skin is closed by a 6-0 Prolene suture.

2.4.4 Neonatal heart injury model

To study the possible roles of SCF during neonatal heart regeneration, SCF-CreER^{T2} x eGFP-Anillin mice were subjected to a neonatal heart injury model consisting of heat induced cauterization of the LAD coronary artery of P0 mice. The experimental procedure was a modification from a previous study by Porrello and colleagues. [111]

Mice were sedated by hypothermia by putting P0 pups directly on ice for 7-10 min. The mice were then put on a self-made cooling plate consisting of a metal platform on top of ice (0°C). Two medium size forceps were used to immobilize the mice by placing them on the limbs with thorax region free for easy access. The mice on the cooling platform were kept under a surgical microscope. Next, the chest wall was disinfected with 70% ethanol. After cutting a small skin incision on the left side of the chest, the superficial muscle layers were transected to expose the second intercostal space (Fig. 2.11A). After opening of the chest by cutting into the fourth intercostal muscles, a small piece of a paper towel was placed inside the chest cavity to open the wound and absorb leaking fluid, which would otherwise block the vision (Fig. 2.11B). The pericardium was opened, and the left ventricle of the heart exposed. The tip of the cauterizer was placed onto the surface of the heart. The switch of the cauterizer was turned on for 1 sec. and the contact surface was heated to 1000°C, thereby injuring it (Fig. 2.11C). Before closing the chest, the pneumothorax was drained by gently squeezing the chest. An 8-0 prolene suture (Ethicon) was used to make a tight ligation in-between the ribs (Fig. 2.11D). The skin was closed by a 10-0 prolene suture (Ethicon) (Fig. 2.11E). Buprenorphine (10 µg per mouse) was administered to the pups as painkiller via intraperitoneal injection. Postoperatively, the mice were placed into cages with heating lamps and monitored 30 to 60 min. before transferring them to their mother.

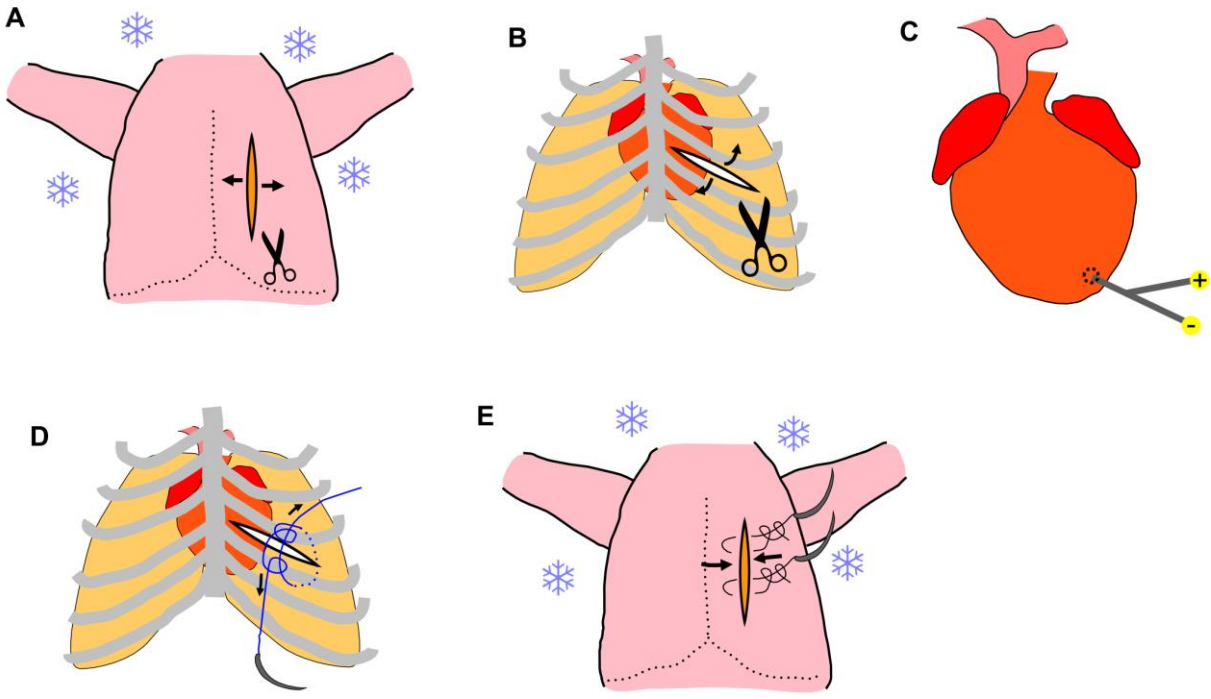

Fig. 2.11 Apex cauterisation of the neonatal mouse heart:

A) After anesthesia by hypothermia, neonatal pup is immobilized in the supine position on a 0 ℃ cooling plate. A skin incision is performed sagittally along the midline. **B)** A muscle incision is performed at fourth intercostal space to get access to the heart. **C)** Apex of the heart is cauterised for 1 sec. at 1000 ℃, which leaves a small scar. **D)** After removal of pneumothorax by gentle squeezing, an 8-0 prolene suture is used to close the chest wall. **E)** The skin is closed by a 10-0 prolene suture.

2.5 Disclaimer

The LAD coronary artery ligation in mice was performed by Dr. Annika Ottersbach from the Department of cardiac surgery, University of Bonn. The breeding and genotyping of the VECad-CreERT2 x Ai9 x c-kit^{BAC}-eGFP compound transgenic mouse line, cardiac cryo-injury, and tissue fixation of hearts from VECad-CreERT2 x Ai9 x c-kit^{BAC}-eGFP triple transgenic mice were performed by the group of Prof. Michael I. Kotlikoff, Cornell University, USA, namely Jane C. Lee, Shaun Reining, and Frank. K. Lee. All the other experiments were performed by myself with the help from my colleagues at the Institute of Physiology I, the staff of the animal core facility at the UKB, the members of GRK1873 and my supervisors, Prof. Bernd K. Fleischmann and PD Dr. Michael Hesse.

3. RESULTS

The c-kit$^+$ cardiac cells had been proposed to play important roles during heart regeneration by many studies over the last 20 years. [8]–[12] However, other independent studies failed to reproduce the similar results. [13][14] More recently, several studies using Cre-loxP based gene-targeted mouse models to directly examine the identities of c-kit$^+$ cardiac lineages and refuted the possibility of a significant contribution of c-kit$^+$ cells to neomyogenesis in adult heart. [15]–[17] On the other hand, the ligand of c-kit, SCF has also been proposed to play important role during heart recovery by several studies. [46]–[49] However, these results must be rigorously verified by independent experiment designs, since the underlying mechanism and the identities of the SCF$^+$ cells in the heart is currently unknown. In the current study, I took advantage of SCF-CreER^{T2} mouse line and other genetic mouse models to independently identify the SCF$^+$ cardiac lineages and verify their proclaimed roles during ischemic heart disease.

3.1 Whole-mount microscopic pictures of early embryos from the SCF-CreER^{T2} mouse line revealed high level of SCF expression in endodermal-derived organs

In the first description of the SCF-CreER^{T2} mouse line 2nd generation sequencing was used to verify the faithful recapitulation of endogenous SCF by tdTomato expressed in adult thymus. [41] However, it is still unclear if SCF-CreER^{T2} line can reproduce the same SCF expression pattern in early endoderm-derived organs as reported by several studies in the early 1990s. [53]–[55] To further verify the faithful recapitulation of endogenous SCF expression by the SCF-CreER^{T2} line, I first used whole-mount fluorescent microscopy to directly visualize the expression pattern of tdTomato in the SCF-CreER^{T2} line. tdTomato signals were found in the endoderm derived foregut, midgut and hindgut in e8.0 embryos. The strongest signal could be seen at the thickening hepatic endoderm below the cardiac crescent (Fig. 3.1A and A'). In contrast, the primary mesoderm which contributes to the future heart fields did not have obvious tdTomato expression that could be distinguished from background (Fig. 3.1B and B'). During the looping of the primitive heart tube at e8.5, the endoderm derived organs continued to have strongest tdTomato expression in the whole embryo, whereas, the heart did not have detectable tdTomato expression (Fig. 3.1C and C'). After the specification of the right ventricle at e9.5, the endodermal

derived organs displayed strong tdTomato signals with the highest expression located at the liver bud and lung bud initiation sites. Furthermore, the mesodermal derived pharyngeal arches which partially contribute to the outflow tract also start to express SCF, as indicated by tdTomato signals (Fig.3.1D), but there was no obvious tdTomato signal in the heart (Fig. 3.2D). These findings suggest that tdTomato as expressed by the SCF-CreER^{T2} transgene has primarily an endodermal expression pattern in early embryos. Furthermore, the early embryonic heart (before e10.5) does not display any tdTomato signal. These observations are highly consistent with previously reported SCF expression patterns in early embryos using in situ hybridization. [54][55]

However, one previous study reported that SCF is expressed in the cardiac cushions of e11.5 hearts, which has not been reported by other studies using similar approaches. [53] To verify this interesting finding, I further analyzed the tdTomato expression pattern in e11.5 hearts of SCF-CreER^{T2} mice.

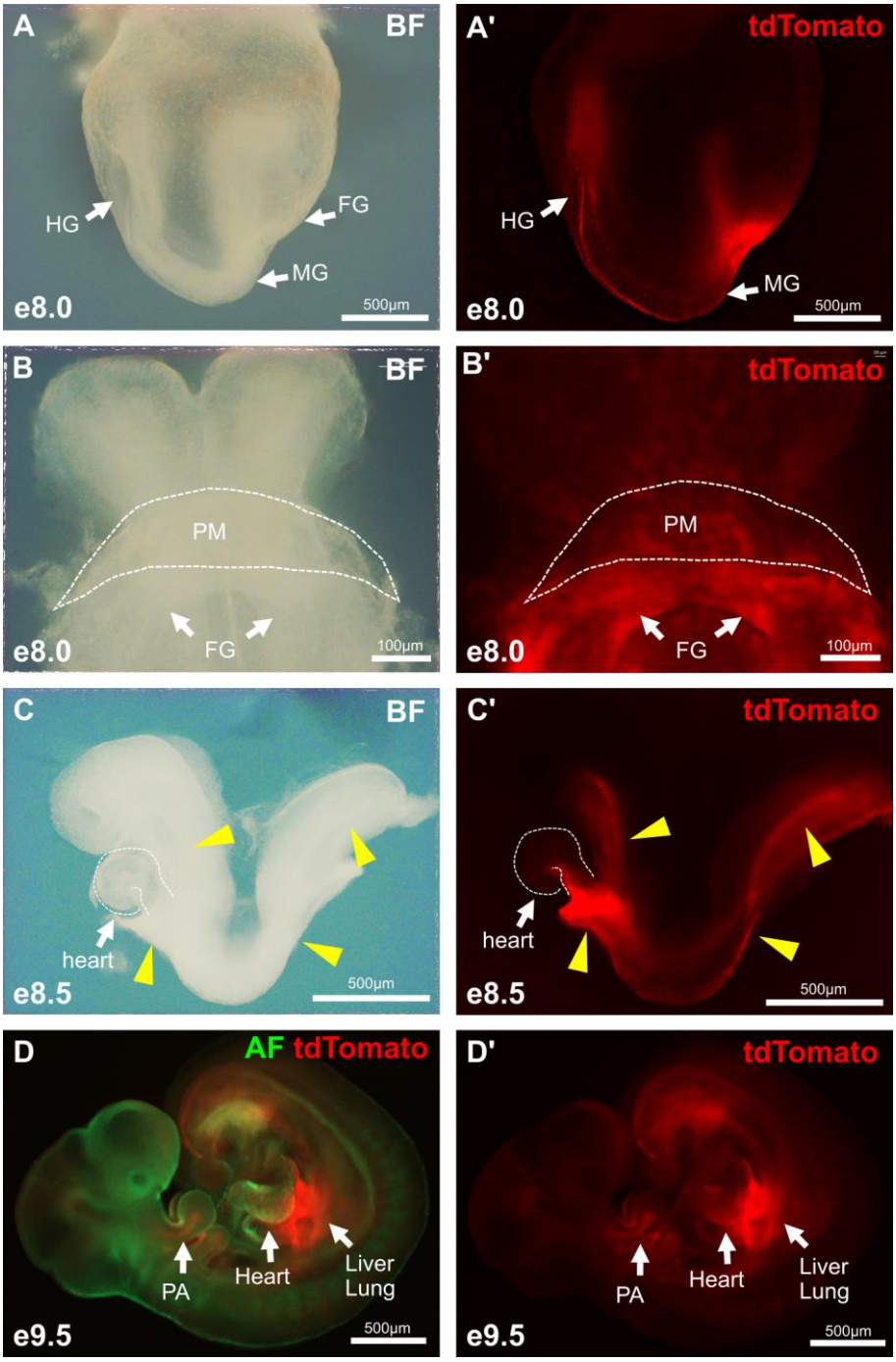

Fig. 3.1 SCF is predominantly expressed in endoderm-derived organs during early to mid-gestation (e8.0 - e9.5):

A-A') Right lateral view of an e8.0 SCF-CreER^{T2} embryo with yolk sac under bright field (BF, A) and RFP channel (A'). White arrows indicate different parts of early endodermal derived tissues. FG, foregut; MG, midgut; HG, hindgut. **B-B')** Magnified anterior view of an e8.0 SCF-CreER^{T2} embryo without yolk sac under BF (B) and RFP channel (B'). Pharyngeal mesoderm (PM), which will develop into 1st and 2nd heart fields, has no obvious tdTomato signal in comparison to foregut (white arrows). **C-C')** Left lateral view of an e8.5 SCF-CreER^{T2} embryo under Bright field (C) and RFP channel (C'). Primary heart tube (white arrow) at e8.5 has much less tdTomato signal in comparison to endodermal derived tissues (yellow arrow heads). **D-D')** Right lateral view of an e9.5 SCF-CreER^{T2} embryo under GFP/RFP double channel (D) and RFP channel (D'). Early heart has much less tdTomato signal in

comparison to early liver and lung. Mesoderm derived pharyngeal arches (PA) which partially contribute to the heart start to express tdTomato signal. (AF, autofluorescence)

3.2 Endocardial cushions express high levels of SCF

After the initial investigations verifying SCF to be preferentially expressed in endoderm-derived organs during early gestation, I wanted to analyze the possible SCF expression in the forming endocardial cushions. After the embryo reaches midgestation, the tdTomato signal intensity from the SCF-CreER^{T2} mouse line is not sufficient for direct observation in whole embryos due to increased thickness and autofluorescence of tissues. Therefore, I dissected the heart from an e11.5 embryo for whole-mount fluorescent microscopy and found high levels of SCF as indicated by tdTomato expression in the endocardial cushions located in the atrioventricular canal and outflow tract (Fig. 3.2A-B). Furthermore, the right ventricle had a very low level of tdTomato signal which was almost undistinguishable from the autofluorescence (Fig. 3.2A-B left panels). Such a low expression of SCF in the e11.5 heart has not been reported in early studies. [53]-[55] However, the reason for that is most likely the limited resolution of *in situ* hybridization analysis in early studies rather than the inaccuracy of the SCF-CreER^{T2} reporter line, because all the other regions which were reported to express high level of SCF were verified by the SCF-CreER^{T2} line. However, the previous study also indicated that tdTomato has lower photostability in fixed tissues in comparison to eGFP. [98] This could be a caveat when using tdTomato in SCF-CreER^{T2}-mice to identify low SCF expressing cell populations on heart sections. Since embryonic hearts have been shown to express only low levels of tdTomato in comparison to the thymus, which was originally used to characterize the SCF-CreER^{T2} line [41], I looked for alternative, more sensitive approaches to identify the reporter gene in the SCF-CreER^{T2} line. SCF-CreER^{T2} –mice express CreER^{T2} under control of the SCF promoter and CreER^{T2} should therefore mimic SCF expression in the same way as tdTomato does. To verify the simultaneous expression of CreER^{T2} and tdTomato in SCF-CreER^{T2} line in vivo, co-immunostaining of these two proteins on cardiac sections was performed to analyze their cellular expression pattern. For this, a human specific monoclonal antibody was used that binds to the c-terminus of human estrogen receptor α (ER). A potential cross-reactivity with endogenous mouse antigens has been ruled out by previous research. [78] Due to the generally lower expression level in the gene distal to IRES-site in a bicistronic vector, [112] I used a RFP antibody to improve the signal of

endogenous tdTomato on sections. As a result, nearly perfect signal colocalization between CreER^{T2} and tdTomato in the heart was observed (Fig. 3.2C). Thus, immunostaining of CreER^{T2} in SCF-CreER^{T2}-mice is a reliable method to detect bona fide SCF^{+} cell populations in the heart. Since the proposed SCF expression in endocardial cushions has not been supported by other studies, I performed co-immunostaining for ER (for SCF expression) and CD31 (EC marker, used as a reference for the luminal side of the OT) on e11.5 heart sections near the region of the cardiac cushions. A high level of SCF expression was found in all the interstitial cells of the valves, but not in the nearby endocardial cells (Fig. 3.2C). Therefore, the SCF expression pattern at embryonic stages as acquired by the SCF-CreER^{T2} mouse line was fully supported by early studies. [53]-[55] Interestingly, I did found very low SCF expression in the right ventricle of the e11.5 heart which has never been reported before. Such low levels of SCF expression are very likely below the detection threshold of methods such as in situ hybridization and antibody based immunostaining. To further identify the cell populations with low SCF expression in the right ventricle of the e11.5 heart, sections of e11.5 hearts were analysed.

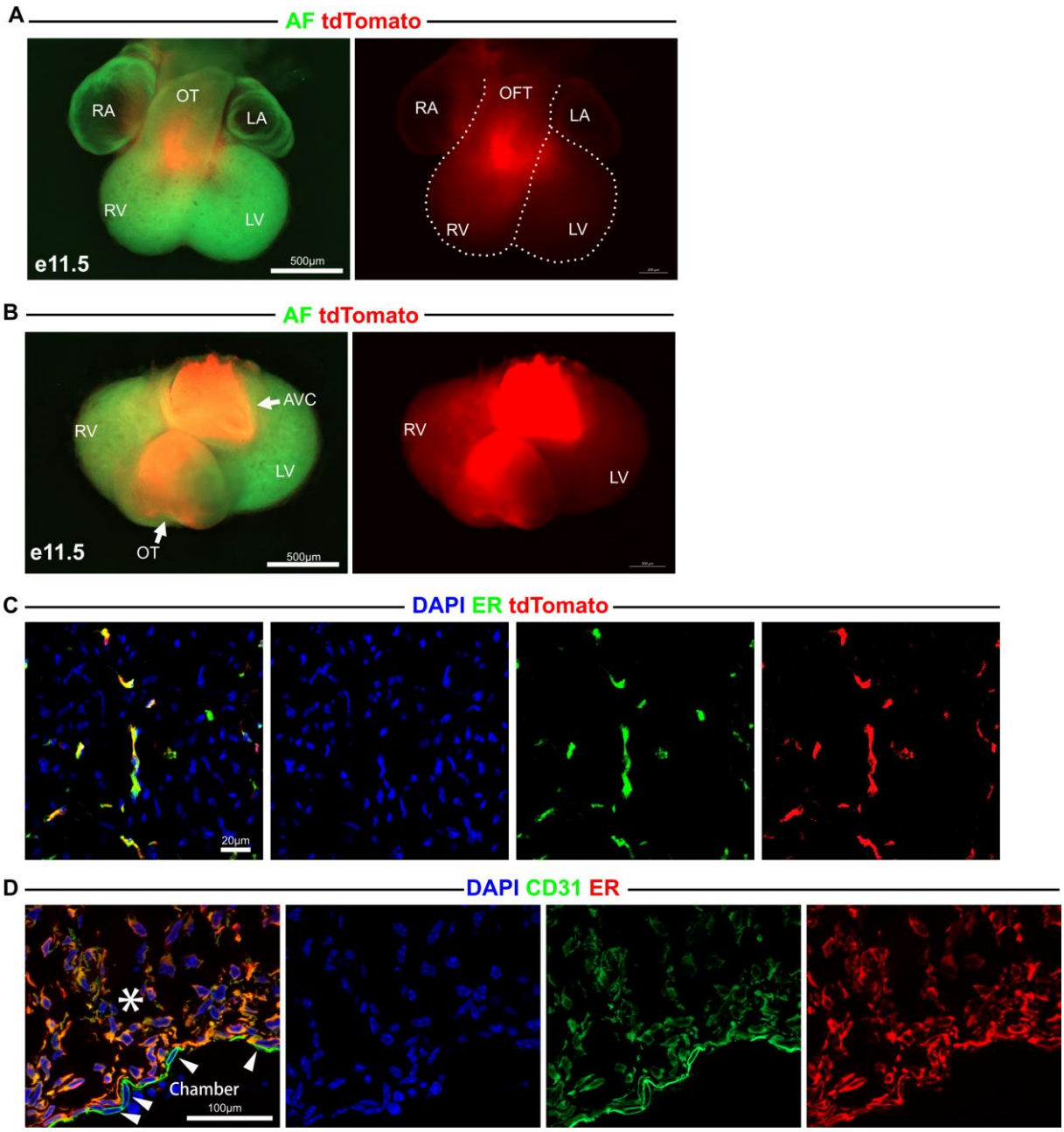

Fig. 3.2 SCF is highly expressed in the developing heart valves at e11.5:
A) Anterior view of an e11.5 heart from SCF-CreER^{T2} transgenic mice. GFP channel was used to show autofluorescence. tdTomato signal is clearly visible in the developing heart valves near the OT. Right ventricle has very low tdTomato signal, which is only slightly higher in signal intensity in comparison to the left ventricle. **B)** Superior view of the e11.5 heart from (A) after removal of atria. Developing heart valves from OT and AVC have very high SCF expression in comparison to other parts of the heart. SCF expression patterns in the right ventricle are not easily distinguishable from background, but can be identified by comparing to the left ventricle. **C)** Costaining for ER (green) and tdTomato (red) on cardiac sections from an adult SCF-CreER^{T2} mouse shows co-expression of CreER^{T2} and tdTomato. **D)** Co-staining of a section through the heart valve from (A) with CD31 (green) to mark endocardial cells and ER (red). CD31+ endocardial cells (arrowheads) near endocardial cushion (asterisk) migrate into the compact heart tubes to form SCF^{+} valve interstitial cells by epithelial to mesenchymal transition. RA, right atrium; LA, left atrium; RV, right ventricle; LV, left ventricle.

3.3 SCF$^+$ cardiomyocytes at e11.5 are spatially confined to the right ventricle and outflow tract

To identify cell populations with low SCF expression in the right ventricle of the e11.5 heart, as detected by whole-mount microscopy of the e11.5 heart, co-immunostainings against CD31, ER and α-actinin, a cardiomyocyte specific marker, was performed. ECs and cardiomyocytes were chosen as candidates for SCF$^+$ cell populations, because they are the most abundant cell types in the right ventricle of the e11.5 heart. The results showed that almost no SCF expression was found in CD31$^+$ cells in the e11.5 hearts (Fig. 3.3). Furthermore, a subset of the cardiomyocytes (identified by α-actinin staining) had very low levels of ER expression. The majority of these cells were located in the right ventricle and outflow tract (Fig. 3.3A). The right ventricular localization of the SCF$^+$ cardiomyocytes at e11.5 was more prominent in the forming ventricular septum, in which the majority of the SCF$^+$ cardiomyocytes formed the left part of the septum (Fig. 3.3B). These data indicate that, at least in e11.5 heart, the SCF expression is spatially confined to cardiomyocytes derived from the SHF. According to this, SCF could potentially be used as a marker for the SHF. However, based on these data, it was unclear if cardiac progenitor cells from the SHF would also express SCF or if other cardiomyocytes would express SCF at a different time window. To investigate the possibility of using SCF as a marker for SHF, I took advantage of the Cre recombinase in the SCF-CreER^{T2} mouse line to perform tracing experiments for the SCF$^+$ cell lineages at different time points.

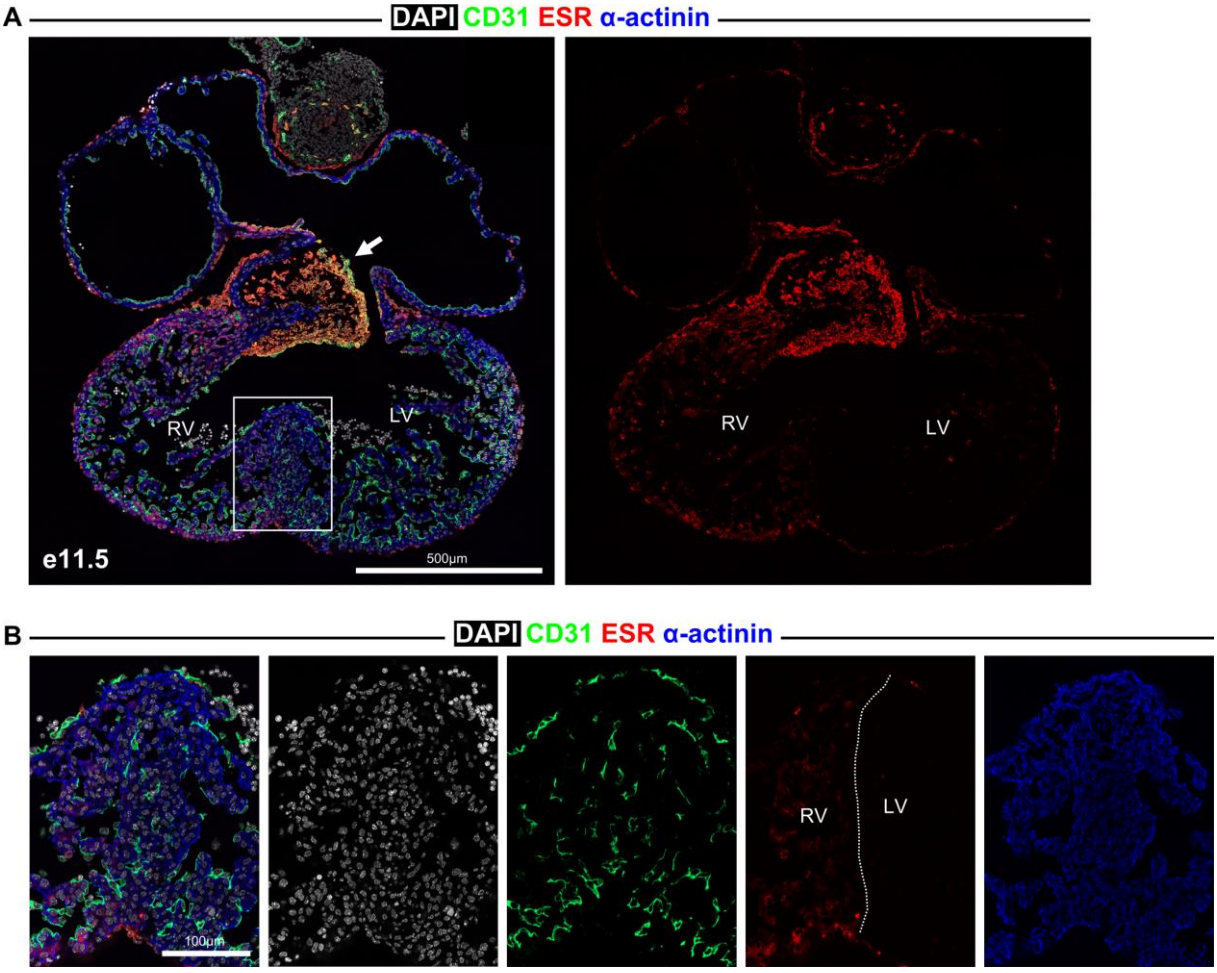

Fig. 3.3 SCF expression patterns in the embryonic heart:
A) Co-staining of CD31 (green), ER (red) and α-actinin (blue) on an e11.5 heart section from SCF-CreER^{T2} mice. Endocardial cushion (white arrow) shows clear signals of strong SCF expression as indicated by ER staining. Right ventricle has much lower level of SCF expression as judged by the ER signal. Left ventricle has almost no SCF expression. **B)** Magnified view of the forming ventricular septum from (A). Cardiac endothelial cells (marked by CD31) do not have SCF expression at e11.5. Cardiomyocytes (marked by α-actinin) have low level of SCF expression in the right part of the ventricular septum.

3.4 Lineage tracing experiments with SCF-CreER^{T2} mice identified a subpopulation of SCF^{+} cardiomyocytes during embryonic development

The observation of SCF expression specific to the right ventricle in e11.5 hearts indicates either that SCF marks for cardiac progenitors from the SHF or that cardiomyocytes originated from SHF retain SCF expression after differentiation. To trace this interesting cardiomyocyte lineage, we took advantage of the SCF-CreER^{T2} mouse line to perform genetic pulse-chase analysis for SCF^{+} cell populations in the developing heart. The SCF-CreER^{T2} mouse line was crossbred with the CAG-mTmG reporter mouse line, in which an ubiquitous CAG promoter drives the expression of membrane-tagged tdTomato protein (mT) prior to the Cre-mediated excision and

membrane-tagged green fluorescent protein (mG) after the excision.[98] In the compound transgenic mouse line, the CreER^{T2} fusion protein will locate to the nucleus after tamoxifen administration and subsequently excise the loxP-flanked mT cDNA, which switches the expression to mG (Fig. 3.4A). To verify the strict regulation of Cre activity by tamoxifen in this double transgenic system and to exclude major leakiness causing specificity issues (level of systemic leakiness), e15.5 embryos were analyzed for GFP expressing cells without applying tamoxifen. Only a few GFP$^+$ cells could be observed in the thymus, heart and skeletal muscle by whole-mount fluorescent macroscopy (Fig. 3.4B). Furthermore, most of the GFP$^+$ cells in e15.5 embryos were located in the liver. This indicated a very high level of CreER^{T2} expression in the liver which had induced Cre activity independent of tamoxifen. This data is consistent with the high SCF expression level in the liver and its progenitors previously observed by whole-mount microscopy of tdTomato signals in early embryos (Fig. 3.4B). To further verify the low leakiness in the heart, co-immunostaining for GFP and ER on sections of the upper body from e15.5 embryos without tamoxifen administration were performed. Most of the SCF$^+$ cells in the heart, lungs and connective tissues at e15.5 did not display GFP expression (Fig. 3.4C). However, a few GFP$^+$ cell clusters were infrequently visible in the heart (Fig. 3.4D). Upon further observation, it was found that, in nearly all cases, these GFP$^+$ cells formed small colonies. This observation suggested that leaky expression takes place in single cells at earlier stages, which were most likely progenitor cells that subsequently expanded into cell clusters at e15.5. Thus, the double transgenic line has the potential to effectively trace SCF$^+$ cells and their potential progeny in the embryonic heart in a tamoxifen dependent manner.

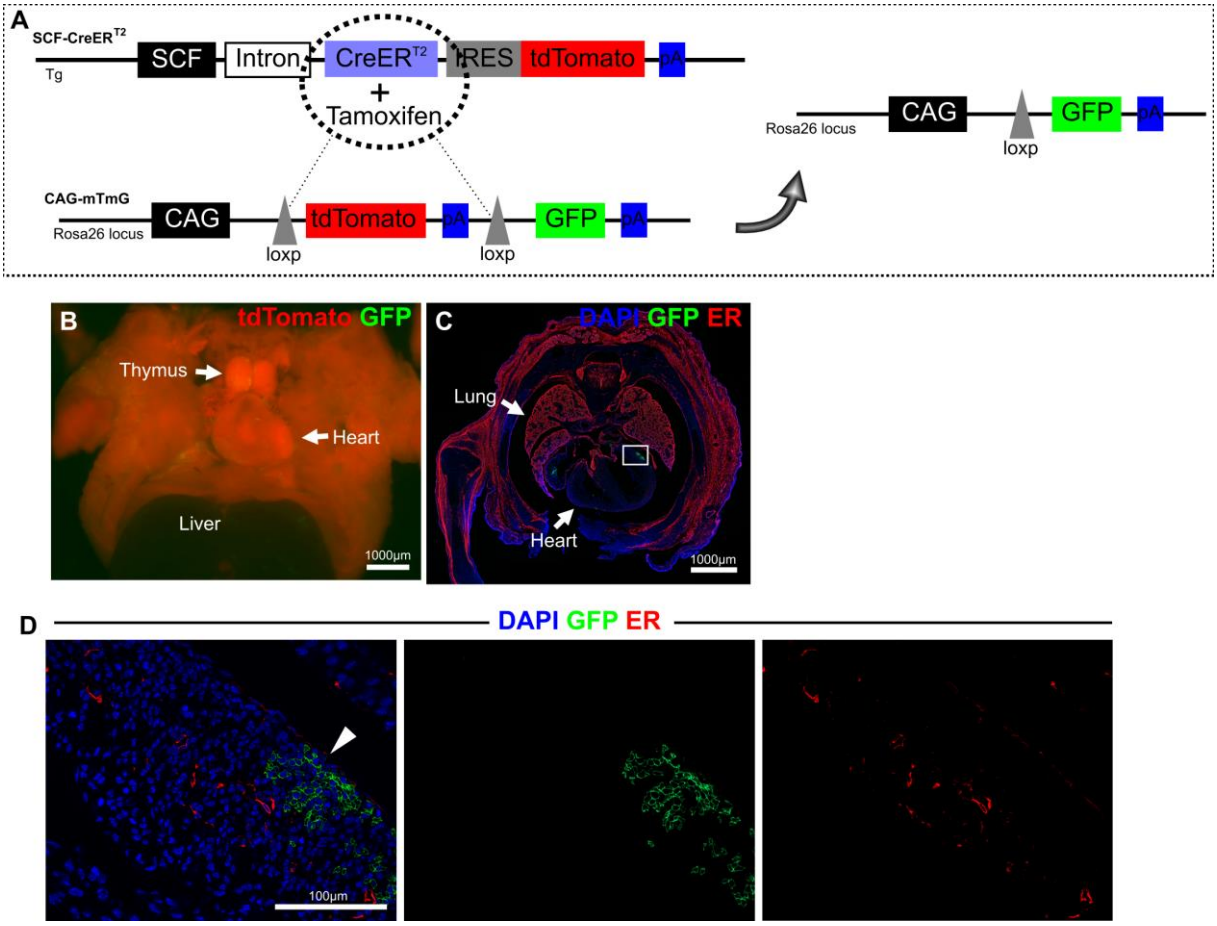

Fig. 3.4 Lineage tracing system used to identify the fate maps of SCF$^+$ cells in the heart:

A) Schematic representation of the system used in the current study to trace the lineage of SCF$^+$ cells. The SCF-CreER^{T2} mouse line was crossbred with the CAG-mTmG reporter line, in which the CAG promoter drives a loxP flanked tdTomato expression cassette, which can be replaced by GFP expression after addition of Tamoxifen. **B)** Frontal view of the upper body cavity of an e15.5 SCF-CreER^{T2} X CAG-mTmG compound transgenic mouse without the presence of Tamoxifen. Very few GFP signal can be seen in the heart indicating that the lineage tracing system has almost no tamoxifen independent recombination induced by leaky Cre expression. **C)** Transverse section of an e15.5 SCF-CreER^{T2} X CAG-mTmG embryo without the administration of tamoxifen co-stained for ER (red) and eGFP (green). As an example, eGFP$^+$ cell clusters which indicate early tamoxifen independent recombination (leakiness) can be found infrequently in the heart. **D)** Magnified picture from the boxed insert in (C). These GFP$^+$/ER$^-$ cells (arrowhead) are in close proximity indicating an early random recombination event which had expanded into a GFP$^+$ cell cluster.

By administrating a single dose of tamoxifen during embryonic development, it is possible to genetically label all the cells that have SCF expression during the period of intracellular tamoxifen presence. A previous study using a similar lineage tracing system had determined that the activation period of CreER^{T2} in the embryos started at approximately 24 h after application of 4 mg tamoxifen to the pregnant mouse by gavage and lasted for approximately 48 h. [73] In the current study, the same method was applied, but with a reduced dosage of tamoxifen of 1 mg. This was done to

shorten the CreER^{T2} activation window to be able to identify timely precise changes of SCF expression patterns during heart formation. To cover all the major events during heart development, a single dose of tamoxifen was given by gavage at all developmental days between e6.5 to e13.5. All hearts were subsequently analyzed at e15.5, a time point at which the embryonic heart has fully formed and displays all structural elements of the postnatal heart (Fig. 3.5A). Macroscopic imaging of whole hearts revealed that the SCF expression gradually shifts from the venous to the arterial end of the heart along with the progression of heart formation. In detail, the gavage of tamoxifen at e6.5 resulted in very few GFP^{+} cells in the e15.5 heart, which indicates that cardiac progenitors from the cardiac crescent at e7.5 had almost no SCF expression. Tamoxifen application at e7.5 resulted in strong GFP expression in derived atria and left ventricle, which are derived from the FHF. This indicated that most parts of the primitive heart at e8.5 express SCF. Subsequent tamoxifen application at e8.0 to e9.5 resulted in the gradual increase of GFP^{+} cells over time in the right ventricle and outflow tract, in contrast to the gradual decline of GFP^{+} cells in the atria and left ventricle. This indicated a gradual turning-on of SCF expression in the forming right ventricle and outflow tract and a gradual turning-off in atria and left ventricle during cardiac looping. The subsequent tamoxifen application at e10.5 resulted in GFP expression in the right ventricle and outflow tract, which indicated that SCF expression in e11.5 hearts is restricted to structures derived from the SHF. Finally, the e13.5 gavage resulted in limited GFP expression near the outflow tract, indicating that most parts of the e14.5 heart do not express SCF (Fig. 3.5B). To verify the observation that the SCF-CreER^{T2} line can effectively distinguish cardiomyocytes derived from either the FHF or SHF, co-immunostaining of GFP and α-actinin was performed. Analysis revealed that only the cardiomyocytes, which originated from the FHF could be effectively traced by the lineage tracing system after tamoxifen administration at e7.5 (Fig. 3.5C). On the other hand, only the cardiomyocytes, which originated from the SHF could be effectively traced after tamoxifen administration at e10.5 (Fig. 3.5D). Surprisingly, these data indicate that SCF expression can only be found in newly formed cardiomyocytes shortly after their differentiation from cardiac progenitor cells at e8.5 and e11.5 residing in the FHF and SHF, respectively. Furthermore, these newly differentiated cardiomyocytes will retain SCF expression for only 2 to 3 days after differentiation. Thus, the SCF can potentially be used as a marker for a subpopulation of newly differentiated cardiomyocytes *in vivo*.

Another major developmental event that takes place shortly after looping of the primitive heart tube is the formation of the coronary vessels. As embryos grow bigger over the course of development, the myocardium can no longer sufficiently supplied with oxygen and nutrients by diffusion. Timely establishment of a functional coronary vasculature is critical for further embryonic development and postnatal growth. Because, SCF was proposed to have significant clinical impacts in the revascularization of infarcted heart (see 1.4), understanding its expression pattern in the forming coronary vessel networks could provide valuable insights in the physiological functions of SCF during coronary revascularization.

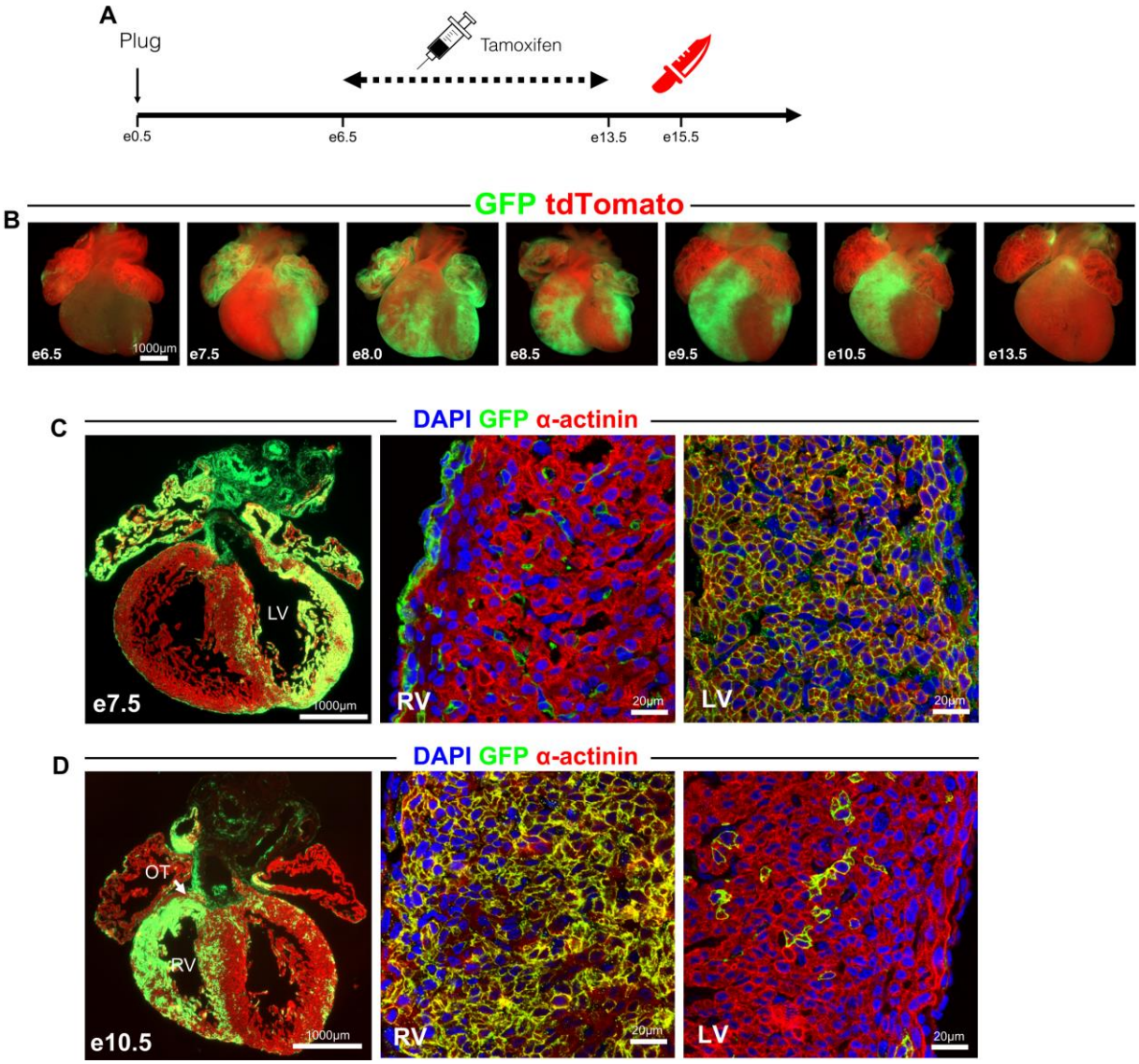

Fig. 3.5 Embryonic cardiomyocytes express SCF during defined developmental windows:

A) Schematic representations of the lineage tracing experiment using SCF-CreER^{T2} x CAG-mTmG double transgenic mice to analyse the SCF expression pattern of embryonic cardiomyocytes. A single dose of tamoxifen was given to pregnant mice at a defined time after coitus ranging from e6.5 to

e13.5. All embryonic hearts were collected for analysis at e15.5. **B)** Fluorescent pictures of freshly harvested e15.5 hearts after administration of single doses of tamoxifen at given time points (indicated at lower left corner). SCF expression in heart and its progenitors was almost not visible before e6.5 and after e13.5. Between e7.5 to e13.5 SCF expression pattern shifts from atria and left ventricle to right ventricle and outflow tract. **C)** Coronal section of an e15.5 heart treated with tamoxifen at e7.5 and stained for GFP and α-actinin to show the SCF fate map from e7.5. Most of the GFP^+ cardiomyocytes are restricted to atria and LV, which are both derived from the 1st heart field. **D)** Coronal section of an e15.5 heart treated with tamoxifen at e10.5 and stained for GFP and α-actinin to show the SCF fate map from e10.5. Most of the GFP^+ cardiomyocytes are restricted to the RV and OT, which are derived from the 2nd heart field.

3.5 Analysis of SCF expression patterns during the formation of embryonic coronary vessels

To determine if SCF could potentially be important for the formation of coronary vessels, SCF expression patterns of the embryonic coronary vessels were examined at various stages of the developing coronary vasculature. The subepicardial endothelial cells sprouting from sinus venosus at the back of the heart at e11.5 are the progenitors of the majority of the future coronary vessels in the outer layers of the myocardium including two major arteries that supply blood from the aorta to the left and right ventricles. [73][74] These initial subepicardial coronary vessel progenitor cells are believed to be dedifferentiated from venous endothelial cells and migrate dorsally around the atrioventricular canal to the interventricular groove and outflow tract. [74] To investigate if SCF is expressed in these progenitor cells, co-immunostainings of ER, CD31 and α-actinin were performed on sections of e11.5 and e12.5 hearts from the SCF-$CreER^{T2}$ mouse line. The purpose of α-actinin staining was to visualize the compact myocardium and to provide auxiliary guidance to find the initial sprouting location of coronary vessel progenitors. Confocal microscopy revealed that neither the subepicardial progenitors nor the endocardium displayed SCF expression at e11.5 (Fig. 3.6A-B). Also at e12.5, when these vessel progenitors continue to invade the compact myocardium, they did not express SCF (Fig. 3.6C-D). These observations strongly indicated that subepicardial coronary vessel progenitors do not express SCF.

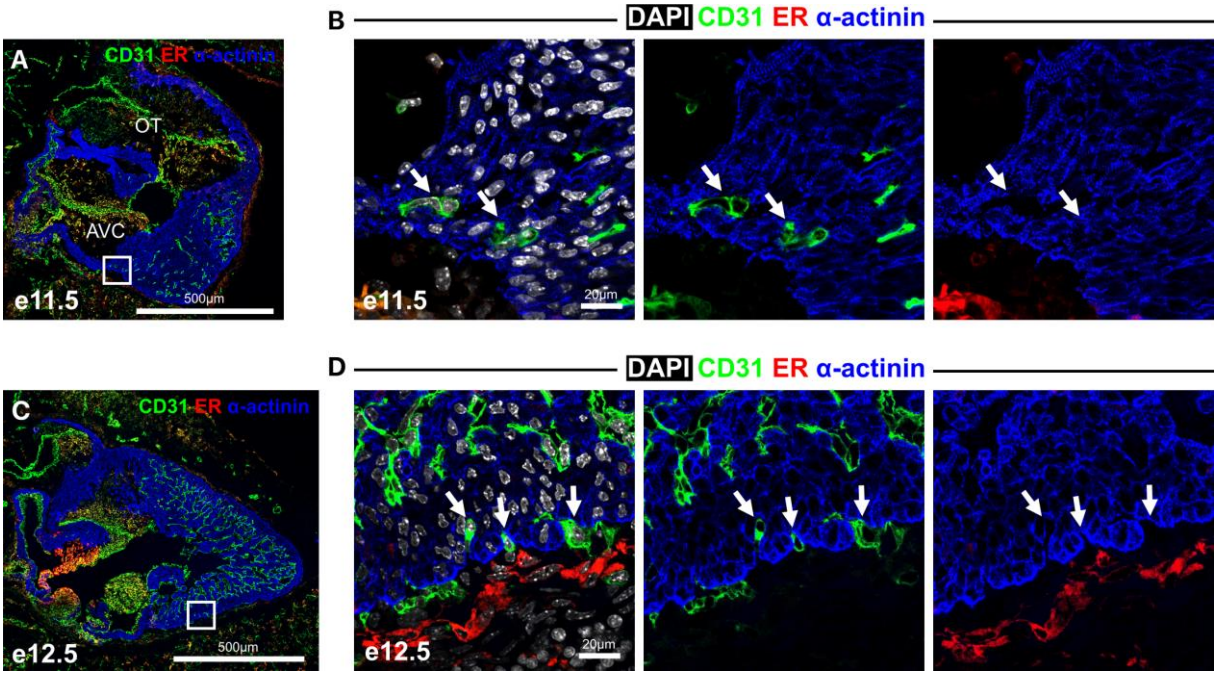

Fig. 3.6 Subepicardial coronary vessel progenitors do not express SCF expression:

A) Sagittal section of an e11.5 heart from SCF-CreER^{T2} mice co-stained with CD31, ER and α-actinin. **B)** Magnified picture from boxed insert in (A) shows that the sprouting subepicardial vessel progenitors (white arrows) originated from sinus venosus, which typically appear at e11.5 on the back side of the heart, are negative for SCF expression. **C)** Sagittal section of an e12.5 heart co-stained with CD31, ER and α-actinin. **D)** Magnified picture from boxed insert in (C) shows that subepicardial vessel progenitors (white arrows), that continue to spread onto the back side of the heart while invading the compact myocardium, are negative for SCF expression.

At approximately e14.5, the previous sparsely distributed endothelial cells start to align and to recruit vascular pericytes at the anterior region of the left and right to the dorsal side of the right ventricle to prepare for the formation of the left and right coronary arteries. [73][74][77] To investigate the SCF expression pattern during the initial arterial specification of subepicardial VECs at e14.5, specific heart sections covering the region of coronary arteries were chosen and co-immunostaining for CD31, ER and PDGFRβ was performed. PDGFRβ staining was used to specifically label the vascular pericytes recruited to wrap around the future major arteries, which eased the identification of the developing major coronary arteries on sections from e14.5 hearts. The newly formed small capillary-sized coronary arteries had high levels of SCF expression (Fig. 3.7A-B). At approximately e15.5, the newly formed coronary arteries connect to the aorta and start to work as a true vessel as they start to transport blood into the developing heart. [73][74][77] A co-immunostaining for CD31, ER and PDGFRβ was performed on e15.5 heart sections covering the regions of major coronary arteries to investigate the expression pattern of SCF in newly

formed arteries. Analysis revealed that SCF is highly expressed in all newly lumenized coronary arteries (Fig. 3.7C-D). The data indicated that the initiation of arteriogenesis in major coronary arteries is concurrent with the turning-on of SCF expression, which indicates potentially important roles of SCF during arteriogenesis.

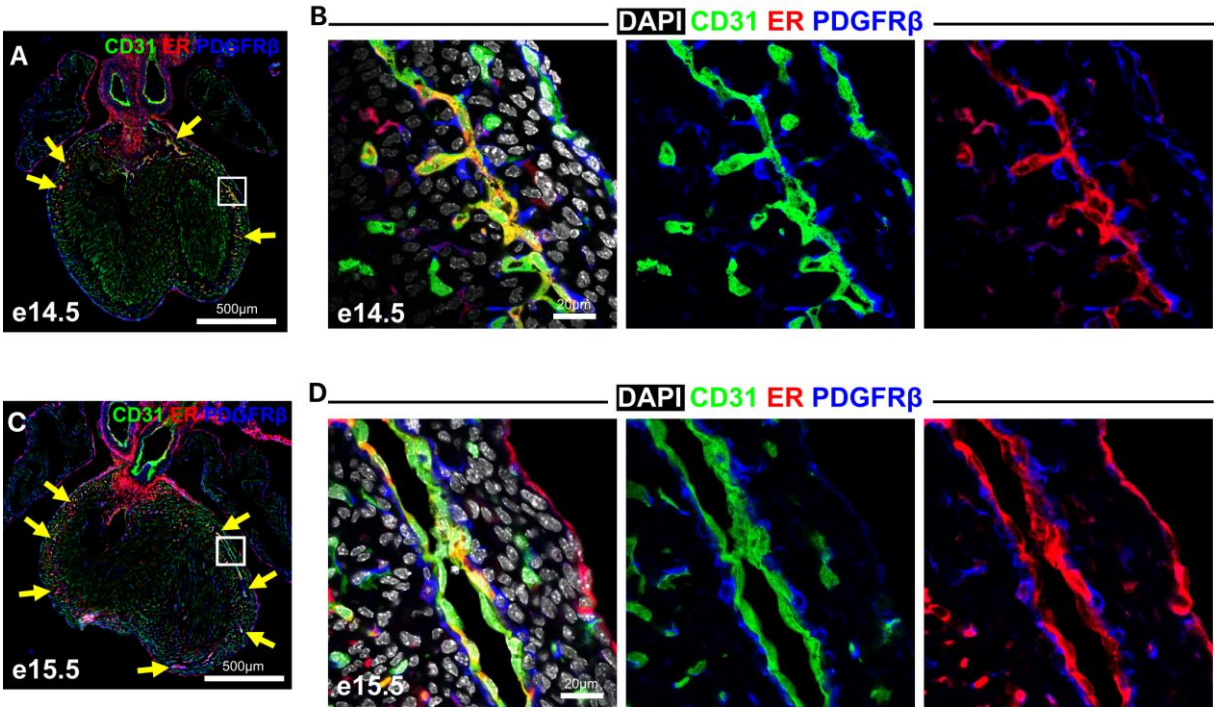

Fig. 3.7 SCF expression pattern during the initiation of coronary artery formation:

A) Transverse section of an e14.5 heart from SCF-CreER^{T2} mice co-stained with CD31, ER and PDGFRβ (vascular pericyte marker). The future major coronary arteries (yellow arrows) start to express SCF. **B)** Magnified picture from boxed insert in (A) shows that the newly emerged capillary which will eventually develop into future LAD coronary artery start to express SCF. **C)** Transverse section of an e15.5 heart co-stained with CD31, ER and PDGFRβ. The capillary sized major coronary arteries (yellow arrows) have SCF expression. **D)** Magnified picture from boxed insert in (C) shows that the newly lumenized LAD coronary artery, that starts to supply blood originated from aorta into coronary vasculature, has SCF^{+} VECs.

The analysis of embryonic hearts has revealed a surprising SCF expression pattern during heart and coronary vessel formation. In particular, SCF is expressed in newly differentiated cardiomyocytes but not in cardiac progenitors and more mature embryonic cardiomyocytes. This observation indicates that SCF may potentially mark a previously undefined subpopulation of newly differentiated cardiomyocytes. Furthermore, VECs start to express SCF during the formation of coronary arteries. SCF could play important roles during initial arterial specification and arteriogenesis.

In light of these interesting findings, I further looked into the expression pattern of SCF in cardiomyocytes and coronary VECs in the postnatal heart.

3.6 Analysis of the SCF expression pattern in cardiomyocytes of postnatal hearts

Neonatal cardiomyocytes undergo rapid transition from proliferating mononuclear cells to binucleated mature cells, most likely to support the increasing cardiac output during growth. [113] SCF expression in postnatal cardiomyocytes was investigated by co-immunostaining for ER and α-actinin in P0, P3, P7 and adult hearts from SCF-CreER^{T2} mice. Due to rapid phenotypic changes of cardiomyocytes during the very first days after birth, we select P0 pups by constant check of birth and absence of milk in the stomach. I found that a small population of cardiomyocytes displayed low expression of SCF during neonatal stages (P0-P7) (Fig. 3.8A). In very rare cases, adult cardiomyocytes had SCF expression, too (Fig. 3.8B). However, our analysis showed that the number of SCF$^+$ cardiomyocytes in adult hearts was negligible. In one set of experiments, I examined three 6 weeks old male adult hearts with three sections per heart and found less than 10 SCF$^+$ cardiomyocytes in total. I quantified the percentage of SCF$^+$ cardiomyocytes in total cardiomyocytes at P0 and found approximately 3% of cardiomyocytes to be SCF$^+$ at P0. To further analyse the SCF$^+$ cardiomyocyte population, the number of SCF$^+$ cardiomyocytes was quantified per square millimeter (mm^2) at different developmental ages. [111][114] The data showed that in neonatal P0 hearts there is the highest number of SCF$^+$ cardiomyocytes of ~650 per mm^2. During neonatal growth, the number of SCF$^+$ cardiomyocytes dropped rapidly to ~ 250 per mm^2 at P3 and ~150 per mm^2 at P7. In adulthood, the number of SCF$^+$ cardiomyocytes declined to less than 1 per mm^2 (Fig. 3.8C). My data suggested that SCF expression in cardiomyocytes decrease rapidly after birth, which is concurrent with the decline of mononucleated cardiomyocytes and cell cycle exit. [113] In the previous chapter, I have demonstrated that SCF is expressed briefly in almost all newly differentiated embryonic cardiomyocytes. Although mature mammalian cardiomyocytes cannot robustly contribute to regeneration after cardiac injury, postnatal cardiomyocytes have been reported to dedifferentiate, to re-express embryonic markers and to adopt relative “young” phenotype.[115]-[118] In lower vertebrates, such as zebrafish and newts, heart regeneration seems to rely predominantly on the proliferation of dedifferentiated cardiomyocytes. [114][119] Investigating the SCF expression pattern, as an

embryonic marker in cardiomyocytes after neonatal injury may provide valuable information about the underlying mechanism behind neonatal heart regeneration in mouse.

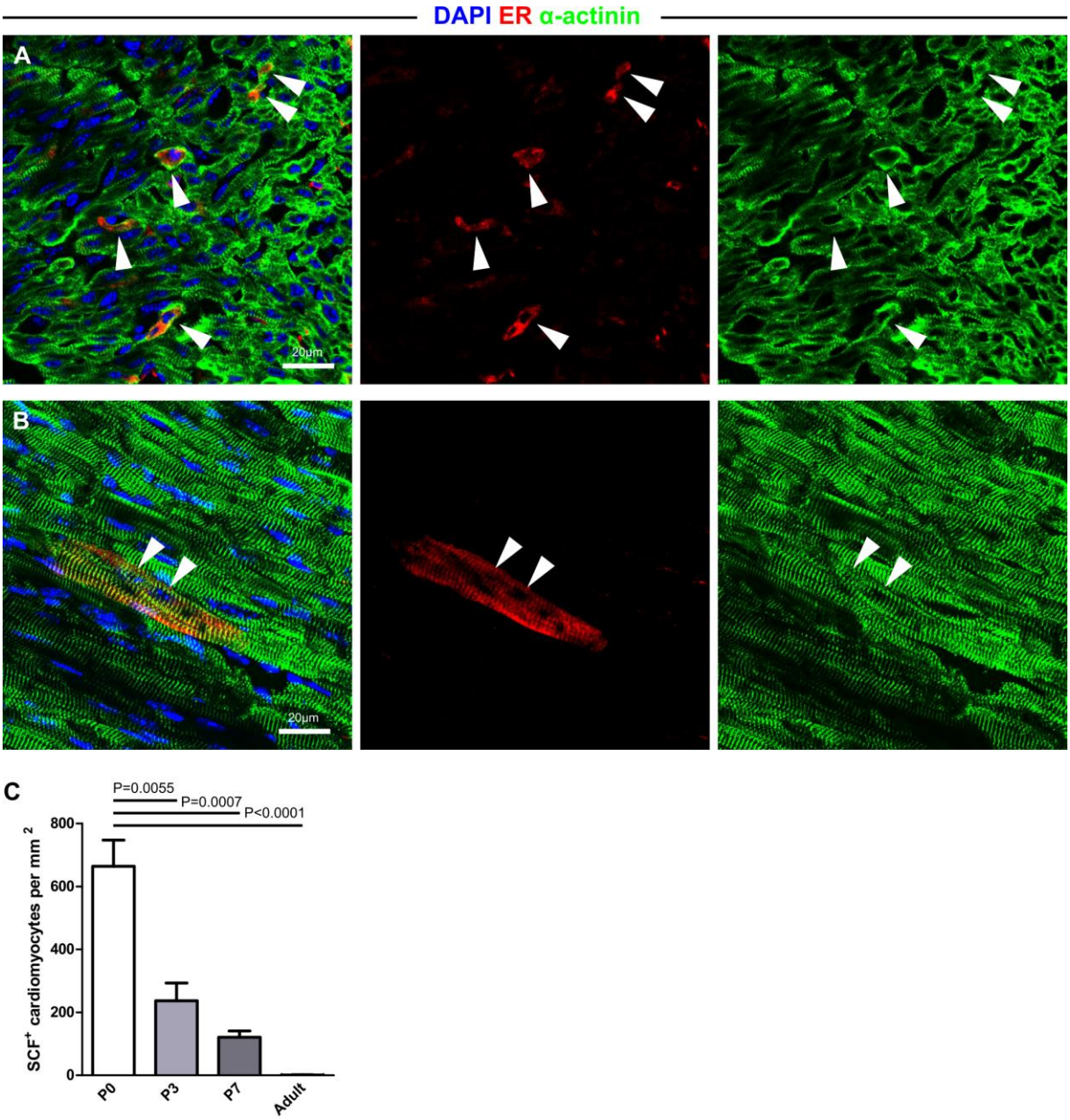

Fig. 3.8 SCF expression pattern in cardiomyocytes of the postnatal heart:

A) Representative picture of a neonatal heart section stained for ER (red) and α-actinin (green). ER signals were over-exposed to visualise much lower SCF expression in cardiomyocytes in comparison to endothelial cells. Arrowheads indicate the SCF^+ cardiomyocytes. **B)** Representative picture of one SCF^+ cardiomyocyte from an adult heart section stained for ER (red) and α-actinin (green). Double arrowheads indicate two adjacent nuclei in the SCF^+ cardiomyocyte. **C)** Quantification of SCF^+ cardiomyocytes in postnatal hearts. Data are shown as mean ± SEM. P value is shown on the top of each bar (Student's t-test), $n \geq 3$.

3.7 Analysis of the SCF expression pattern in cardiomyocytes after neonatal heart injury

Unlike adult hearts, neonatal hearts can recover from myocardial injury by regeneration. [120] To study the potential contribution of SCF signaling during the recovery after neonatal heart injury, the expression pattern of SCF was analyzed after cauterization of a small region on the apex of the left ventricle. The SCF-CreER^{T2} mouse line was crossbred to the eGFP-Anillin mouse line, in which cell cycle activity can be visualized directly through the intracellular localization of an eGFP-Anillin fusion protein.[99] P1 mice were subjected to either cauterization injury or sham operation. Mice were then sacrificed on 7dps for analysis by co-immunostaining for eGFP, ER and α-actinin. Approximately 0.1 mg of tamoxifen was injected intraperitoneally 2 days before sacrifice to induce localization of CreER^{T2} to the nucleus to ease detection by immunofluorescence staining (Fig. 3.9A). Hearts were harvested at 7dps and subsequently co-stained for eGFP, ER and α-actinin. As expected, the injured hearts had substantially more nuclear eGFP^{+} cardiomyocytes in comparison to sham operated hearts (Fig. 3.9B-G). However, these nuclear eGFP^{+} cardiomyocytes were not restricted to the injury site but were distributed over the whole heart (Fig. 3.9F). During prometaphase of the M-phase, the nuclear membrane breaks down, which causes the nuclear eGFP-anillin signals to locate to the cytosol. Accordingly, a few M-phase cardiomyocytes with cytosolic eGFP-anillin signals could be detected. Condensed chromatin as evidenced by DAPI staining and disarranged sarcomere structure as evident by α-actinin staining further confirmed their M-phase status. Interestingly, most of these M-phase cardiomyocytes also coincidentally and exclusively expressed low levels of SCF (Fig. 3.9H). However, this phenomenon was not observed in sham operated hearts. Based on these observations, SCF may be important for the initiation or progression of the M-phase of the cell cycle in cardiomyocytes in neonatal hearts.

In summary, low levels of SCF expression have been found in all newly differentiated embryonic cardiomyocytes, a small portion of neonatal cardiomyocytes and very few cell cycle active cardiomyocytes in M-phase after neonatal injury. These SCF^{+} cardiomyocytes may display an undifferentiated phenotype and constitute a previously undefined subpopulation of cardiomyocytes. On the other hand, SCF expression in coronary VECs has not been correlated with proliferation. Instead, the expression map from embryonic coronary VECs indicated a strong correlation with

arterial fate determination. Analysis of SCF expression in postnatal coronary VECs may provide further information about the identity of SCF^{+} VECs.

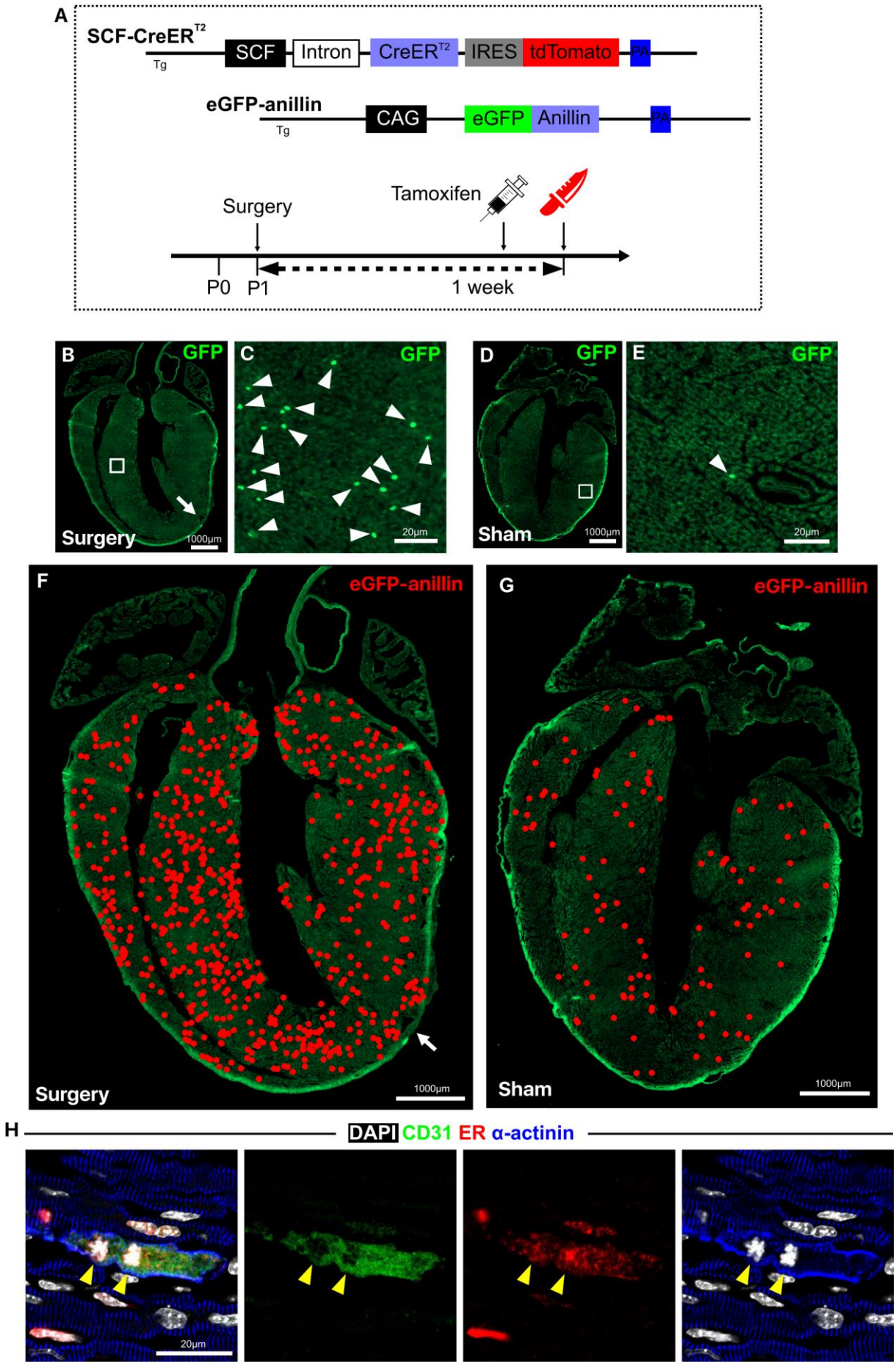
A
SCF-CreER^{T2}
Tg
SCF
Intron
CreER^{T2}
IRES
tdTomato
PA
eGFP-anillin
Tg
CAG
eGFP
Anillin
PA
Surgery
Tamoxifen
P0
P1
1 week
B
GFP
Surgery
1000μm
C
GFP
20μm
D
GFP
Sham
1000μm
E
GFP
20μm
F
eGFP-anillin
Surgery
1000μm
G
eGFP-anillin
Sham
1000μm
H
DAPI CD31 ER α-actinin
20μm

Fig. 3.9 SCF expression may indicate cell cycle M-phase in neonatal cardiomyocytes after injury:

A) Schematic presentation of an experiment to investigate SCF expression pattern in cardiomyocytes after neonatal injury. P1 double transgenic SCF-CreER^{T2} and eGFP-anillin (a cell cycle reporter line) mice were subjected to either heat induced apex injury or sham operation. Mice were sacrificed 7 dps for analysis. Tamoxifen was given to each mouse 2 days before the sacrifice to relocate the CreER^{T2} protein into the nuclei, which in turns improve the weak signals of ER staining in cardiomyocytes. **B)** Coronal sections of neonatal P8 hearts 7 days after lesion at the apex at P1 stained with GFP to intensify endogenous eGFP signals. White arrow indicates the lesion site. **C)** Magnified picture of the boxed insert in (C). White arrowheads indicate eGFP$^+$ signals. **D)** Coronal sections of neonatal P8 hearts 7 days after sham operation at P1 stained with eGFP to intensify endogenous eGFP signals. **E)** Magnified picture of the boxed insert in (D). White arrowhead indicates eGFP$^+$ signal. **F-G)** Artificial red dots indicating eGFP signals were added to the ventricular part of (B) and (D) to show the distribution of M-phase cells. White arrow indicates the lesion site. Cell cycle activity increased substantially after neonatal heart injury. **H)** Representative picture of an SCF$^+$ cardiomyocyte from P8 heart injured at P1. Double yellow arrowheads indicate colocalization of cytosolic eGFP-anillin and ER signals. DAPI staining shows condensed chromatin, which indicates M-phase of mitosis. α-actinin staining shows disarranged sarcomere structure, which also indicates cell cycle activity.

3.8 Analysis of SCF expression patterns in the coronary vessels of postnatal mouse hearts

To investigate the SCF expression pattern in coronary vessels during postnatal growth, co-immunostaining for ER and CD31 was performed on P1, P7 and P15 hearts from SCF-CreER^{T2} mice. High levels of SCF expression could be found in some VECs in postnatal hearts (Fig. 3.10A). I found that most of the SCF$^+$ VECs belonged to the relative bigger vessels in comparison to the surrounding small capillaries (Fig. 3.10A-B). Those vessels are likely to be intramyocardial arteries and arterioles. However, the identity of these SCF$^+$ VECs was difficult to confirm due to a lack of proper arterio-venous markers in the postnatal heart. [121] Nevertheless, I took advantage of one of the hallmarks of artery morphology, which is their surrounding smooth muscle cells, to identify arterial VECs. To investigate the SCF expression pattern in the arterial VECs, co-immunostaining for CD31, ER and α-SMA (alpha smooth muscle actin, a smooth muscle cell marker) was performed on P1, P7 and P15 hearts. Interestingly, almost all the small arteries had SCF$^+$ VECs (Fig. 3.10C). However, there was still a small portion of SCF$^+$ capillary VECs. To characterize the SCF$^+$ VECs in the capillaries, a co-immunostaining for CD31, ER and PDGFRβ (pericyte marker) was performed. Nearly all SCF$^+$ VECs had pericytes encircled around them (Fig. 3.10D), which indicated that most of the SCF$^+$ VECs in capillaries belonged to the stabilized phalanx cell type instead of tip and stalk cell type. [122] These observations suggested that the SCF$^+$ VECs in the neonatal and juvenile hearts had a predominately arterial phenotype. To see if such SCF

expression pattern was conserved in the adult heart, I next applied the same methods to investigate the arterio-venous identities of SCF$^+$ VECs in the adult heart.

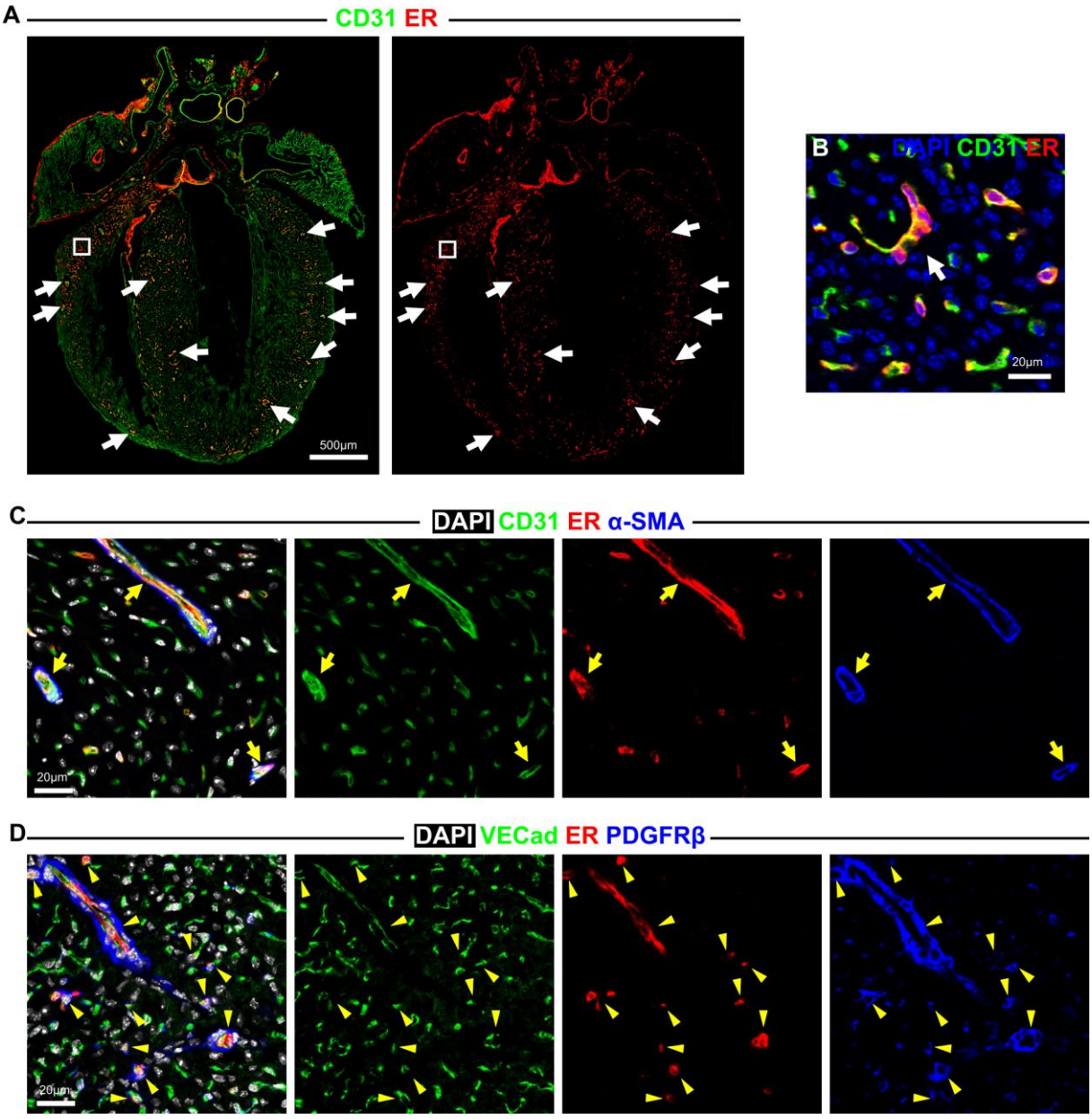

Fig. 3.10 SCF expression pattern in endothelial cells of the young hearts:

A) Coronal section of a P1 neonatal heart stained for CD31 (green) and ER (red). Strong SCF expression (as indicated by ER) can be found in relative large vessels among capillaries (white arrows) in the compact area of the ventricles. **B)** Magnified picture from the boxed region in (A) of a relative large vessel (white arrow) with ER$^+$ /CD31+ endothelial cells. **C)** Representative picture of a juvenile heart (P15) stained for CD31, ER and α-SMA (smooth muscle marker). Arterial identity of capillary-size arteries was defined by the encirclement by smooth muscle cells. All small arterial VECs (yellow arrows) are SCF$^+$. **D)** Representative picture of a neonatal P1 heart stained for VeCad (endothelial cell marker), ER and PDGFRβ (vascular pericyte marker). Most of the SCF$^+$ VECs (yellow arrowheads) have pericytes in close proximity.

3.9 Analysis of the SCF expression pattern in the coronary vessels of the adult heart

To investigate the SCF expression pattern in the adult coronary vessels, co-immunostaining for CD31 and ER was performed on adult heart sections from the SCF-CreER^{T2} mouse line. High levels of SCF expression could be found in a subset of vessels (Fig. 3.11). Furthermore, the VECs of relative larger vessels in comparison to small capillaries often had high levels of SCF expression (Fig. 3.11B). To see if the adult hearts had similar SCF expression patterns in comparison to the neonatal and juvenile hearts, co-immunostaining for CD31, ER and α-SMA was performed to identify small arterial VECs in 6 to 22 weeks old mice. Analysis revealed that most of the small arteries had SCF^{+} VECs (Fig. 3.11C). To investigate the SCF expression pattern in the capillaries, co-immunostaining for CD31, ER and PDGFRβ was performed on 6 to 22 weeks old hearts. Most of the SCF^{+} VECs in capillaries were encircled by vascular pericytes (Fig. 3.11D), which indicated a stabilized phalanx-like cell type similar to the SCF^{+} capillaries in the neonatal hearts. These observations, together with the expression pattern in embryonic, neonatal and juvenile hearts, strongly suggested that SCF is mostly expressed in the VECs of small arterial-like coronary vessels. However, further quantification is necessary to establish SCF as an arterial VEC marker.

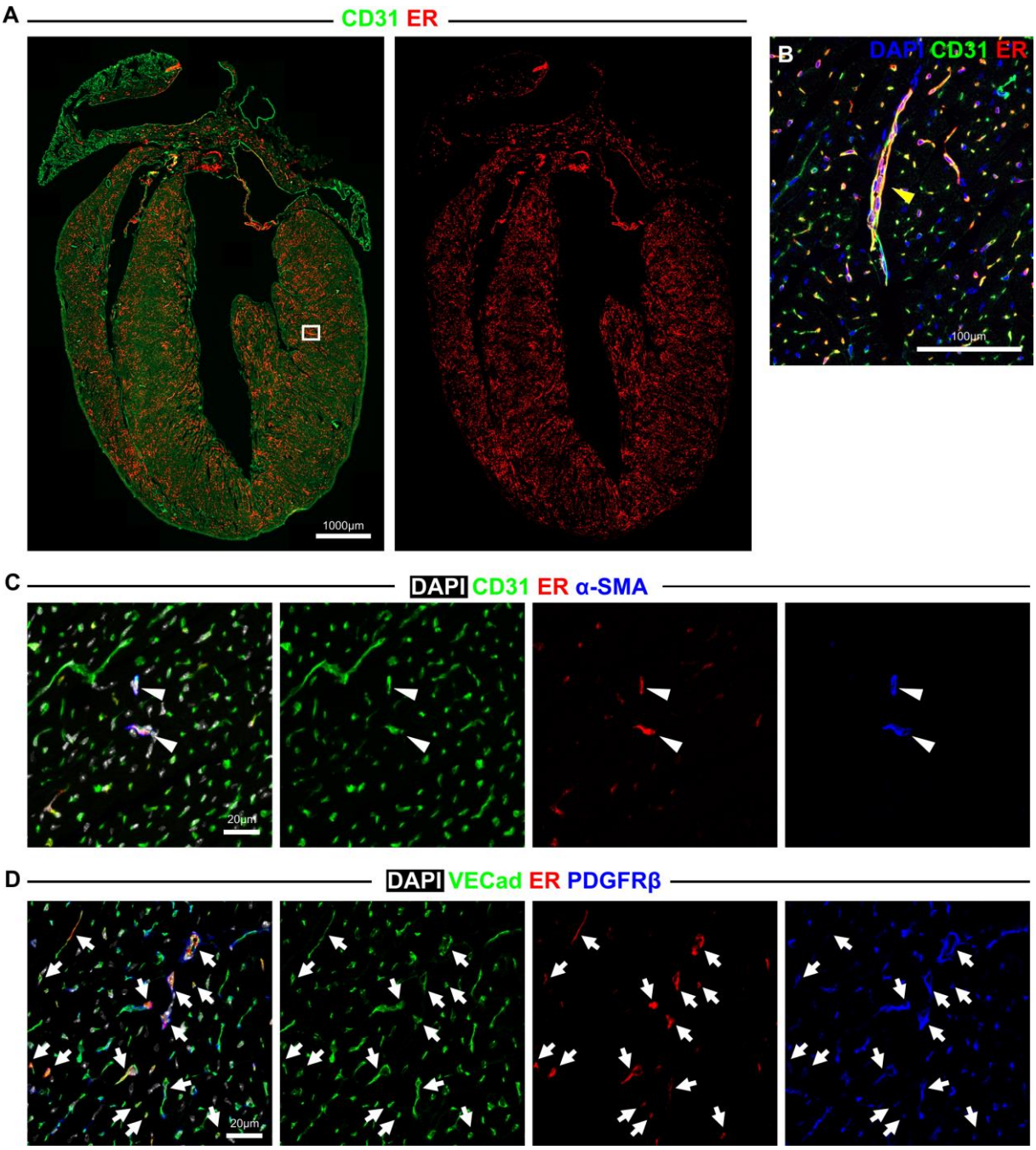

Fig. 3.11 SCF expression patterns in the endothelial cells of the adult heart:

A) Coronal section of a neonatal heart stained for CD31 (green) and ER (red). Strong SCF expression can be found in a subset of VECs in the ventricles. **B)** Magnified picture from boxed insert of (A) showed SCF^+ VECs in relative large vessels (yellow arrowheads) in comparison to capillaries. **C)** Representative picture of an adult heart stained for CD31, ER and α-SMA. Arterial identity of capillary-size arterioles was defined by the encirclement by smooth muscle cells (α-SMA^+). White arrowheads indicate SCF^+ VECs in very small arteries. **D)** Representative picture of an adult heart stained for VeCad, ER and PDGFRβ. Most of the $SCF^+/CD31^+$ endothelial cells (white arrows) have pericytes in close proximity.

3.10 Quantification of SCF$^+$ VECs reveals SCF as a marker for small coronary arteries

To verify our observation that small arteries express SCF$^+$ in their VECs, the percentage of SCF$^+$ VECs was quantified in all small coronary arteries. These were identified in P7, P15 and adult hearts by staining for α-SMA$^+$ cells surrounding CD31$^+$ cells. Due to the technically poor immunostaining of the α-SMA antibody in P0 hearts, only major coronary arteries were selected for quantification at that time point. This was possible, because the major coronary arteries had the size of the small arteries at P0 and could be easily recognized by their location and morphology. At later stages α-SMA staining showed high specificity and reproducibility for smooth muscle cells. Furthermore, the major coronary arteries were excluded from quantification starting at P7 when the major coronary arteries start to grow into mature arteries. The quantification showed that over 93% of the small arteries had SCF$^+$ VECs in all age groups (Fig. 3.12A). On the other hand, less than 16% of VECs in capillaries are SCF$^+$ (Fig. 3.12B). To investigate the SCF$^+$ fraction of VECs in capillaries, the percentage of stable VECs as marked by encirclement of PDGFRβ^+ vascular pericytes was quantified in all SCF$^+$ capillaries in P0, P7, P15, and adult hearts. I found that almost 100% of SCF$^+$ capillaries had pericytes adjacent, indicating relative stable and phalanx-like phenotypes in comparison to tip-stalk cell phenotypes (Fig. 3.12C). In summary, the findings indicate that SCF can potentially be a marker for small arterial VECs and stable capillaries. It is also very likely that SCF expression in VECs is associated with a distinct phenotype, such as arteriogenic potential, as showed in embryonic coronary artery formation. VECs of big arteries are morphologically and functionally different to VECs of small arteries. In fact, global VEC expression profiling using RNAseq has showed the most prominent differences between large and small vessels rather than arterial and venous vessels. [123] To verify if SCF can discriminate between VECs of small and big arteries, I further explored the SCF expression pattern in major coronary arteries.

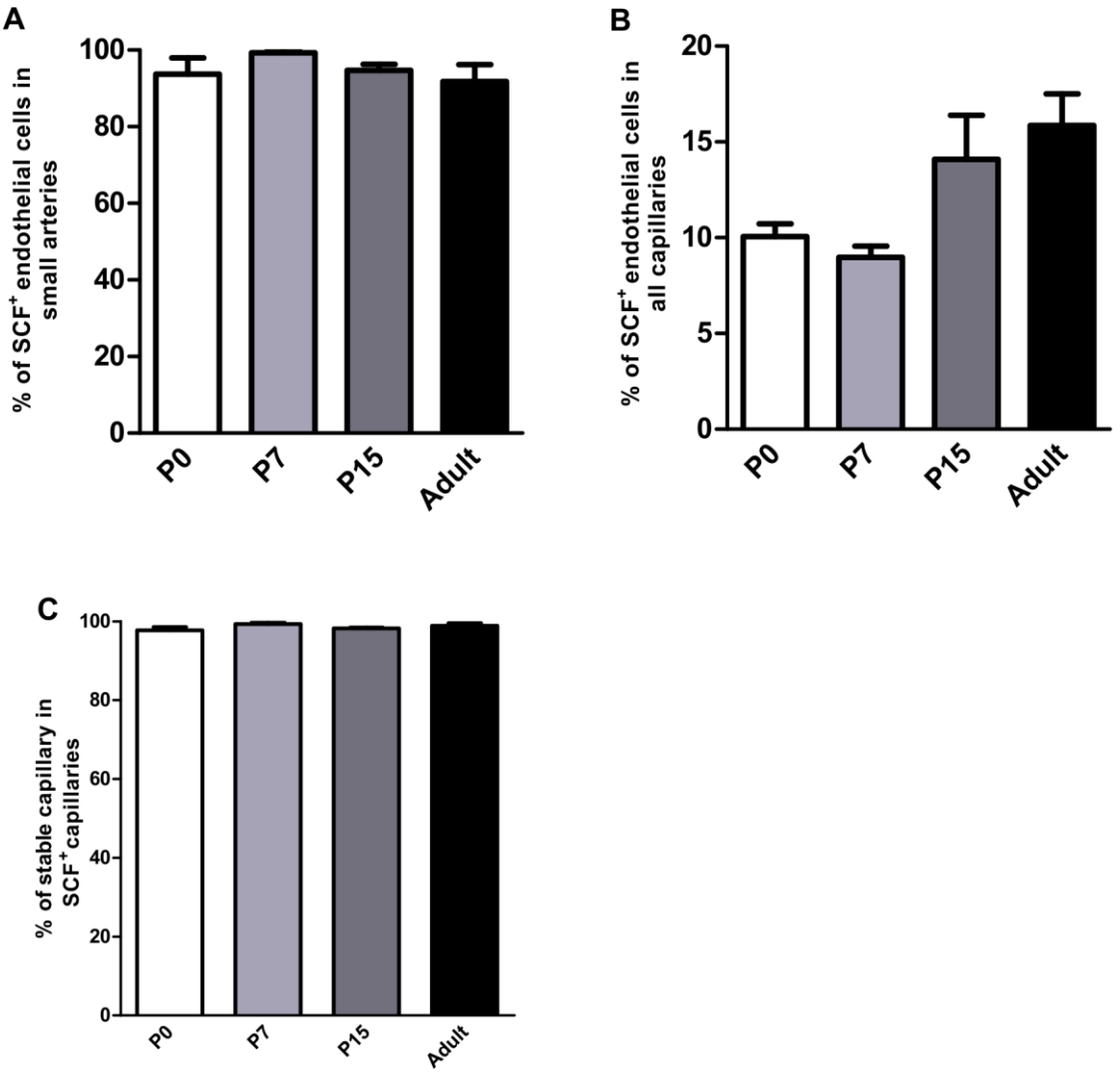

Fig. 3.12 Quantification of SCF$^+$/CD31$^+$ endothelial cells in small arterioles and stable capillaries indicates arterial specificity of SCF expression:

A) Quantification of the percentage of SCF$^+$/CD31$^+$ endothelial cells in total endothelial cells of the small artery fractions (as defined by the encirclement of α-SMA$^+$ smooth muscle cells) at different ages (indicated in the bottom of each chart). **B)** Quantification of the percentage of SCF$^+$/CD31$^+$ endothelial cells in total endothelial cells of the capillary fractions (as defined by the absence of the α-SMA$^+$ smooth muscle cells) at different ages (indicated in the bottom of each chart). **C)** Quantification of the percentage of stable capillaries (defined by encirclement by PDGFRβ$^+$ vascular pericytes) in all SCF$^+$ capillaries. All data are shown as mean ± SEM. n≥3.

3.11 Analysis of the SCF expression pattern in the major coronary arteries during postnatal growth and maturation

Major coronary arteries increase in diameter during postnatal growth to cope with increasing cardiac demand for blood. To verify if SCF expression is restricted to small, immature arteries but not to big, mature arteries, the SCF expression pattern in the major coronary arteries of different maturation levels was analyzed by co-

immunostaining for CD31, ER and α-SMA. We found that neonatal major coronary arteries had strong SCF expression in almost all the VECs until P7 when some of the VECs of major coronary arteries start to downregulate SCF expression (Fig. 3.13A). From P15 to adulthood, the VECs of major coronary arteries no longer express SCF (Fig. 3.13B-C). In addition, major coronary veins have no SCF expression, too (Fig. 13D). These observations confirmed that SCF^+ VECs were restricted to small arterial-like vessels but not big arteries in the heart. It is also worth to mention that there is no clear discriminator for the definitions of small and big arteries. SCF expression may be a useful tool to discriminate VECs in the border area of small and big arteries, which could be potentially useful for studies of VEC heterogeneity. The pathological changes in VECs of major coronary arteries, especially the LAD coronary artery, are the major cause of myocardial infarction. [124] Since SCF was proposed to have profound clinical significance in coronary artery disease (see part 1.4), it was worthwhile to explore SCF expression in the heart after myocardial infarction.

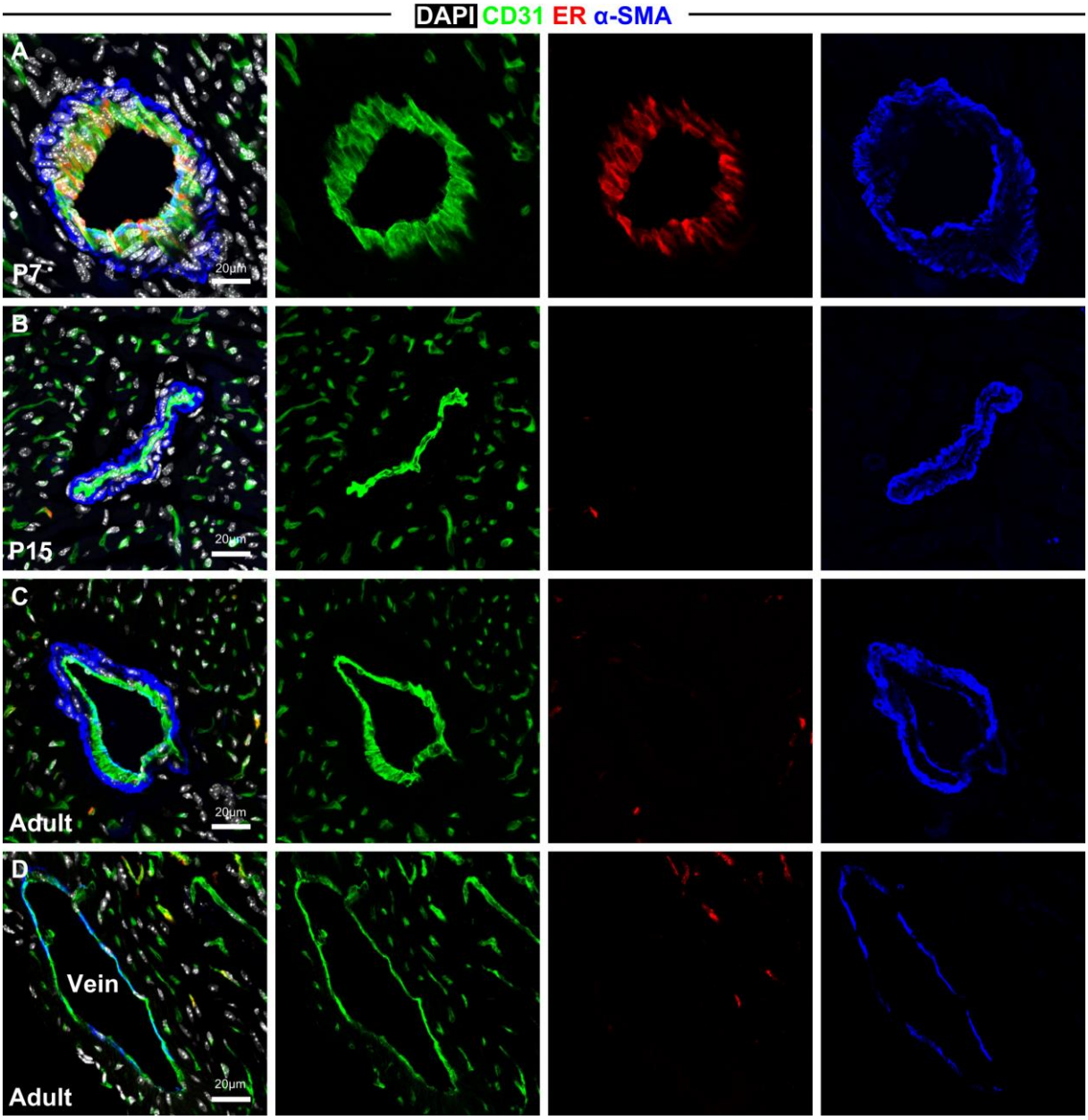

Fig. 3.13 Major coronary arteries lose SCF expression after maturation:

A-C) Representative pictures of the sections in the anterior left descending coronary artery stained for CD31 (green), ER (red) and α-SMA (blue). **A)** Major coronary arteries start to turn off the SCF expression in the endothelial cells at P7. **B)** By P15, major coronary arteries no longer express SCF. **C)** In adult hearts, major coronary arteries also do not express SCF. **D)** Representative picture of the section of a major vein on the backside of the adult heart. VECs ($CD31^+$) in the coronary veins do not have SCF expression.

3.12 Analysis of the SCF expression pattern during myocardial infarction

To analyze if SCF may play a role after acute myocardial infarction, the SCF expression pattern was examined using SCF-$CreER^{T2}$ mice after artificial occlusion of the LAD coronary artery to mimic myocardial infarction. Since most of the SCF^+ cells in adult heart are VECs, co-immunostaining for CD31 and ER was performed on

heart sections at 2, 7 and 14 days after myocardial infarction. A steep decline of SCF^+ VECs was found in the affected area at 2 days post-surgery (dps). Furthermore, results from mice analyzed at 7dps and 14dps revealed that the infarcted area of the heart remained to be scarce of SCF^+ VECs after the acute phase of myocardial infarction. Only the connective tissues from the surface of the injury sites did express high levels of SCF (Fig. 3.14A). At 2dps, the pre-existing vessels in the infarcted area started to die as was evident by the loss of structural integration of $CD31^+$ VECs. Almost no SCF^+ VECs or other types of SCF^+ cells could be found in the infarcted area. Furthermore, a substantial decline in SCF expression in the vessels of the border area of the infarct could be observed. Although the vasculature in the border area was intact, nearly all the VECs close to the infarcted area lost SCF expression, whereas the VECs close to the unaffected remote area had similar SCF expression pattern as the remote area (Fig. 3.14B). These observations do not support the proposed notion that SCF signaling may have a functionally significant role during the repair processes following acute myocardial infarction. To verify that SCF may be negligible during the repair processes after acute myocardial infarction, a conditional loss-of-function of SCF in VECs in a transgenic mouse was analyzed.

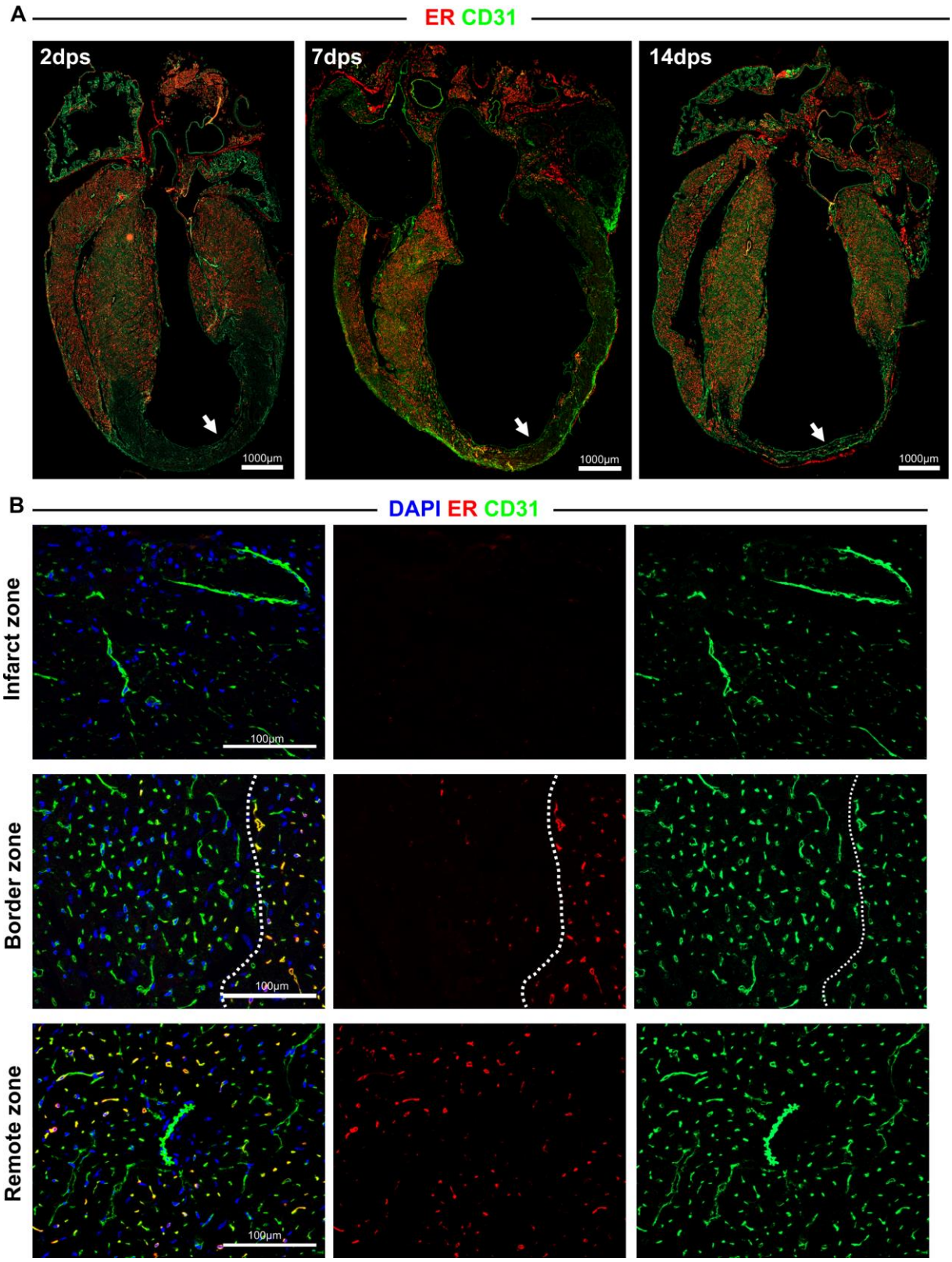

Fig. 3.14 SCF expression pattern after acute myocardial infarction in adult hearts:

A) Coronal sections of infarcted adult hearts at 2 to 14 dps stained for ER (red) and CD31 (green). The infarcted areas have reduced level of SCF expression (white arrows). **B)** Magnified pictures from different areas of the heart at 2 dps. The infarcted zone has only sparse SCF expression. The border zone has the normal SCF expression pattern similar to a healthy heart in the unaffected area (right to

the dashed line) but reduced SCF expression next to the infarcted zone (left to the dashed line). The remote zone has similar SCF expression to healthy adult heart.

3.13 Systematic VEC specific knock down of SCF does not produce an obvious phenotype after acute myocardial infarction

The Tie2-Cre transgenic mouse line, in which Cre recombinase is expressed in all the VECs, was crossbred to the $SCF^{\Delta EX7}$ mouse line, in which exon 7 of the SCF gene, which encodes for the membrane anchoring of SCF, is flanked by two loxP sites. [41][100] Homozygotes $SCF^{\Delta EX7}$/Tie2-Cre transgenic mice are knockouts for membrane-anchored SCF (mSCF) in all VECs starting from early embryonic stages (Fig. 3.15A). Again, a myocardial infarction model consisting of ligation of the LAD coronary artery was used to mimic myocardial infarction on these VEC specific mSCF knockout and control mice. Subsequently, co-immunostaining for CD31 and CD45 were performed on heart sections at 7dps. There was no obvious morphological difference between knockout and control hearts after infarction (Fig. 3.15B). Furthermore, a similar pattern of loss of cellularity was evident in the infarcted area as well as an invasion of hematopoietic cells in knockouts and controls (Fig. 3.15C). This observation suggested that SCF signaling is unlikely to have substantial influence on the outcome of acute myocardial infarction. The source of neovascularization in the infarcted area is unlikely to be SCF^{+} cells, because SCF is not expressed in or near the infarcted area. To further address this issue the expression pattern of c-kit, the receptor of SCF, was studied after acute myocardial infarction.

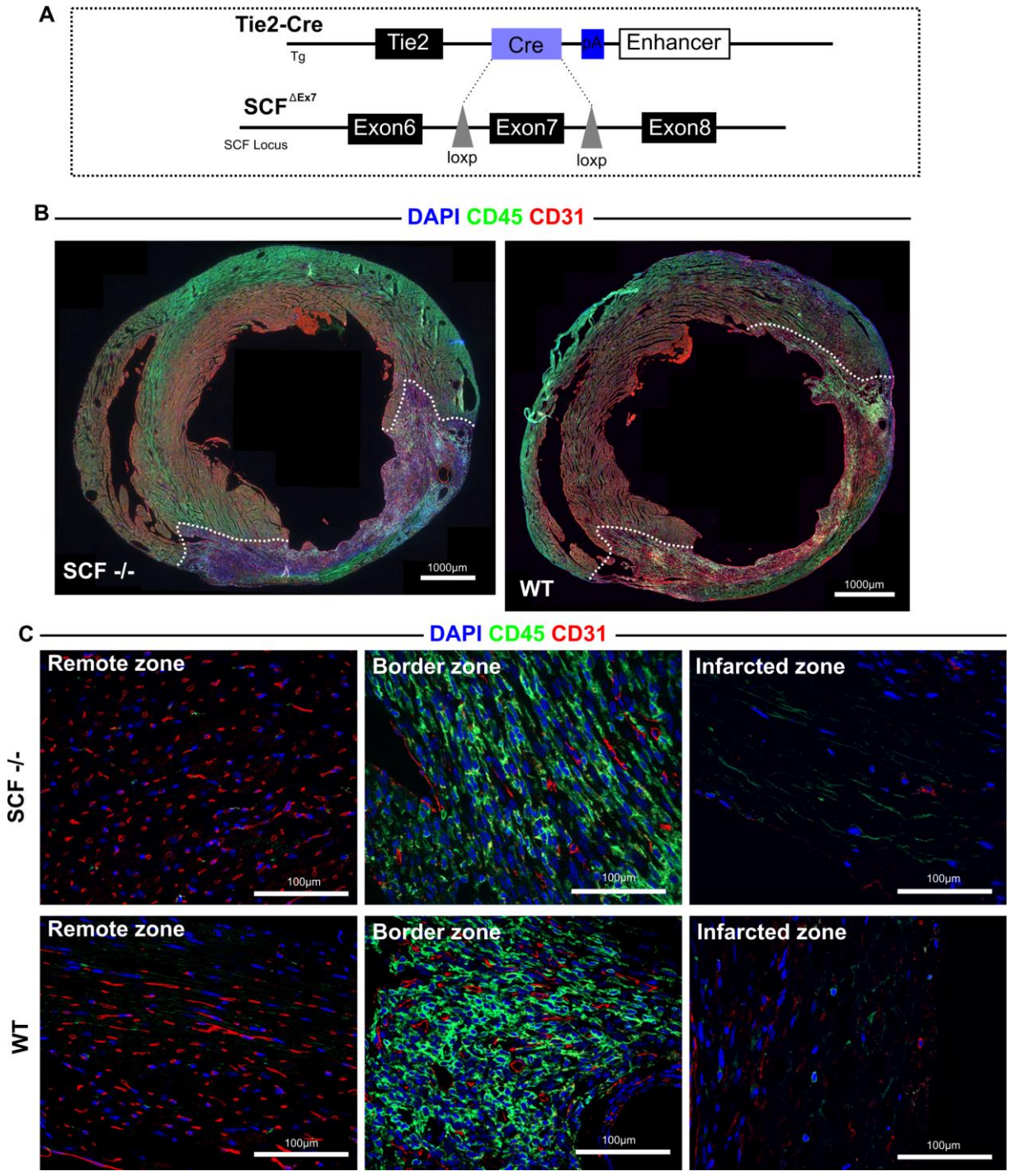

Fig. 3.15 SCF endothelial specific knockout does not produce an obvious phenotype after myocardial infarction:

A) Schematic representation of endothelial specific SCF loss-of-function strategy. In short, Tie2-Cre mouse line was bred with SCF-floxed^{Ex7} mouse line to create pan-VEC specific homozygous knockout of membrane bound SCF. Ligations of the LAD coronary artery were inflicted to create lesions in adult hearts. Mice were sacrificed for analysis one week after surgery. **B)** Transverse sections of infarcted heart at 7dps stained for CD45 (leukocyte marker, green) and CD31 (red). Very similar area of infarction (indicated by dashed line) can be observed for both SCF endothelial knockout (SCF-/-) and wild type (WT) mice. **C)** Magnified pictures from different areas of the infarcted hearts. Similar patterns of vessel distribution and leukocytes infiltration can be observed in hearts from knockout and wildtype mice.

3.14 C-kit signaling may be important for revascularization after myocardial infarction

C-kit$^+$ cells were reported to be involved in regeneration of the heart after myocardial infarction. Whether c-kit$^+$ cells contribute to the revascularization of infarcted hearts is under debate. [125] In order to address this question, we have collaborated with the working group of Prof. Kotlikoff from Cornell University (USA). This group has done the breeding of mice, the tamoxifen treatment and the operations and shipped the hearts to me. I have sectioned, immunostained and quantified the data over here at Bonn. To identify the potential origins of revascularized vessels in the infarcted heart and the involvement of c-kit signaling, lineage tracing experiments for all pre-existing VECs before myocardial infarction were performed. In detail, three mouse lines were crossbred together by the colleagues in the US to generate a triple transgenic mouse line: The VeCad-CreER^{T2} mouse line, [101] in which the VEC specific promoter VE-Cadherin drives CreER^{T2} expression, the Ai9 reporter mouse line, [126] consisting of the ubiquitous CAG promoter followed by a loxP-flanked STOP cassette and tdTomato, and a c-kit^{BAC}eGFP mouse line, [96] in which the c-kit promoter drives the expression of eGFP to identify c-kit+ cells *in vivo*. In the triple transgenic mice, approximately 2 to 4 grams of tamoxifen was injected by intraperitoneal injection for 3 times in one week to induce high levels of Cre-loxP recombination in the Ai9 reporter line. The mice were then kept in stock without additional tamoxifen for at least one week to ensure the clearance of tamoxifen from the organism. The mice were then subjected to either sham operation or cryo-injury, in which a liquid nitrogen cooled metal probe was used to inflict damage in the left ventricle. These mice were subsequently sacrificed at 7dps for analysis (Fig. 3.16A). For a whole expression map of the possible correlation between c-kit$^+$ cells and new vessels after acute injury co-immunostaining of CD31, tdTomato and eGFP was performed. We found that almost all CD31$^+$ cells were also tdTomato$^+$ in the remote and border area of the cryo-injured hearts and sham operated hearts, indicating very high Cre recombination efficiencies (Fig. 3.16B). Surprisingly, we also found a small portion of CD31$^+$ cells which did not have tdTomato signals in the infarcted area, indicating that alternative cellular origins other than pre-existing vessels contributed to these new vessels after injury (Fig. 3.16B). Most of the c-kit$^+$ cells were found in the infarcted area with the majority of them being CD31$^+$/tdTomato$^+$ (Fig. 3.16C). In addition, a few c-kit$^+$/CD31$^-$/tdTomato$^-$ large cells were found in the border area, too. They were

confirmed to be cardiomyocytes after co-immunostaining for eGFP, tdTomato and α-actinin (Fig. 3.16D).

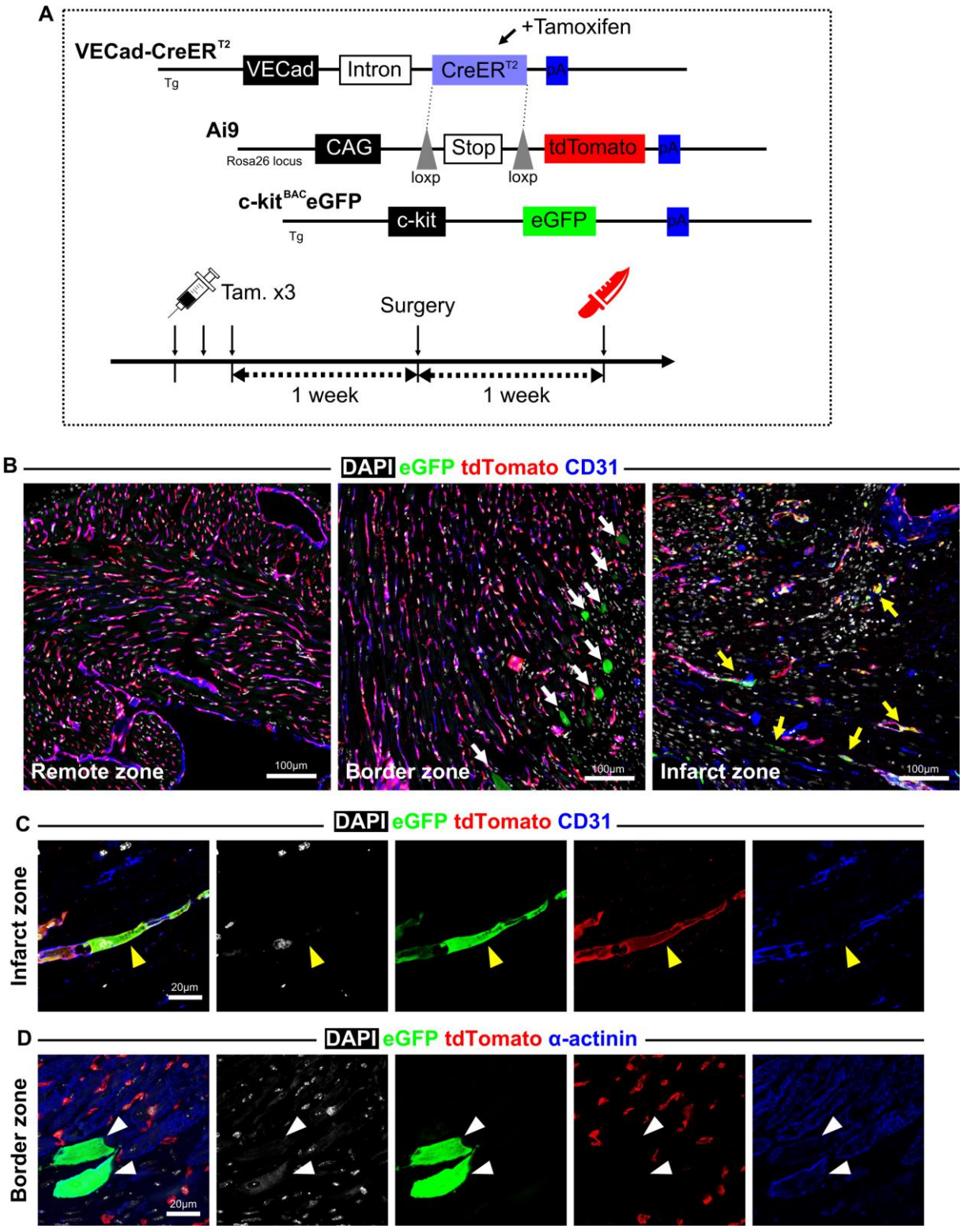

Fig. 3.16 C-kit^{+} cardiac cells may play a role in the revascularisation process after myocardial infarction:

A) Schematic presentation of a lineage tracing experiment designed to determine the potential function of c-kit during heart recovery after acute infarction in the adult mouse. The mice used in this experiment have a triple transgenic background consisting of VECad-CreER^{T2} (a vascular endothelial specific, inducible Cre line), Ai9 (a robust Cre reporter line expressing tdTomato after Cre recombinase) and c-kit^{BAC}eGFP (c-kit^{+} cell reporter line expresses eGFP under the control of c-kit promoter.). Tamoxifen was injected for 3 times during a week to label all endothelial cells. Cryo-injury to the left ventricle was performed 1 week after tamoxifen withdraw. Hearts were collected for analysis at 7 dpi. This part of the experiments was performed at Cornell University. **B)** Representative pictures of heart sections stained for eGFP (green), tdTomato (red) and CD31 (blue) from different regions of the infarcted heart (indicated in the lower left corner). C-kit^{+} cardiomyocytes (white arrows) are only seen in the border zone. The majority of the c-kit^{+} endothelial cells (yellow arrows) were found in the infarcted zone. **C)** Representative picture of a c-kit^{+}/tdTomato^{+}/CD31^{+} endothelial cell (yellow arrowhead) in the infarcted zone. **D)** Representative picture of two c-kit^{+} cardiomyocytes (white arrowheads) in the border zone.

To confirm these observations, quantifications of c-kit^{+} VECs and cardiomyocytes after acute infarction were performed. The results showed that almost no c-kit^{+} cardiomyocytes could be found in sham operated hearts or the remote areas of cryo-injured hearts, but approximately 18% of cardiomyocytes in the border area expressed c-kit (Fig. 3.17A). Nearly 100% of VECs in the sham operated hearts and the remote areas of the cryo-injured hearts colocalized with tdTomato signals, indicating that the method to induce Cre-loxP is efficient in labeling all pre-existing VECs (Fig. 3.17B). However, the results also demonstrated that approximately 20% of the VECs in the infarcted areas of the cryo-injured hearts do not express tdTomato, which indicates that these are new vessels arising from currently unidentified cells other than pre-existing VECs (Fig. 3.17C). In addition, c-kit^{+} VECs can be found almost exclusively in the infarcted area and compromise ~22% of total VECs in the infarcted area (Fig. 3.17D). Finally, ~21% of the VECs in the infarcted area are c-kit^{+}/tdTomato^{+}, which is substantially higher than the number of the VECs in the infarcted area that are c-kit^{+}/tdTomato^{-} (~1%) (Fig. 3.17E). These data suggested that c-kit signaling might be functionally active in cardiomyocytes in the border area of the infarct and the VECs in the infarcted area during the repair processes after acute myocardial infarction. However, c-kit activation by endogenous SCF is unlikely, as SCF is not expressed in or near the infarcted area. Furthermore, pre-existing vessels are the major source of the revascularization in the infarcted heart.

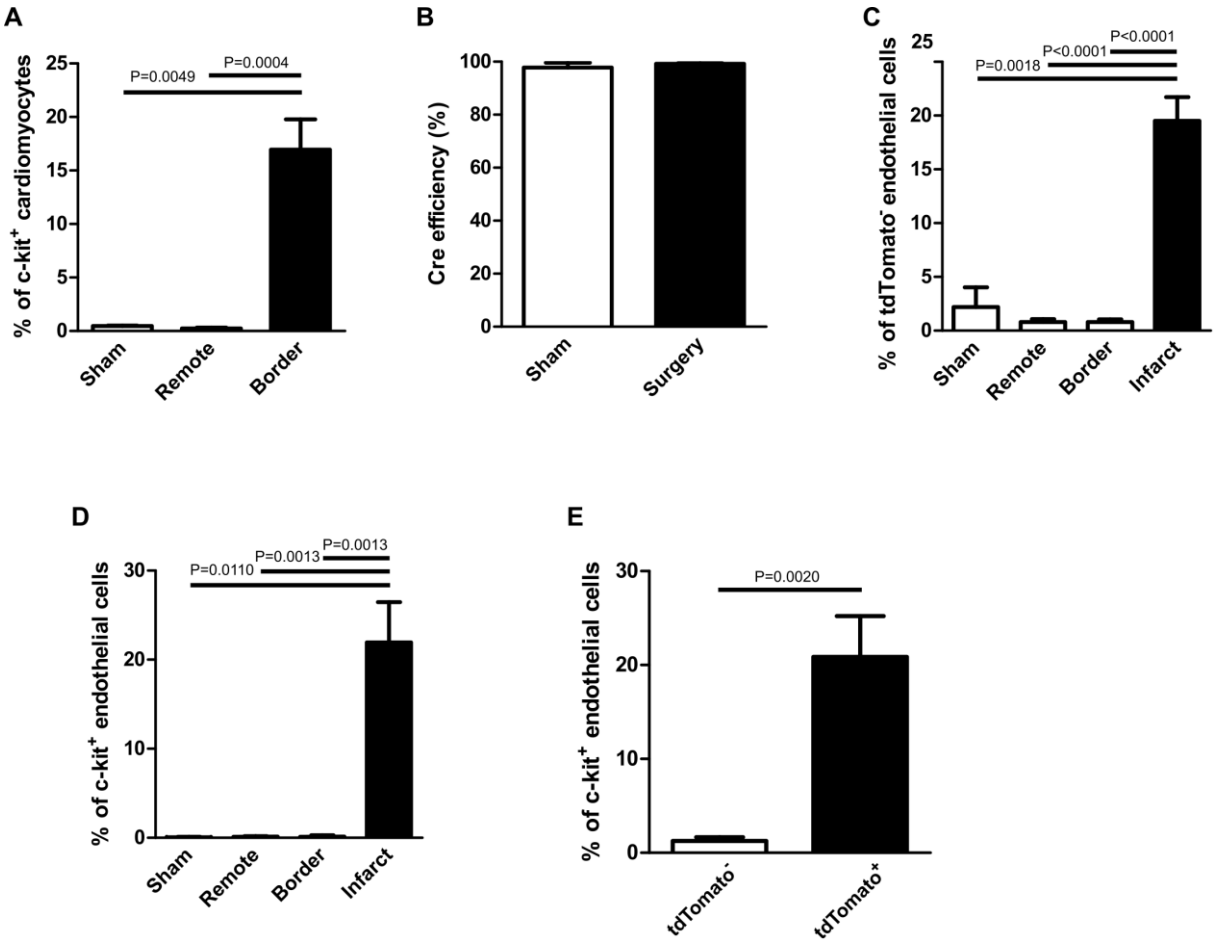

Fig. 3.17 Quantification of c-kit$^+$ cell types in the infarcted heart:

A) Quantification of c-kit$^+$ cardiomyocytes in different areas of the infarcted and in sham operated heart. **B)** Quantification of Cre efficiency in the VECad-CreER^{T2}/Ai9 lineage tracing system by counting the percentage of tdTomato$^+$/CD31$^+$ cells with respect to total CD31$^+$ cells. Cre efficiency in the surgery group was calculated by the recombination efficiency of CD31$^+$ cells in the right ventricle. **C)** Quantification of tdTomato$^-$ VECs, indicating a non-pre-existing endothelial origin in different areas of the infarcted. **D)** Quantification of c-kit$^+$ endothelial cells in different areas of the infarcted and sham operated heart. **E)** Quantification of tdTomato$^-$/c-kit$^+$ and tdTomato$^+$/c-kit$^+$ endothelial cells in the infarcted area. All data are shown as mean ± SEM. P values are indicated on the top bars (Student's t-test), n≥3.

4. Discussion

The role of c-kit$^+$ cardiac cells in heart repair after lesion has been under debate mainly due to the techniques applied to identify c-kit$^+$ cells in the heart. [3][18][127] Recent studies have resolved this controversy by using multiple genetic mouse models and suggested a minimal contribution of c-kit$^+$ cells to heart regeneration. [15]–[17] Additionally, the endogenous ligand of c-kit, SCF, has also been proposed to have clinical importance in the treatment of ischemic heart disease (see part 1.4). However, the underlying mechanism is unclear partially due to the technical difficulties in identifying SCF$^+$ cells in the heart. In the present study, I used multiple genetic mouse models to systematically analyze SCF expression in the heart during embryonic development, postnatal growth, adult homeostasis and pathological conditions. The results from my SCF expression analysis and SCF loss-of-function experiments during myocardial infarction do not support the previously claimed role of SCF during pathogenesis of the heart. However, I surprisingly identified SCF as a marker for two previously undefined subpopulations in the heart: small-arterial like coronary VECs and newly differentiated embryonic cardiomyocytes. Further characterization of these two important subpopulations could potentially improve our understanding of arteriogenesis and cardiomyocyte differentiation and cell cycle activity after myocardial infarction.

4.1 The SCF-CreER^{T2} mouse line recapitulates endogenous SCF expression

In the 1970s, early studies of mouse mutants on the steel locus, later identified as SCF, found strong phenotypes in the hematopoietic system, such as macrocytic anaemia. Since then, SCF expression has been studied intensively in hematopoietic organs, especially bone marrow. Endothelial expression of SCF in bone marrow was proposed by several studies based on data collected from qPCR, *in situ* hybridization and immunohistochemistry. [34][38][128]–[131] However, SCF$^+$ cells in bone marrow have not been systematically characterized until recently. [33] One of the main reasons for that is the low reliability of the mouse SCF antibodies used for immunohistochemistry. To overcome this limitation, Ding and colleagues generated a Scf^{gfp} transgenic mouse line in which exon 2 of SCF in the genome was replaced by an GFP-polyA cassette. [33] This knock-in mouse line can be used as a reporter line, expressing GFP under the regulation of the endogenous SCF promoter. In addition, homozygous mice are SCF knockouts displaying perinatal death due to severe anaemia. Furthermore, heterozygous Scf^{gfp} mice exhibit reduced HSCs frequency, reduced cellularity in newborn liver and abnormal pigmentation in the abdominal region. [33] These phenotypes indicate that impairing one of the two copies of the SCF gene causes severe disturbance in the health status of the mouse and therefore expression of SCF in Scf^{gfp} mice may differ from its expression pattern in wildtype mice. In contrast, the SCF-CreER^{T2} mouse line used in my thesis to identify SCF expression in the heart has certain advantages. Firstly,

this line expresses CreER^{T2} and tdTomato simultaneously. It can therefore be used as a direct detection and lineage tracing tool for SCF expressing cells. Secondly, the dimerized mutated red fluorescence protein, tdTomato, has several advantages when compared to GFP: It has its maximum emission at 581 nm, which creates lower background during whole-mount imaging in comparison to the emission maximum of GFP at 509 nm. It also provides a signal, which is 6 times brighter compared to eGFP (Clontech Inc.). Thirdly, SCF-CreER^{T2} mice have no obvious phenotype ensuring that the detection of SCF expression is comparable to the wildtype. However, the usage of the SCF-CreER^{T2} line also has drawbacks: Firstly, the tdTomato cDNA is located downstream of an IRES, which can potentially result in a much lower expression level of tdTomato in comparison to CreER^{T2}, which is located upstream of IRES. Secondly, the SCF promoter and its enhancers have so far not been properly characterized. Accordingly, in transgenic mouse line using “artificial promoters” there is always the risk of losing important regulatory elements of the targeted gene. Importantly, the SCF-CreER^{T2} line utilized a bacterial artificial chromosome (BAC) containing a very large region (229 kb) of the SCF gene from the mouse genome. It is well known [132] and also the experience in our lab that this this approach minimizes the possibility of losing important regulatory elements of the promoter. Importantly, in their first publication reporting this mouse line the Oxford group has carefully investigated the expression pattern of the transgene in endothelial cells of the thymus using RNA-seq as well as single cell analysis clearly demonstrating that transgene expression is specific and appears to recapitulate the endogenous expression pattern [41]. In my studies I have corroborated this important aspect by analyzing co-immunostainings of CreER^{T2} and tdTomato. The ligand binding domain of CreER^{T2} is derived from the human estrogen receptor, which allows staining for CreER^{T2} with the same antibody being used to stain for the ligand binding domain of human estrogen receptor. Unlike antibodies against mouse SCF or Cre, the antibody against human estrogen receptor (see part 2.1.6) used in the present study is highly specific, reproducible and reliable, as has been also demonstrated several times in heart sections in independent studies. [77][133][134] In order to visualize cells with low SCF expression, I have used a signal amplification protocol for CreER^{T2} staining to identify SCF^{+} cells on cardiac sections. In addition, I have compared the sparse SCF expression data from previous studies with my obtained tdTomato expression pattern in early embryos. The regions that had strong tdTomato expression, such as endodermal derived tissue, have been in fact also reported earlier. Particularly in the heart, the developing cardiac cushions displayed strong tdTomato signals, which is consistent with the RNA expression data from *in situ* hybridization analysis. [53] The low level of tdTomato expression in e11.5 heart is also consistent with data from previous Northern blot analysis. [54] These data indicate that the expression map acquired from the SCF-CreER^{T2} mouse line is fully

supported by multiple previous studies using different approaches. Thus, I consider the SCF-CreER^{T2} mouse line to be a very good tool to identify and study *bona fide* SCF^{+} cells in the heart.

4.2 SCF expression marks small-arterial like coronary VECs

In the present study, I found most of the SCF expressing cells in the postnatal heart to be coronary VECs. Contrariwise, only a part of the coronary VECs did express SCF. The expression of SCF in coronary VECs seemed to be randomly distributed on histological sections. However, it was apparent that coronary vessels with bigger diameters in comparison to their surrounding vessels did contain SCF^{+} VECs. To identify the exact cell types of SCF+ VECs α-SMA (smooth muscle marker) was used to distinguish intramyocardial arteries and arterioles from capillaries. The rational to discriminate these VEC subtypes by the existence of smooth muscle cells in close proximity to the cells was as follows: a) Pulsation is one of the hall marks of arteries, which require vascular smooth muscle cells; b) Although veins possess smooth muscle layers, they do not exist in the compact myocardium [135]; c) Canonical arterial and venous markers for VECs, such as the seminal EphrinB2/EphB4, were discovered during early vascular development and angioblasts specification, which can be difficult for the identification of arterial or venous VECs in the adult heart [85]; d) Antibodies for these markers may not work in postnatal heart. As a result, I found that over 90% of VECs in the intramyocardial arteries (excluding major coronary arteries) in postnatal heart were SCF^{+}. In comparison, less than 16% of VECs in the capillaries did express SCF. In the coronary vascular bed, major coronary arteries on the surface of the heart arise from aorta and branch into intramyocardial arteries, arterioles and eventually capillaries. [136] However, in the intermediate regions between arterioles and capillaries it is difficult to determine the arterial or venous identity of VECs. Thus, to expect any of the molecular markers of arterial VECs to have 100% colocalization with α-SMA encircled VECs is unrealistic. My data strongly suggest that SCF expression in coronary VECs indicates an arterial phenotype. Furthermore, I also identified the SCF^{+} capillary VECs by their correlation with vascular pericytes. In a prototypic angiogenesis model, VECs in the nascent sprout adopt two distinct cellular phenotypes, the migrating tip cells and the proliferating stalk cells. [137] Vascular pericytes are later recruited to support new vessel formation. [138] I found nearly 100% SCF^{+} VECs in capillaries to be encircled by vascular pericytes. This indicated that SCF^{+} VECs have a phalanx-like phenotype rather than a tip/stalk-like phenotype. Since pericytes are the progenitors for coronary artery smooth muscles [139], the SCF^{+} VECs may have more similarities to the arterial phenotype than SCF^{-} VECs in the capillary compartment.

However, I also found that VECs from major coronary arteries in adult hearts do not express SCF. Accordingly, I hypothesized that SCF expression in VECs represents a small-arterial phenotype. In contrast, major coronary arteries in neonatal hearts contained SCF^+ VECs. However, the SCF expression in major coronary VECs started to decline at P7. By P15, most of the coronary VECs are SCF^-. These observations further corroborated that SCF marks a subpopulation of small-arterial VECs. Although the two major coronary arteries are big arteries, they both grow from arterioles in newborns. SCF expression is lost in their VECs after they grow bigger and many phenotypic changes take place. It is therefore reasonable to suggest that SCF identifies distinct small arterial VECs in the heart.

The SCF expression pattern was further analyzed in developing coronary vessels. Recent studies [121] on coronary vessel development revealed various phenotypic changes of endocardial cells and VECs in young hearts. Coronary VECs determined to adopt an arterial fate can be easily identified on the surface of the left anterior region and right posterior region of the e14.5 heart. [77] These findings were utilized to verify my theory about the small-arterial identity of SCF^+ VECs in various known VEC populations during coronary vessel formation. I found that early angioblast-like SECs, which form different types of coronary vessels, did not display SCF expression. The first SCF^+ VECs appear in the heart during the formation of major coronary arteries at e14.5. These SCF^+ VECs in the left anterior region of the heart also recruited vascular pericytes and aligned into tubular vascular shape structure. Subsequently, the newly formed coronary arteries continue to mature into lumenized structures and express SCF in VECs. These observations indicated the concurrence of SCF expression and functional phenotypic changes in coronary VECs during initial arteriogenesis. The fact that SCF^+ VECs appear in major coronary arteries before they connect to the aorta/blood flow also indicates genetic predisposition to play important roles in arterial specification of VECs during the formation of major coronary arteries. The phenotypes of arterial and venous VECs may interchangeable according to their environment. [140] Earlier studies suggested an influence of hemodynamics on arterial/venous identity. [141] As an example, coronary artery bypass grafting suggests that veins can adopt arterial-like phenotypes when grafted into arterial circulation. [142] However, my findings suggest that arteriogenesis in coronary arteries is likely to be genetically programmed, because the SCF expression in the developing coronary arteries at e14.5 is prior to the establishment of arterial circulation. SCF could potentially mark a subpopulation of VECs that has more arteriogenic potential.

4.3 The SCF-CreER^{T2} mouse line can be used to genetically trace the lineage of SCF^{+} cardiac cells during embryonic development

The SCF-CreER^{T2} mouse line was crossbred with the CAG-mTmG mouse line to be able to trace the lineage of SCF^{+} cardiac cells during mouse embryonic development. The recombination of loxP sites by CreER^{T2} has been proven to be highly ligand-dependent *in vitro*. [94] Because of this, it is necessary to verify Cre activity in each individual transgenic mouse line, since different transgenic engineering strategies can severely affect the outcome of Cre activity. [92] To analyze the leakiness of the SCF-CreER^{T2} x CAG-mTmG mouse line I examined mice without administration of tamoxifen. In e15.5 hearts from these mice there were almost no GFP^{+} cells detectable. This indicated that CreER^{T2}, driven by the SCF promoter has an expression level, which is not so high that unspecific Cre activity causes spontaneous recombination. The GFP^{+} cells also formed clusters at random locations of the heart. This indicated early activity of CreER^{T2} in single cells and subsequent proliferation leading to the formation of clones of cardiac cells. The very small amount, but not absence, of leakiness indicates that the CreER^{T2} is expressed in an adequate dosage in the SCF-CreER^{T2} line, since the expression level of CreER^{T2} is high enough to cause leakiness but not as high as to make the Cre activity no longer tamoxifen dependent. This rendered the SCF-CreER^{T2} x CAG-mTmG mouse line particularly suitable for genetic tracing of cell lineages. The activation of CreER^{T2} causes irreversible recombination of the reporter gene, which triggers expression of GFP driven by the strong ubiquitous promoter CAG. The cells labeled by this event and all their progeny will continuously express GFP in disregard of SCF promoter activity. This enabled me to find cell populations that only transiently express SCF at a certain time point during development and cells expressing a very low amount of SCF. I administered a single dose of tamoxifen via oral gavage to each pregnant mouse at certain developmental stage. My data showed that each time point of injection has its unique fate map in the heart, which in turn verified that the experimental strategy enabled a 24 h window of CreER^{T2} activation. Thus, our lineage tracing system can discover transient SCF^{+} cell populations during embryonic development.

4.4 SCF marks newly differentiated cardiomyocytes

Besides SCF^{+} VECs, also some of the embryonic cardiomyocytes expressed SCF. However, the expression level of SCF was substantially lower in cardiomyocytes than VECs and cardiac cushions, respectively. To overcome this, I stained for CreER^{T2} by tyramide signal amplification to intensify the signals. As a result, I identified SCF^{+} cardiomyocytes only in the right ventricle of e11.5 embryos. This was inconsistent with previous *in situ* hybridization analysis[53]-[55] and has never been reported before. However, I considered the SCF^{+} signals not to be staining artifacts, but to be specific, because the left ventricle worked as an internal control for SCF^{-} cardiomyocytes. Furthermore, the sensitivity of *in situ* hybridization

methods does vary substantially [143] and with this technique it is easily possible to miss cells with low mRNA expression. Since the right ventricle originates from the SHF, SCF expression in cardiomyocytes at e11.5 may be functionally related to the formation of the SHF. I used the SCF-CreER^{T2} x CAG-mTmG mouse line to trace the potential SCF^{+} cardiac progenitors at e7.5, when the cardiac crescent, that contains progenitors from both FHF and SHF, starts to form the heart. As a result, I found that almost no cardiomyocytes were traceable in the e15.5 heart. This result indicates that cardiac progenitors do not express SCF. However, when the SCF^{+} cell lineages were labelled in e8.5, left ventricle and atria could be traced in e15.5 hearts. Such an expression pattern coincides with the fate map of progenitor cells from the FHF. At e8.5, the primitive heart tube has formed and progenitors from SHF gradually migrate to the arterial and venous poles of the heart. [144] The e8.5 traced cardiomyocytes can be reasonably assigned to the newly differentiated cardiomyocytes on the heart tube expressing SCF. As I continued to label SCF^{+} cells at different stages, I found that the SCF^{+} cell lineage shifted gradually from atria and left ventricle to right ventricle and OT. In summary, virtually all cardiomyocytes express SCF at some time point of their differentiation and maturation. Based on the different time points of labelling and the resulting spatial distribution of the SCF^{+} cell lineage, I concluded that SCF^{+} cardiac cells are fate determined new cardiomyocytes and different from HCN4^{+} and ISL1^{+} cardiac progenitors from FHF and SHF, respectively. According to my data, the SCF expression in newly differentiated cardiomyocytes lasts for less than 3 days. The initially SCF^{+} cardiomyocytes in atria and left ventricle at e8.5 and the right ventricle and OT at e11.5 lost their SCF expression after 3 days. These observations suggest that SCF expression marks a previously undefined population of newly differentiated cardiomyocytes in the embryonic heart.

In contrast to the controversy about postnatal cardiomyocytes, embryonic cardiomyocytes have a proliferative capacity. [145] My identification of a SCF expressing, newly differentiated cardiomyocyte population in embryonic hearts may provide new insight into the proliferative potential of the neonatal heart. I examined the neonatal heart at P0 and found less than 3% of the cardiomyocytes to express SCF. However, this population quickly disappeared after P7 and could not be found in adult hearts. However, the methods used in the quantification could potentially introduce biases into the results due to currently technical limitations. Firstly, the low expression level of SCF in cardiomyocytes and the increasing signal background in aging heart tissue could result in false positives. Secondly, since the identification of cardiomyocytes relies on the co-staining of α-actinin on heart sections, the identity of an individual cardiomyocyte cannot be unequivocally determined. This could falsify the total number of cardiomyocytes used in the quantification of the percentage of SCF^{+} cardiomyocytes. To prevent this the absolute number of SCF^{+} cardiomyocytes per mm^{2} was

further quantified using a previously published method [111][114] in a random area of the heart and obtained similar results. After birth, the heart needs to quickly adapt from the connection to the maternal circulation to the circulation system of the newborn. During this period neonatal cardiomyocytes undergo many phenotypic changes, such as trabecular compaction, binucleation and reduction of cell cycle activity. SCF expression represents a newly differentiated stage of embryonic cardiomyocytes. Re-expression of SCF in a very small portion of neonatal cardiomyocytes may indicate either new cardiomyocytes being differentiated from progenitors, which is rather unlikely, or that pre-existing cardiomyocytes acquire a more undifferentiated phenotype to support heart growth. However, the exact mechanism behind SCF expression in cardiomyocytes is currently unknown. The decrease in the number of SCF^+ cardiomyocytes coincides with the decrease of cell cycle activity, which may indicate the depletion of phenotypically young cardiomyocytes over time.

4.5 SCF expression in diseased hearts

Many previous studies made numerous claims about potential clinical benefits of $c\text{-}kit^+$ stem cells during heart regeneration. [8]–[12] However, such claims need to be verified and have been refuted by recent studies [15]–[17]. I investigated the SCF expression pattern in the injured heart after cryo-infarction, in order to tackle the role of SCF/C-kit signalling during heart disease and repair. The data obtained demonstrated that after the lesion SCF expression in the infarcted area almost completely disappeared after 2 days. In addition, I did not find any substantial increase of SCF^+ cells after 7 or 14 days. As the activation of C-kit relies on binding of SCF and several independent studies (see 1.2.2) have discovered SCF^+ cells to act as niches to support different stem cells in a c-kit dependent manner in other systems, the loss of SCF^+ cells would most likely abolish the potential c-kit signaling and diminish the potential c-kit+ cardiac stem cells in the infarcted area. Furthermore, the EC specific knockout of membrane bound SCF did not show any changes after myocardial infarction in terms of revascularisation and immune cell infiltration in comparison to wild type mice. Recent studies also showed that knockout of membrane bound SCF could phenocopy the total SCF knockout and the steel mutant, indicating a predominant role of this isoform over soluble SCF. Therefore, it is unlikely that soluble SCF could compensate the loss of endogenous SCF^+ cells. Thus, my observations do not support previous claims about the important roles of endogenous SCF/c-kit+ cardiac stem cells during heart regeneration.

Nevertheless, these data partially supported my hypothesis about the small arterial-like VEC identity in SCF^+ coronary VECs. Revascularization of infarcted regions requires angiogenesis from pre-existing coronary vessels, especially from the vessels in the border area of the infarct. On the other hand, hypoxia as induced by ischemia, also promotes vessel sprouting by upregulating multiple pro-angiogenic pathways. Thus, the VECs in the border zone of the

infarct are likely to differentiate to tip/stalk-cells instead of phalanx-like/arterioles, which coincides with loss of SCF^+ VECs in the border zone of the infarct.

It is known that the neonatal mouse heart still possesses a certain level of regenerative capacity, which was described to be mediated primarily by cardiomyocyte proliferation. [111] I investigated the SCF expression pattern during neonatal heart regeneration by using a new lesion variation. Previously established neonatal heart injury models included apex resection [111], cryo-injury [14] and LAD coronary artery ligation [146]. I used a small vessel cauteriser to inflict a small injury on the apex of the heart for the following three reasons: 1) Apex resection results in massive blood loss which could potentially slow down the regenerative response. 2) Cryo-injury, which uses a liquid nitrogen cooled probe to inflict injury is a highly reproducible model in terms of infarction size and does not result in blood loss. However, in order to inflict an injury, the pre-cooled probe must contact the heart surface for a very long time (e.g. 3x10 sec), which could partially damage the surrounding tissue and leave the scars of cryo-injured hearts without clear borders. This would complicate the analysis of a regenerative response in the border zone of the injury. 3) Ligation of the LAD coronary artery is technically very challenging, resulting in different levels of severity of the injury. More importantly, neonatal coronary arteries respond differently to injury in comparison to adult ones [147], which results in huge inconsistencies in each mouse. My method used a small vessel cauteriser to inflict injury to the apex of the heart, which was created by heating to over 1000°C for 1 sec. This method reduces inconsistencies between surgeries and creates an unaffected border zone.

Cardiomyocytes are known to undergo various cell cycle variants not resulting in cell division, such as endoreduplication and acytokinetic mitosis, which makes it almost impossible to identify authentic cell division by using antibody based M-phase specific markers.[99] The transgenic line eGFP-anillin used in the current study provides an independent genetic tool to identify cell cycle activity. After applying cauterization injury to mice from this mouse line, I found 3 times more cell cycle activity in injured hearts than in sham operated ones at 7 dpi. Furthermore, the distribution of the $eGFP^+$ cells did not show higher abundance near the injury site. Instead, the $eGFP^+$ cells were almost evenly distributed all over the heart. Unlike amphibian regeneration models, in which animals can restore entire complex structures such as limbs, injured neonatal hearts always leave scars and other permanent morphological changes, despite seemingly full functional recovery. [111] My data implied that lost cardiac tissue and decreased heart function are restored by accelerated proliferation and, perhaps, also terminal differentiation of cardiomyocytes in the entire heart rather than only in the border area of the injury. This result suggests regeneration in neonatal heart to be mediated by compensatory proliferation and growth of the unaffected surviving cardiomyocytes in the

entire heart. Furthermore, we also found a very small portion of cardiomyocytes with cytosolic eGFP-anillin signals, disassembled sarcomeres, condensed chromatins and SCF expression. Cardiomyocytes with these four characteristics could be proliferative for the following reasons: a) Cytosolic eGFP-anillin signals indicate the breakdown of the nuclear membrane during M-phase. b) Sarcomere disassembly has been observed in dividing embryonic cardiomyocytes. [148][149] c) Chromatin condensation is another hall mark of mitosis. [150] d) SCF is expressed in newly differentiated embryonic cardiomyocytes (this thesis). Re-expression of embryonic markers in cardiomyocytes has been associated with a proliferative phenotype in both zebrafish [151] and mouse [111]. To unequivocally identify proliferative cardiomyocytes *in vivo* is almost impossible, because cardiomyocytes are known to undergo various cell cycle variants [99]. My data shows, by combining SCF expression, eGFP-anillin localization and other proliferation markers, it may be possible to improve the identification of proliferative cardiomyocytes in neonatal hearts. However, this method also faces several technical challenges: a) The cytosolic eGFP-anillin signals are much weaker than their nuclear signals. High background caused by autofluorescence may interfere with the real signals; b) SCF expression levels in neonatal cardiomyocytes are also very low and hard to detect. I injected tamoxifen 1-2 days before sacrifice, to concentrate the $CreER^{T2}$ signal into the nucleus. However, proliferating cardiomyocytes break down their nuclear membranes, which disperses the $CreER^{T2}$ signal back into the cytosol. In conclusion, injured neonatal mouse hearts restore function by compensatory proliferation and terminal differentiation of cardiomyocytes. SCF expression may be correlated with the M-phase of cell cycle active cardiomyocytes during neonatal heart regeneration.

4.6 Contribution of c-kit$^+$ cells to repair mechanisms after myocardial lesion

The possible contribution of c-kit$^+$ cells to cardiomyocytes after myocardial infarction was under debate for more than a decade. [18] Recently, new evidence from c-kit based genetic lineage tracing suggested that their contribution to cardiomyocytes is extremely low. [15][16] In the current study, I investigated the contribution of potential resident cardiac progenitor cells to the revascularization after myocardial infarction and if c-kit$^+$ cells were involved. I used genetic cell lineage tracing to label all pre-existing VECs, which allowed me to identify vessels originating from a resident progenitor pool. About 20% of the new vessels in the infarcted area were derived from un-identified progenitor cells. This result differed substantially from a recently published study using almost the same experimental setting, which claimed that virtually all neovascularization after myocardial infarction originates from pre-existing VECs. [152] The possible explanation for this discrepancy could be the different injury models used in the two studies. The ischemia reperfusion model used in the above mentioned study inflicts a milder injury compared to cryo-injury model used in my study.

Although the ischemia-reperfusion model can create large areas of fibrosis, the pre-existing vessel network is still intact after injury, due to the reperfusion and provides a source of sprouting VECs for new vessels. On the other hand, cryo-injury results in large areas of necrosis at the injury site and destroys the pre-existing vessel network which makes sprouting angiogenesis impossible in certain regions of the injury. My data showed that new vessels originating from unknown progenitors only exist in those regions of the infarcted area that cannot be reached by pre-existing VECs, but not in the border area of the infarction where pre-existing vessels are in close proximity. These observations indicate that cellular origins of neovascularization in the injured heart are based on spatial availability. Such spatial mechanisms are similar to the developmental progression of coronary vessel during which origins of coronary vessels are determined also by proximity, which may have evolved as the fastest way to re-vascularize the myocardium after injury. Pre-existing vessels contributed to 80% of new vessels in the infarcted area, indicating a predominant role of angiogenesis during revascularization of the injured heart. In these experiments c-kit$^+$ cells were identified as VECs in the infarcted area and cardiomyocytes in the border area. The majority of c-kit$^+$ VECs originated from pre-existing vessels, as the lineage tracing experiments suggested. The c-kit$^+$ cardiomyocytes in the border zone at 7 dpi were terminally differentiated and mature cardiomyocytes, which made it unlikely that they originated from c-kit$^+$ progenitors. In summary, my data did not support the notion that c-kit$^+$ cells contribute to revascularization and neomyogenesis after myocardial infarction in the adult. However, so far unidentified progenitors do contribute to revascularization in the infarcted heart.

4.7 Outlook

In the current study, I identified SCF$^+$ cells in the adult heart to be VECs. However, the function of SCF expression in these cells is still unclear. Furthermore, I found SCF expression to mark a small-arterial like subpopulation of VECs. To verify the small-arterial like identity of SCF$^+$ VECs, I am planning to provide more molecular information in regard to the expression of other key markers for arterial and venous identity. In fact, FACS based cell sorting can help purifying the SCF$^+$ and SCF$^-$ VEC populations and RNA-seq transcriptome sequencing can provide gene expression profiles of SCF$^+$ VECs, which will help to understand the functional roles of SCF$^+$ VECs in the heart and to verify the small-arterial like identity of SCF$^+$ VECs. In the current study, the small-arterial like identity of SCF$^+$ VECs was verified during the progression of coronary vessel development. Accordingly, the (epi)genetically pre-programmed arterial specification of coronary major arteries seems to coincide with the expression of SCF. Transcriptome analysis of these initial SCF$^+$ major coronary VECs could potentially lead to new findings of key regulators determining arterial

specification of coronary arteries. Such experiments are technically challenging, because initial major coronary arteries only contain approximately 50 cells. One option could be laser capture microdissection combined with 3rd generation single cell RNA transcriptome sequencing in order to obtain in the future information about the gene expression profiles of these cells.

I also identified SCF^+ cardiomyocytes as newly differentiated embryonic cardiomyocytes. Presumably, these cardiomyocytes had an increased proliferative capacity. As neonatal hearts also possess a small amount of SCF^+ cardiomyocytes they may have an increased proliferative capacity after injury as well. However, the correlation between SCF^+ embryonic and neonatal cardiomyocytes has not been shown so far. The low expression level of SCF in neonatal cardiomyocytes as well as the low percentage of SCF^+ cardiomyocytes brings substantial technical difficulties to the characterization of these cells. Further improvement of genetic mouse tools or SCF identification methods is necessary to carry out such studies. Interestingly, the percentage of SCF^+ embryonic cardiomyocytes can be as high as 50% in e11.5 hearts, making it possible to study the gene expression profile of embryonic SCF^+ cardiomyocytes by 3rd generation single cell RNA transcriptome sequencing. This information combined with bioinformatic analysis of data depositories from previously sequenced data may provide useful information about SCF^+ cardiomyocytes in regard to the regulatory signalling networks of the (sub)lineage conversion between phenotypically “young” and proliferative cardiomyocytes and terminally differentiated quiescent cardiomyocytes.

5. SUMMARY

Proper regulation of c-kit receptor tyrosine kinase by its ligand, Stem Cell Factor (SCF), is essential for survival, growth, migration and differentiation of many types of stem/progenitor cells. However, its role in the heart has remained elusive. Previous studies identified c-kit$^+$ cells as hematopoietic or resident cardiac stem cells, which were supposed to play an important role in heart regeneration after myocardial infarction. However, more recent studies indicate that c-kit$^+$ cells minimally contribute to new cardiomyocytes after cardiac injury or during aging. The nature of c-kit$^+$ cardiac cell populations has been at least partially clarified by the use of recently developed genetic mouse models, whereas the cell populations expressing the endogenous ligand SCF have not been identified. In my current study, I have therefore analyzed the expression pattern of SCF during mouse heart development and after cardiac injury by taking advantage of a transgenic mouse line, SCF-CreER^{T2}, which expresses a Cre/mutated human estrogen receptor (ER^{T2}) fusion protein and a tdTomato fluorescence protein under control of the SCF promoter. This model enables to identify SCF expressing cells in the heart and to genetically trace the lineage of these cells under various conditions.

I discovered that SCF was strongly expressed in a part of the VECs in neonatal and adult hearts. Quantification of the SCF$^+$ VECs in arteries and capillaries revealed SCF expression to be restricted to small-arterial like vessels in the postnatal heart. In addition, I found that the VECs of major coronary arteries only express SCF during neonatal stages. As soon as the major coronary arteries grew bigger, they lost their SCF expression in VECs. Furthermore, I also found that the undifferentiated coronary VECs in early embryos did not express SCF, whereas coronary VECs adopting an arterial fate expressed SCF during the formation of major coronary arteries in e14.5 hearts. These findings strongly suggested that SCF expression marks a previously undefined small-arterial like VEC subpopulation.

I also found that SCF was expressed in some of the embryonic cardiomyocytes at a much lower level in comparison to the coronary VECs. By deploying genetic lineage tracing of the SCF$^+$ cells from different stages of the embryo, I found nearly all cardiomyocytes to have expressed SCF for a short time period after their differentiation. I hypothesised that SCF expression in embryonic cardiomyocytes marks a newly differentiated cardiomyocyte subpopulation. Furthermore, I also found

neonatal P0 hearts to have approximately 3% SCF^+ cardiomyocytes. However, this population quickly diminishes within the first week after birth. These observations may indicate the depletion of a population of phenotypically young cardiomyocytes. In addition, SCF expression co-localized with M-phase cardiomyocytes in neonatal mice during regeneration after experimental heart injury. These findings suggested that SCF expression may indicate proliferative cell cycle activity in cardiomyocytes.

To investigate the involvement of c-kit signalling during myocardial infarction, I examined the expression pattern of SCF after myocardial infarction in adult mice. I found substantial decrease of SCF^+ cells in the border zone and infarct area of the injured heart after 2, 7, and 14 dpi, which might indicate decreased SCF/C-kit activity after myocardial infarction. To investigate if $c\text{-}kit^+$ cells or other possible progenitors contribute to neovascularization, all pre-existing VECs were labelled by using genetic lineage tracing tools prior to myocardial infarction. I found the majority of the new vessels in the infarcted area to have originated from pre-existing vessels. Furthermore, most of the $C\text{-}kit^+$ cells in the infarcted heart are either VECs originating from pre-existing vessels or mature cardiomyocytes in the border zone. My findings suggested that cardiac endogenous $C\text{-}kit^+$ cells are unlikely to contribute to VECs and cardiomyocytes after myocardial infarction.

In conclusion, this study did not support the notion that potential $C\text{-}kit^+$ stem cells contribute to the regeneration of infarcted hearts. Instead, I found that SCF expression marked a small-arterial like subpopulation of VECs and newly differentiated embryonic cardiomyocytes. Further molecular characterization of these two cell populations could provide useful insights into the regulatory mechanisms of coronary arteriogenesis and cardiomyocyte proliferation.

6. REFERENCES

[1] "WHO | Cardiovascular diseases (CVDs)," *WHO*, 2017.

[2] R. R. Nadig, "Stem cell therapy - Hype or hope? A review.," *J. Conserv. Dent.*, vol. 12, no. 4, pp. 131–8, Oct. 2009.

[3] M. Hesse, B. K. Fleischmann, and M. I. Kotlikoff, "Concise Review: The Role of C-kit Expressing Cells in Heart Repair at the Neonatal and Adult Stage," *Stem Cells*, vol. 32, no. 7, pp. 1701–1712, Jul. 2014.

[4] S. A. Doppler, M.-A. Deutsch, V. Serpooshan, G. Li, E. Dzilic, R. Lange, M. Krane, and S. M. Wu, "Mammalian Heart Regeneration: The Race to the Finish Line.," *Circ. Res.*, vol. 120, no. 4, pp. 630–632, Feb. 2017.

[5] S. S.-K. Chan, Y.-Z. Shueh, N. Bustamante, S.-J. Tsai, H.-L. Wu, J.-H. Chen, and P. C. H. Hsieh, "Genetic Fate-Mapping for Studying Adult Cardiomyocyte Replenishment After Myocardial Injury," 2010, pp. 201–211.

[6] S. E. Senyo, M. L. Steinhauser, C. L. Pizzimenti, V. K. Yang, L. Cai, M. Wang, T.-D. Wu, J.-L. Guerquin-Kern, C. P. Lechene, and R. T. Lee, "Mammalian heart renewal by pre-existing cardiomyocytes," *Nature*, vol. 493, no. 7432, pp. 433–436, Dec. 2012.

[7] P. C. H. Hsieh, V. F. M. Segers, M. E. Davis, C. MacGillivray, J. Gannon, J. D. Molkentin, J. Robbins, and R. T. Lee, "Evidence from a genetic fate-mapping study that stem cells refresh adult mammalian cardiomyocytes after injury.," *Nat. Med.*, vol. 13, no. 8, pp. 970–4, Aug. 2007.

[8] A. P. Beltrami, L. Barlucchi, D. Torella, M. Baker, F. Limana, S. Chimenti, H. Kasahara, M. Rota, E. Musso, K. Urbanek, A. Leri, J. Kajstura, B. Nadal-Ginard, and P. Anversa, "Adult cardiac stem cells are multipotent and support myocardial regeneration.," *Cell*, vol. 114, no. 6, pp. 763–76, Sep. 2003.

[9] K. Matsuura, T. Nagai, N. Nishigaki, T. Oyama, J. Nishi, H. Wada, M. Sano, H. Toko, H. Akazawa, T. Sato, H. Nakaya, H. Kasanuki, and I. Komuro, "Adult Cardiac Sca-1-positive Cells Differentiate into Beating Cardiomyocytes," *J. Biol. Chem.*, vol. 279, no. 12, pp. 11384–11391, Mar. 2004.

[10] E. Messina, L. De Angelis, G. Frati, S. Morrone, S. Chimenti, F. Fiordaliso, M. Salio, M. Battaglia, M. V. G. Latronico, M. Coletta, E. Vivarelli, L. Frati, G. Cossu, and A. Giacomello, "Isolation and Expansion of Adult Cardiac Stem Cells From Human and Murine Heart," *Circ. Res.*, vol. 95, no. 9, pp. 911–921, Oct. 2004.

[11] G. M. Ellison, C. Vicinanza, A. J. Smith, I. Aquila, A. Leone, C. D. Waring, B. J. Henning, G. G. Stirparo, R. Papait, M. Scarfò, V. Agosti, G. Viglietto, G. Condorelli, C. Indolfi, S. Ottolenghi, D. Torella, and B. Nadal-Ginard, "Adult c-kitpos cardiac stem cells are necessary and sufficient for functional cardiac regeneration and repair," *Cell*, vol. 154, no. 4, pp. 827–842, 2013.

[12] J. Ferreira-Martins, B. Ogorek, D. Cappetta, A. Matsuda, S. Signore, D. D'Amario, J. Kostyla, E. Steadman, N. Ide-Iwata, F. Sanada, G. Iaffaldano, S. Ottolenghi, T. Hosoda, A. Leri, J. Kajstura, P. Anversa, and M. Rota, "Cardiomyogenesis in the Developing Heart Is Regulated by C-Kit-Positive Cardiac Stem Cells," *Circ. Res.*, vol. 110, no. 5, pp. 701–715, Mar. 2012.

[13] M. M. Zaruba, M. Soonpaa, S. Reuter, and L. J. Field, "Cardiomyogenic potential of C-kit+-expressing cells derived from neonatal and adult mouse hearts," *Circulation*, vol. 121, no. 18, pp. 1992–2000, May 2010.

[14] S. A. Jesty, M. A. Steffey, F. K. Lee, M. Breitbach, M. Hesse, S. Reining, J. C.

Lee, R. M. Doran, A. Y. Nikitin, B. K. Fleischmann, and M. I. Kotlikoff, “c-kit+ precursors support postinfarction myogenesis in the neonatal, but not adult, heart,” *Proc. Natl. Acad. Sci.*, vol. 109, no. 33, pp. 13380–13385, Aug. 2012.
[15] J. H. van Berlo, O. Kanisicak, M. Maillet, R. J. Vagnozzi, J. Karch, S. J. Lin, R. C. Middleton, E. Marbán, and J. D. Molkentin, “c-kit+ cells minimally contribute cardiomyocytes to the heart,” *Nature*, vol. 509, no. 7500, pp. 337–341, May 2014.
[16] N. Sultana, L. Zhang, J. Yan, J. Chen, W. Cai, S. Razzaque, D. Jeong, W. Sheng, L. Bu, M. Xu, G. Y. Huang, R. J. Hajjar, B. Zhou, A. Moon, and C. L. Cai, “Resident c-kit + cells in the heart are not cardiac stem cells,” *Nat. Commun.*, vol. 6, no. 1, p. 8701, Dec. 2015.
[17] Q. Liu, R. Yang, X. Huang, H. Zhang, L. He, L. Zhang, X. Tian, Y. Nie, S. Hu, Y. Yan, L. Zhang, Z. Qiao, Q.-D. Wang, K. O. Lui, and B. Zhou, “Genetic lineage tracing identifies in situ Kit-expressing cardiomyocytes,” *Cell Res.*, vol. 26, no. 1, pp. 119–130, Jan. 2016.
[18] T. Eschenhagen, R. Bolli, T. Braun, L. J. Field, B. K. Fleischmann, J. Frisén, M. Giacca, J. M. Hare, S. Houser, R. T. Lee, E. Marbán, J. F. Martin, J. D. Molkentin, C. E. Murry, P. R. Riley, P. Ruiz-Lozano, H. A. Sadek, M. A. Sussman, and J. A. Hill, “Cardiomyocyte Regeneration: A Consensus Statement,” *Circulation*, pp. 1–8, 2017.
[19] D. M. Anderson, D. E. Williams, R. Tushinski, S. Gimpel, J. Eisenman, L. A. Cannizzaro, M. Aronson, C. M. Croce, K. Huebner, and D. Cosman, “Alternate splicing of mRNAs encoding human mast cell growth factor and localization of the gene to chromosome 12q22-q24.,” *Cell Growth Differ.*, vol. 2, no. 8, pp. 373–8, Aug. 1991.
[20] M. K. Majumdar, L. Feng, E. Medlock, D. Toksoz, and D. A. Williams, “Identification and mutation of primary and secondary proteolytic cleavage sites in murine stem cell factor cDNA yields biologically active, cell-associated protein.,” *J. Biol. Chem.*, vol. 269, no. 2, pp. 1237–42, Jan. 1994.
[21] Z. Zhang, R. Zhang, A. Joachimiak, J. Schlessinger, and X. P. Kong, “Crystal structure of human stem cell factor: implication for stem cell factor receptor dimerization and activation.,” *Proc. Natl. Acad. Sci. U. S. A.*, vol. 97, no. 14, pp. 7732–7, Jul. 2000.
[22] J. Lennartsson and L. Rönnstrand, “Stem cell factor receptor/c-Kit: from basic science to clinical implications.,” *Physiol. Rev.*, vol. 92, no. 4, pp. 1619–49, 2012.
[23] D. E. Williams, J. Eisenman, A. Baird, C. Rauch, K. Van Ness, C. J. March, L. S. Park, U. Martin, D. Y. Mochizuki, and H. S. Boswell, “Identification of a ligand for the c-kit proto-oncogene.,” *Cell*, vol. 63, no. 1, pp. 167–74, Oct. 1990.
[24] N. G. Copeland, D. J. Gilbert, B. C. Cho, P. J. Donovan, N. A. Jenkins, D. Cosman, D. Anderson, S. D. Lyman, and D. E. Williams, “Mast cell growth factor maps near the steel locus on mouse chromosome 10 and is deleted in a number of steel alleles.,” *Cell*, vol. 63, no. 1, pp. 175–83, Oct. 1990.
[25] B. Chabot, D. A. Stephenson, V. M. Chapman, P. Besmer, and A. Bernstein, “The proto-oncogene c-kit encoding a transmembrane tyrosine kinase receptor maps to the mouse W locus,” *Nature*, vol. 335, no. 6185, pp. 88–89, Sep. 1988.
[26] E. N. Geissler, M. A. Ryan, and D. E. Housman, “The dominant-white spotting (W) locus of the mouse encodes the c-kit proto-oncogene,” *Cell*, vol. 55, no. 1, pp. 185–192, Oct. 1988.
[27] S. Lev, J. M. Blechman, D. Givol, and Y. Yarden, “Steel factor and c-kit

protooncogene: genetic lessons in signal transduction.," *Crit. Rev. Oncog.*, vol. 5, no. 2–3, pp. 141–68, 1994.
[28] P. Besmer, K. Manova, R. Duttlinger, E. J. Huang, A. Packer, C. Gyssler, and R. F. Bachvarova, "The kit-ligand (steel factor) and its receptor c-kit/W: pleiotropic roles in gametogenesis and melanogenesis.," *Dev. Suppl.*, pp. 125–37, 1993.
[29] S. A. Keller, S. Liptay, A. Hajra, and M. H. Meisler, "Transgene-induced mutation of the murine steel locus.," *Proc. Natl. Acad. Sci. U. S. A.*, vol. 87, no. 24, pp. 10019–22, Dec. 1990.
[30] E. Keshet1 ', S. D. Lyman2, D. E. Williams2, D. M. Anderson2, N. A. Jenkins1, N. G. Copeland1, and L. F. Parada1, "Embryonic RNA expression patterns of the c-kit receptor and its cognate ligand suggest multiple functional roles in mouse development," *EMBO J.*, vol. 10, no. 9, pp. 2425–2435, 1991.
[31] V. Alexeev and K. Yoon, "Distinctive role of the cKit receptor tyrosine kinase signaling in mammalian melanocytes.," *J. Invest. Dermatol.*, vol. 126, no. 5, pp. 1102–10, May 2006.
[32] E. S. Russell, "Hereditary anemias of the mouse: A review for geneticists," *Adv. Genet.*, vol. 20, no. C, pp. 357–459, 1979.
[33] L. Ding, T. L. Saunders, G. Enikolopov, and S. J. Morrison, "Endothelial and perivascular cells maintain haematopoietic stem cells," *Nature*, vol. 481, no. 7382, pp. 457–462, 2012.
[34] Y. Kimura, B. Ding, N. Imai, D. J. Nolan, J. M. Butler, and S. Rafii, "c-Kit-Mediated Functional Positioning of Stem Cells to Their Niches Is Essential for Maintenance and Regeneration of Adult Hematopoiesis," *PLoS One*, vol. 6, no. 10, p. e26918, Oct. 2011.
[35] M. Hanoun and P. S. Frenette, "This niche is a maze; an amazing niche.," *Cell Stem Cell*, vol. 12, no. 4, pp. 391–2, Apr. 2013.
[36] E. Gussoni, Y. Soneoka, C. D. Strickland, E. A. Buzney, M. K. Khan, A. F. Flint, L. M. Kunkel, and R. C. Mulligan, "Dystrophin expression in the mdx mouse restored by stem cell transplantation," *Nature*, vol. 401, no. 6751, pp. 390–394, Sep. 1999.
[37] D. Lyden, K. Hattori, S. Dias, C. Costa, P. Blaikie, L. Butros, A. Chadburn, B. Heissig, W. Marks, L. Witte, Y. Wu, D. Hicklin, Z. Zhu, N. R. Hackett, R. G. Crystal, M. A. S. Moore, K. A. Hajjar, K. Manova, R. Benezra, and S. Rafii, "Impaired recruitment of bone-marrow-derived endothelial and hematopoietic precursor cells blocks tumor angiogenesis and growth.," *Nat. Med.*, vol. 7, no. 11, pp. 1194–1201, Nov. 2001.
[38] L. M. Calvi, G. B. Adams, K. W. Weibrecht, J. M. Weber, D. P. Olson, M. C. Knight, R. P. Martin, E. Schipani, P. Divieti, F. R. Bringhurst, L. A. Milner, H. M. Kronenberg, and D. T. Scadden, "Osteoblastic cells regulate the haematopoietic stem cell niche," *Nature*, vol. 425, no. 6960, pp. 841–846, Oct. 2003.
[39] B. O. Zhou, R. Yue, M. M. Murphy, J. G. Peyer, and S. J. Morrison, "Leptin-receptor-expressing mesenchymal stromal cells represent the main source of bone formed by adult bone marrow," *Cell Stem Cell*, vol. 15, no. 2, pp. 154–168, Aug. 2014.
[40] H. C. Blair, S. S. Dong, and B. A. Julian, "Expression of stem cell factor by osteoblasts in normal and hyperparathyroid bone: relation to ectopic mast cell differentiation.," *Virchows Arch.*, vol. 435, no. 1, pp. 50–7, Jul. 1999.
[41] M. Buono, R. Facchini, S. Matsuoka, S. Thongjuea, D. Waithe, T. C. Luis, A. Giustacchini, P. Besmer, A. J. Mead, S. E. W. Jacobsen, and C. Nerlov, "A

dynamic niche provides Kit ligand in a stage-specific manner to the earliest thymocyte progenitors," *Nat. Cell Biol.*, vol. 18, no. 2, pp. 157–167, Jan. 2016.
[42] C. Liao, R. C. Booker, S. J. Morrison, and L. Q. Le, "Identification of hair shaft progenitors that create a niche for hair pigmentation," pp. 1–13, 2017.
[43] M. E. Rothenberg, Y. Nusse, T. Kalisky, J. J. Lee, P. Dalerba, F. Scheeren, N. Lobo, S. Kulkarni, S. Sim, D. Qian, P. A. Beachy, P. J. Pasricha, S. R. Quake, and M. F. Clarke, "Identification of a cKit+ Colonic Crypt Base Secretory Cell That Supports Lgr5+ Stem Cells in Mice," *Gastroenterology*, vol. 142, no. 5, p. 1195–1205.e6, May 2012.
[44] S. S. Fazel, L. Chen, D. Angoulvant, S.-H. Li, R. D. Weisel, A. Keating, and R.-K. Li, "Activation of c-kit is necessary for mobilization of reparative bone marrow progenitor cells in response to cardiac injury," *FASEB J.*, vol. 22, no. 3, pp. 930–940, Oct. 2007.
[45] F.-L. Xiang, X. Lu, L. Hammoud, P. Zhu, P. Chidiac, J. Robbins, and Q. Feng, "Cardiomyocyte-Specific Overexpression of Human Stem Cell Factor Improves Cardiac Function and Survival After Myocardial Infarction in Mice," *Circulation*, vol. 120, no. 12, pp. 1065–1074, Sep. 2009.
[46] E. Yaniz-Galende, J. Chen, E. Chemaly, L. Liang, J.-S. Hulot, L. McCollum, T. Arias, V. Fuster, K. M. Zsebo, and R. J. Hajjar, "Stem cell factor gene transfer promotes cardiac repair after myocardial infarction via in situ recruitment and expansion of c-kit+ cells.," *Circ. Res.*, vol. 111, no. 11, pp. 1434–45, Nov. 2012.
[47] K. Ishikawa, K. Fish, J. Aguero, E. Yaniz-Galende, D. Jeong, C. Kho, L. Tilemann, L. Fish, L. Liang, A. A. Eltoukhy, D. G. Anderson, K. Zsebo, K. D. Costa, and R. J. Hajjar, "Stem Cell Factor Gene Transfer Improves Cardiac Function After Myocardial Infarction in Swine," *Circ. Hear. Fail.*, vol. 8, no. 1, pp. 167–174, Jan. 2015.
[48] H. Björkbacka, I. Yao Mattisson, M. Wigren, O. Melander, G. N. Fredrikson, E. Bengtsson, I. Gonçalves, P. Almgren, J. O. Lagerstedt, M. Orho-Melander, G. Engström, and J. Nilsson, "Plasma stem cell factor levels are associated with risk of cardiovascular disease and death," *J. Intern. Med.*, Sep. 2017.
[49] M. Wigren, S. Rattik, K. Hultman, H. Björkbacka, G. Nordin-Fredrikson, E. Bengtsson, B. Hedblad, A. Siegbahn, I. Gonçalves, and J. Nilsson, "Decreased levels of stem cell factor in subjects with incident coronary events," *J. Intern. Med.*, vol. 279, no. 2, pp. 180–191, Feb. 2016.
[50] Z. Xu, S. Cang, T. Yang, and D. Liu, "Cardiotoxicity of tyrosine kinase inhibitors in chronic myelogenous leukemia therapy," *Hematol. Rep.*, vol. 1, no. 1, p. 4, Mar. 2009.
[51] T. D. Kim, P. le Coutre, M. Schwarz, P. Grille, M. Levitin, S. Fateh-Moghadam, F. J. Giles, B. Dörken, W. Haverkamp, and C. Köhncke, "Clinical cardiac safety profile of nilotinib," *Haematologica*, vol. 97, no. 6, pp. 883–889, Jun. 2012.
[52] O. Pasvolsky, A. Leader, Z. Iakobishvili, Y. Wasserstrum, R. Kornowski, and P. Raanani, "Tyrosine kinase inhibitor associated vascular toxicity in chronic myeloid leukemia," *Cardio-Oncology*, vol. 1, no. 1, pp. 1–10, Dec. 2015.
[53] E. Keshet, S. D. Lyman, D. E. Williams, D. M. Anderson, N. A. Jenkins, N. G. Copeland, and L. F. Parada, "Embryonic RNA expression patterns of the c-kit receptor and its cognate ligand suggest multiple functional roles in mouse development.," *EMBO J.*, vol. 10, no. 9, pp. 2425–35, Sep. 1991.
[54] Y. Matsui, K. M. Zsebo, and B. L. M. Hogan, "Embryonic expression of a haematopoietic growth factor encoded by the SI locus and the ligand for c-kit," *Nature*, vol. 347, no. 6294, pp. 667–669, Oct. 1990.
[55] B. Motro, D. van der Kooy, J. Rossant, A. Reith, and A. Bernstein, "Contiguous

patterns of c-kit and steel expression: analysis of mutations at the W and Sl loci.," *Development*, vol. 113, no. 4, pp. 1207–21, Dec. 1991.
[56] M. Xin, E. N. Olson, and R. Bassel-Duby, "Mending broken hearts: cardiac development as a basis for adult heart regeneration and repair," *Nat. Rev. Mol. Cell Biol.*, vol. 14, no. 8, pp. 529–541, Aug. 2013.
[57] S. M. Wu, Y. Fujiwara, S. M. Cibulsky, D. E. Clapham, C. Lien, T. M. Schultheiss, and S. H. Orkin, "Developmental Origin of a Bipotential Myocardial and Smooth Muscle Cell Precursor in the Mammalian Heart," *Cell*, vol. 127, no. 6, pp. 1137–1150, Dec. 2006.
[58] K. E. Hatzistergos, L. M. Takeuchi, D. Saur, B. Seidler, S. M. Dymecki, J. J. Mai, I. A. White, W. Balkan, R. M. Kanashiro-Takeuchi, A. V Schally, and J. M. Hare, "cKit + cardiac progenitors of neural crest origin," *Proc. Natl. Acad. Sci.*, vol. 112, no. 42, pp. 13051–13056, Oct. 2015.
[59] A. F. M. MOORMAN and V. M. CHRISTOFFELS, "Cardiac Chamber Formation: Development, Genes, and Evolution," *Physiol. Rev.*, vol. 83, no. 4, pp. 1223–1267, Oct. 2003.
[60] J. Rossant and J. C. Cross, "Placental development: Lessons from mouse mutants," *Nature Reviews Genetics*, vol. 2, no. 7. Nature Publishing Group, pp. 538–548, 01-Jul-2001.
[61] P. P. L. Tam and R. R. Behringer, "Mouse gastrulation: The formation of a mammalian body plan," *Mechanisms of Development*, vol. 68, no. 1–2. Elsevier, pp. 3–25, 01-Nov-1997.
[62] M. Buckingham, S. Meilhac, and S. Zaffran, "Building the mammalian heart from two sources of myocardial cells," *Nat. Rev. Genet.*, vol. 6, no. 11, pp. 826–837, Nov. 2005.
[63] F. Lescroart, S. Chabab, X. Lin, S. Rulands, C. Paulissen, A. Rodolosse, H. Auer, Y. Achouri, C. Dubois, A. Bondue, B. D. Simons, and C. Blanpain, "Early lineage restriction in temporally distinct populations of Mesp1 progenitors during mammalian heart development," *Nat. Cell Biol.*, vol. 16, no. 9, pp. 829–840, Aug. 2014.
[64] X. Liang, G. Wang, L. Lin, J. Lowe, Q. Zhang, L. Bu, Y. Chen, J. Chen, Y. Sun, and S. M. Evans, "HCN4 dynamically marks the first heart field and conduction system precursors," *Circ. Res.*, vol. 113, no. 4, pp. 399–407, Aug. 2013.
[65] K.-L. Laugwitz, A. Moretti, L. Caron, A. Nakano, and K. R. Chien, "Islet1 cardiovascular progenitors: a single source for heart lineages?," *Development*, vol. 135, no. 2, pp. 193–205, Jan. 2008.
[66] M. P. Santini, E. Forte, R. P. Harvey, and J. C. Kovacic, "Developmental origin and lineage plasticity of endogenous cardiac stem cells," *Development*, vol. 143, no. 8, pp. 1242–1258, Apr. 2016.
[67] "Isl1 Identifies a Cardiac Progenitor Population that Proliferates Prior to Differentiation and Contributes a Majority of Cells to the Heart," *Dev. Cell*, vol. 5, no. 6, pp. 877–889, Dec. 2003.
[68] A. Von Gise and W. T. Pu, "Endocardial and epicardial epithelial to mesenchymal transitions in heart development and disease," *Circ. Res.*, vol. 110, no. 12, pp. 1628–1645, Jun. 2012.
[69] I. Washington Smoak, N. A. Byrd, R. Abu-Issa, M. M. Goddeeris, R. Anderson, J. Morris, K. Yamamura, J. Klingensmith, and E. N. Meyers, "Sonic hedgehog is required for cardiac outflow tract and neural crest cell development," *Dev. Biol.*, vol. 283, no. 2, pp. 357–372, Jul. 2005.
[70] B. Zhou, Q. Ma, S. Rajagopal, S. M. Wu, I. Domian, J. Rivera-Feliciano, D. Jiang, A. von Gise, S. Ikeda, K. R. Chien, and W. T. Pu, "Epicardial progenitors

contribute to the cardiomyocyte lineage in the developing heart," *Nature*, vol. 454, no. 7200, pp. 109–113, Jul. 2008.
[71] C.-J. Lin, C.-Y. Lin, C.-H. Chen, B. Zhou, and C.-P. Chang, "Partitioning the heart: mechanisms of cardiac septation and valve development.," *Development*, vol. 139, no. 18, pp. 3277–99, Sep. 2012.
[72] M. P. Santini, E. Forte, R. P. Harvey, and J. C. Kovacic, "Developmental origin and lineage plasticity of endogenous cardiac stem cells," *Development*, vol. 143, pp. 1242–1258, 2016.
[73] X. Tian, T. Hu, H. Zhang, L. He, X. Huang, Q. Liu, W. Yu, L. He, Z. Yang, Z. Zhang, T. P. Zhong, X. Yang, Z. Yang, Y. Yan, A. Baldini, Y. Sun, J. Lu, R. J. Schwartz, S. M. Evans, A. C. Gittenberger-de Groot, K. Red-Horse, and B. Zhou, "Subepicardial endothelial cells invade the embryonic ventricle wall to form coronary arteries.," *Cell Res.*, vol. 23, no. 9, pp. 1075–1090, 2013.
[74] K. Red-Horse, H. Ueno, I. L. Weissman, and M. A. Krasnow, "Coronary arteries form by developmental reprogramming of venous cells," *Nature*, vol. 464, no. 7288, pp. 549–553, Mar. 2010.
[75] H. I. Chen, B. Sharma, B. N. Akerberg, H. J. Numi, R. Kivela, P. Saharinen, H. Aghajanian, A. S. McKay, P. E. Bogard, A. H. Chang, A. H. Jacobs, J. A. Epstein, K. Stankunas, K. Alitalo, and K. Red-Horse, "The sinus venosus contributes to coronary vasculature through VEGFC-stimulated angiogenesis," *Development*, vol. 141, no. 23, pp. 4500–4512, Dec. 2014.
[76] H. I. Chen, A. Poduri, H. Numi, R. Kivela, P. Saharinen, A. S. McKay, B. Raftrey, J. Churko, X. Tian, B. Zhou, J. C. Wu, K. Alitalo, and K. Red-Horse, "VEGF-C and aortic cardiomyocytes guide coronary artery stem development," *J. Clin. Invest.*, vol. 124, no. 11, pp. 4899–4914, Nov. 2014.
[77] X. Tian, T. Hu, L. He, H. Zhang, X. Huang, R. E. Poelmann, W. Liu, Z. Yang, Y. Yan, W. T. Pu, and B. Zhou, "Peritruncal Coronary Endothelial Cells Contribute to Proximal Coronary Artery Stems and Their Aortic Orifices in the Mouse Heart," *PLoS One*, vol. 8, no. 11, p. e80857, Nov. 2013.
[78] X. Tian, T. Hu, H. Zhang, L. He, X. Huang, Q. Liu, W. Yu, L. He, Z. Yang, Y. Yan, X. Yang, T. P. Zhong, W. T. Pu, and B. Zhou, "Vessel formation. De novo formation of a distinct coronary vascular population in neonatal heart.," *Science*, vol. 345, no. 6192, pp. 90–4, Jul. 2014.
[79] C. G. Burns and C. E. Burns, "Development. A crowning achievement for deciphering coronary origins," *Science (80-.).*, vol. 345, no. 6192, pp. 28–29, 2014.
[80] W. C. Aird, "Phenotypic heterogeneity of the endothelium: I. Structure, function, and mechanisms," *Circ. Res.*, vol. 100, no. 2, pp. 158–173, 2007.
[81] M. R. Swift and B. M. Weinstein, "Arterial-Venous Specification During Development," *Circ. Res.*, vol. 104, no. 5, pp. 576–588, Feb. 2009.
[82] C. C. Hong, T. Kume, and R. T. Peterson, "Role of Crosstalk Between Phosphatidylinositol 3-Kinase and Extracellular Signal-Regulated Kinase/Mitogen-Activated Protein Kinase Pathways in Artery-Vein Specification," *Circ. Res.*, vol. 103, no. 6, pp. 573–579, Sep. 2008.
[83] J. Aitsebaomo, A. L. Portbury, J. C. Schisler, and C. Patterson, "Brothers and Sisters: Molecular Insights Into Arterial-Venous Heterogeneity," *Circ. Res.*, vol. 103, no. 9, pp. 929–939, Jul. 2008.
[84] L. T. Krebs, Y. Xue, C. R. Norton, J. R. Shutter, M. Maguire, J. P. Sundberg, D. Gallahan, V. Closson, J. Kitajewski, R. Callahan, G. H. Smith, K. L. Stark, and T. Gridley, "Notch signaling is essential for vascular morphogenesis in mice.," *Genes Dev.*, vol. 14, no. 11, pp. 1343–52, Jun. 2000.

[85] N. W. Gale, P. Baluk, L. Pan, M. Kwan, J. Holash, T. M. DeChiara, D. M. McDonald, and G. D. Yancopoulos, “Ephrin-B2 Selectively Marks Arterial Vessels and Neovascularization Sites in the Adult, with Expression in Both Endothelial and Smooth-Muscle Cells,” *Dev. Biol.*, vol. 230, no. 2, pp. 151–160, Feb. 2001.
[86] O. Nakagawa, M. Nakagawa, J. A. Richardson, E. N. Olson, and D. Srivastava, “HRT1, HRT2, and HRT3: a new subclass of bHLH transcription factors marking specific cardiac, somitic, and pharyngeal arch segments.,” *Dev. Biol.*, vol. 216, no. 1, pp. 72–84, Dec. 1999.
[87] S. S. Gerety, H. U. Wang, Z. F. Chen, and D. J. Anderson, “Symmetrical mutant phenotypes of the receptor EphB4 and its specific transmembrane ligand ephrin-B2 in cardiovascular development.,” *Mol. Cell*, vol. 4, no. 3, pp. 403–14, Sep. 1999.
[88] L. Yuan, D. Moyon, L. Pardanaud, C. Bréant, M. J. Karkkainen, K. Alitalo, and A. Eichmann, “Abnormal lymphatic vessel development in neuropilin 2 mutant mice.,” *Development*, vol. 129, no. 20, pp. 4797–806, Oct. 2002.
[89] L.-R. You, F.-J. Lin, C. T. Lee, F. J. DeMayo, M.-J. Tsai, and S. Y. Tsai, “Suppression of Notch signalling by the COUP-TFII transcription factor regulates vein identity.,” *Nature*, vol. 435, no. 7038, pp. 98–104, May 2005.
[90] B. Ciszek, D. Skubiszewska, and A. Ratajska, “The anatomy of the cardiac veins in mice,” *J. Anat.*, vol. 211, no. 1, pp. 53–63, Jul. 2007.
[91] L. He, X. Huang, O. Kanisicak, Y. Li, Y. Wang, Y. Li, W. Pu, Q. Liu, H. Zhang, X. Tian, H. Zhao, X. Liu, S. Zhang, Y. Nie, S. Hu, X. Miao, Q.-D. Wang, F. Wang, T. Chen, Q. Xu, K. O. Lui, J. D. Molkentin, and B. Zhou, “Preexisting endothelial cells mediate cardiac neovascularization after injury.,” *J. Clin. Invest.*, vol. 127, no. 8, pp. 2968–2981, Aug. 2017.
[92] A. Nagy, “Cre recombinase: The universal reagent for genome tailoring,” *Genesis*, vol. 26, no. 2. pp. 99–109, 2000.
[93] P. C. Orban, D. Chui, and J. D. Marth, “Tissue- and site-specific DNA recombination in transgenic mice.,” *Proc. Natl. Acad. Sci. U. S. A.*, vol. 89, no. 15, pp. 6861–5, Aug. 1992.
[94] R. Feil, J. Wagner, D. Metzger, and P. Chambon, “Regulation of Cre Recombinase Activity by Mutated Estrogen Receptor Ligand-Binding Domains,” *Biochem. Biophys. Res. Commun.*, vol. 237, no. 3, pp. 752–757, Aug. 1997.
[95] E. Casanova, S. Fehsenfeld, T. Lemberger, D. R. Shimshek, R. Sprengel, and T. Mantamadiotis, “ER-based double iCre fusion protein allows partial recombination in forebrain,” *Genesis*, vol. 34, no. 3, pp. 208–214, Nov. 2002.
[96] Y. N. Tallini, K. S. Greene, M. Craven, A. Spealman, M. Breitbach, J. Smith, P. J. Fisher, M. Steffey, M. Hesse, R. M. Doran, A. Woods, B. Singh, A. Yen, B. K. Fleischmann, and M. I. Kotlikoff, “C-Kit Expression Identifies Cardiovascular Precursors in the Neonatal Heart,” *Proc Natl Acad Sci U S A*, vol. 106, no. 6, pp. 1808–1813, 2009.
[97] L. Madisen, T. A. Zwingman, S. M. Sunkin, S. W. Oh, H. A. Zariwala, H. Gu, L. L. Ng, R. D. Palmiter, M. J. Hawrylycz, A. R. Jones, E. S. Lein, and H. Zeng, “A robust and high-throughput Cre reporting and characterization system for the whole mouse brain.,” *Nat. Neurosci.*, vol. 13, no. 1, pp. 133–40, Jan. 2010.
[98] M. D. Muzumdar, B. Tasic, K. Miyamichi, N. Li, and L. Luo, “A global double-fluorescent cre reporter mouse,” *Genesis*, vol. 45, no. 9, pp. 593–605, Sep. 2007.
[99] M. Hesse, A. Raulf, G.-A. Pilz, C. Haberlandt, A. M. Klein, R. Jabs, H. Zaehres,

C. J. Fügemann, K. Zimmermann, J. Trebicka, A. Welz, A. Pfeifer, W. Röll, M. I. Kotlikoff, C. Steinhäuser, M. Götz, H. R. Schöler, and B. K. Fleischmann, “Direct visualization of cell division using high-resolution imaging of M-phase of the cell cycle.,” *Nat. Commun.*, vol. 3, p. 1076, Sep. 2012.

[100] Y. Y. Kisanuki, R. E. Hammer, J. Miyazaki, S. C. Williams, J. A. Richardson, and M. Yanagisawa, “Tie2-Cre Transgenic Mice: A New Model for Endothelial Cell-Lineage Analysis in Vivo,” *Dev. Biol.*, vol. 230, no. 2, pp. 230–242, Feb. 2001.

[101] A. Monvoisin, J. A. Alva, J. J. Hofmann, A. C. Zovein, T. F. Lane, and M. L. Iruela-Arispe, “VE-cadherin-CreERT2 transgenic mouse: A model for inducible recombination in the endothelium,” *Dev. Dyn.*, vol. 235, no. 12, pp. 3413–3422, Dec. 2006.

[102] K. Mullis, F. Faloona, S. Scharf, R. Saiki, G. Horn, and H. Erlich, “Specific enzymatic amplification of DNA in vitro: The polymerase chain reaction,” *Cold Spring Harb. Symp. Quant. Biol.*, vol. 51, no. 1, pp. 263–273, Jan. 1986.

[103] D. Pirici, L. Mogoanta, S. Kumar-Singh, I. Pirici, C. Margaritescu, C. Simionescu, and R. Stanescu, “Antibody elution method for multiple immunohistochemistry on primary antibodies raised in the same species and of the same subtype.,” *J. Histochem. Cytochem.*, vol. 57, no. 6, pp. 567–575, 2009.

[104] N. C. Shaner, R. E. Campbell, P. A. Steinbach, B. N. G. Giepmans, A. E. Palmer, and R. Y. Tsien, “Improved monomeric red, orange and yellow fluorescent proteins derived from Discosoma sp. red fluorescent protein,” *Nat. Biotechnol.*, vol. 22, no. 12, pp. 1567–1572, Dec. 2004.

[105] F. Bernex, P. De Sepulveda, C. Kress, C. Elbaz, C. Delouis, and J. J. Panthier, “Spatial and temporal patterns of c-kit-expressing cells in WlacZ/+ and WlacZ/WlacZ mouse embryos.,” *Development*, vol. 122, pp. 3023–3033, 1996.

[106] K. Manova, R. F. Bachvarova, E. J. Huang, S. Sanchez, S. M. Pronovost, E. Velazquez, B. McGuire, and P. Besmer, “c-kit receptor and ligand expression in postnatal development of the mouse cerebellum suggests a function for c-kit in inhibitory interneurons.,” *J. Neurosci.*, vol. 12, no. 12, pp. 4663–76, Dec. 1992.

[107] S. Gory, M. Vernet, M. Laurent, E. Dejana, J. Dalmon, and P. Huber, “The vascular endothelial-cadherin promoter directs endothelial-specific expression in transgenic mice.,” *Blood*, vol. 93, no. 1, pp. 184–192, Jan. 1999.

[108] P. Soriano, “Generalized lacZ expression with the ROSA26 Cre reporter strain [1],” *Nature Genetics*, vol. 21, no. 1. pp. 70–71, 01-Jan-1999.

[109] T. M. Schlaeger, S. Bartunkova, J. A. Lawitts, G. Teichmann, W. Risau, U. Deutsch, and T. N. Sato, “Uniform vascular-endothelial-cell-specific gene expression in both embryonic and adult transgenic mice.,” *Proc. Natl. Acad. Sci. U. S. A.*, vol. 94, no. 7, pp. 3058–63, Apr. 1997.

[110] W. Roell, Y. Fan, Y. Xia, E. Stoecker, P. Sasse, E. Kolossov, W. Bloch, H. Metzner, C. Schmitz, K. Addicks, J. Hescheler, A. Welz, and B. K. Fleischmann, “Cellular cardiomyoplasty in a transgenic mouse model.,” *Transplantation*, vol. 73, no. 3, pp. 462–5, Feb. 2002.

[111] E. R. Porrello, A. I. Mahmoud, E. Simpson, J. A. Hill, J. A. Richardson, E. N. Olson, and H. A. Sadek, “Transient Regenerative Potential of the Neonatal Mouse Heart,” *Science (80-.).*, vol. 331, no. 6020, pp. 1078–1080, Feb. 2011.

[112] H. Mizuguchi, Z. Xu, A. Ishii-Watabe, E. Uchida, and T. Hayakawa, “IRES-Dependent Second Gene Expression Is Significantly Lower Than Cap-Dependent First Gene Expression in a Bicistronic Vector,” *Mol. Ther.*, vol. 1,

no. 4, pp. 376–382, Apr. 2000.
[113] F. Li, “Rapid Transition of Cardiac Myocytes from Hyperplasia to Hypertrophy During Postnatal Development,” *J. Mol. Cell. Cardiol.*, vol. 28, no. 8, pp. 1737–1746, Aug. 1996.
[114] C. Jopling, E. Sleep, M. Raya, M. Martí, A. Raya, and J. C. I. Belmonte, “Zebrafish heart regeneration occurs by cardiomyocyte dedifferentiation and proliferation,” *Nature*, vol. 464, no. 7288, pp. 606–609, Mar. 2010.
[115] T. Kubin, J. Pöling, S. Kostin, P. Gajawada, S. Hein, W. Rees, A. Wietelmann, M. Tanaka, H. Lörchner, S. Schimanski, M. Szibor, H. Warnecke, and T. Braun, “Oncostatin M Is a Major Mediator of Cardiomyocyte Dedifferentiation and Remodeling,” *Cell Stem Cell*, vol. 9, no. 5, pp. 420–432, Nov. 2011.
[116] R. B. Driesen, F. K. Verheyen, W. Debie, E. Blaauw, F. A. Babiker, R. N. M. Cornelussen, J. Ausma, M.-H. Lenders, M. Borgers, C. Chaponnier, and F. C. S. Ramaekers, “Re-expression of alpha skeletal actin as a marker for dedifferentiation in cardiac pathologies,” *J. Cell. Mol. Med.*, vol. 13, no. 5, pp. 896–908, May 2009.
[117] N. Smart, S. Bollini, K. N. Dubé, J. M. Vieira, B. Zhou, S. Davidson, D. Yellon, J. Riegler, A. N. Price, M. F. Lythgoe, W. T. Pu, and P. R. Riley, “De novo cardiomyocytes from within the activated adult heart after injury,” *Nature*, vol. 474, no. 7353, pp. 640–644, Jun. 2011.
[118] M. Leone, A. Magadum, and F. B. Engel, “Cardiomyocyte proliferation in cardiac development and regeneration: a guide to methodologies and interpretations,” *Am. J. Physiol. Circ. Physiol.*, vol. 309, no. 8, pp. H1237–H1250, Oct. 2015.
[119] F. Laube, M. Heister, C. Scholz, T. Borchardt, and T. Braun, “Re-programming of newt cardiomyocytes is induced by tissue regeneration,” *J. Cell Sci.*, vol. 119, no. 22, pp. 4719–4729, Oct. 2006.
[120] E. R. Porrello, A. I. Mahmoud, E. Simpson, J. A. Hill, J. A. Richardson, E. N. Olson, and H. A. Sadek, “Transient regenerative potential of the neonatal mouse heart.,” *Science*, vol. 331, no. 6020, pp. 1078–80, Feb. 2011.
[121] X. Tian, W. T. Pu, and B. Zhou, “Cellular origin and developmental program of coronary angiogenesis,” *Circ. Res.*, vol. 116, no. 3, pp. 515–530, Jan. 2015.
[122] M. Heil, I. Eitenmüller, T. Schmitz-Rixen, and W. Schaper, “Arteriogenesis versus angiogenesis: Similarities and differences,” *J. Cell. Mol. Med.*, vol. 10, no. 1, pp. 45–55, 2006.
[123] J.-T. Chi, H. Y. Chang, G. Haraldsen, F. L. Jahnsen, O. G. Troyanskaya, D. S. Chang, Z. Wang, S. G. Rockson, M. van de Rijn, D. Botstein, and P. O. Brown, “Endothelial cell diversity revealed by global expression profiling.,” *Proc. Natl. Acad. Sci. U. S. A.*, vol. 100, no. 19, pp. 10623–8, Sep. 2003.
[124] M. Barnes, A. E. Heywood, A. Mahimbo, B. Rahman, A. T. Newall, and C. R. Macintyre, “Acute myocardial infarction and influenza: a meta-analysis of case-control studies.,” *Heart*, vol. 101, no. 21, pp. 1738–47, Nov. 2015.
[125] X. L. Tang, Q. Li, G. Rokosh, S. K. Sanganalmath, N. Chen, Q. Ou, H. Stowers, G. Hunt, and R. Bolli, “Long-Term Outcome of Administration of c-kitPOSCardiac Progenitor Cells after Acute Myocardial Infarction: Transplanted Cells Do not Become Cardiomyocytes, but Structural and Functional Improvement and Proliferation of Endogenous Cells Persist for at Leas,” *Circ. Res.*, vol. 118, no. 7, pp. 1091–1105, Apr. 2016.
[126] S. D. Clarke, “Regulation of fatty acid synthase gene expression: an approach for reducing fat accumulation.,” *Journal of animal science*, vol. 71, no. 7. NIH Public Access, pp. 1957–1965, Jan-1993.

[127] J. H. van Berlo and J. D. Molkentin, “Commentaries on Cutting Edge Science: Most of the Dust Has Settled,” *Circ. Res.*, vol. 118, pp. 17–20, 2016.
[128] S. Méndez-Ferrer, T. V Michurina, F. Ferraro, A. R. Mazloom, B. D. Macarthur, S. A. Lira, D. T. Scadden, A. Ma’ayan, G. N. Enikolopov, and P. S. Frenette, “Mesenchymal and haematopoietic stem cells form a unique bone marrow niche.,” *Nature*, vol. 466, no. 7308, pp. 829–34, Aug. 2010.
[129] Y. Omatsu, T. Sugiyama, H. Kohara, G. Kondoh, N. Fujii, K. Kohno, and T. Nagasawa, “The Essential Functions of Adipo-osteogenic Progenitors as the Hematopoietic Stem and Progenitor Cell Niche,” *Immunity*, vol. 33, no. 3, pp. 387–399, Sep. 2010.
[130] M. C. Heinrich, D. C. Dooley, A. C. Freed, L. Band, M. E. Hoatlin, W. W. Keeble, S. T. Peters, K. V Silvey, F. S. Ey, and D. Kabat, “Constitutive expression of steel factor gene by human stromal cells.,” *Blood*, vol. 82, no. 3, pp. 771–83, Aug. 1993.
[131] H. C. Blair, B. A. Julian, X. Cao, S. E. Jordan, and S.-S. Dong, “Parathyroid Hormone-Regulated Production of Stem Cell Factor in Human Osteoblasts and Osteoblast-like Cells,” *Biochem. Biophys. Res. Commun.*, vol. 255, no. 3, pp. 778–784, Feb. 1999.
[132] X. W. Yang and S. Gong, “An Overview on the Generation of BAC Transgenic Mice for Neuroscience Research,” in *Current Protocols in Neuroscience*, vol. Chapter 5, Hoboken, NJ, USA: John Wiley & Sons, Inc., 2005, p. Unit 5.20.
[133] Q. Chen, H. Zhang, Y. Liu, S. Adams, H. Eilken, M. Stehling, M. Corada, E. Dejana, B. Zhou, and R. H. Adams, “Endothelial cells are progenitors of cardiac pericytes and vascular smooth muscle cells,” *Nat. Commun.*, vol. 7, p. 12422, Aug. 2016.
[134] C. Villa del Campo, G. Lioux, R. Carmona, R. Sierra, R. Muñoz-Chápuli, C. Clavería, and M. Torres, “Myc overexpression enhances epicardial contribution to the developing heart and promotes extensive expansion of the cardiomyocyte population,” *Sci. Rep.*, vol. 6, no. 1, p. 35366, Dec. 2016.
[135] W. C. Aird, “Phenotypic heterogeneity of the endothelium: II. Representative vascular beds,” *Circ. Res.*, vol. 100, no. 2, pp. 174–190, 2007.
[136] M. Hauser, “Congenital anomalies of the coronary arteries.,” *Heart*, vol. 91, no. 9, pp. 1240–5, Sep. 2005.
[137] W. Risau, “Mechanisms of angiogenesis,” *Nature*, vol. 386, no. 6626, pp. 671–674, Apr. 1997.
[138] P. C. Stapor, R. S. Sweat, D. C. Dashti, A. M. Betancourt, and W. L. Murfee, “Pericyte dynamics during angiogenesis: new insights from new identities.,” *J. Vasc. Res.*, vol. 51, no. 3, pp. 163–74, 2014.
[139] K. S. Volz, A. H. Jacobs, H. I. Chen, A. Poduri, A. S. McKay, D. P. Riordan, N. Kofler, J. Kitajewski, I. Weissman, and K. Red-Horse, “Pericytes are progenitors for coronary artery smooth muscle,” *Elife*, vol. 4, p. e10036, Oct. 2015.
[140] K. Othman-Hassan, K. Patel, M. Papoutsi, M. Rodriguez-Niedenführ, B. Christ, and J. Wilting, “Arterial identity of endothelial cells is controlled by local cues.,” *Dev. Biol.*, vol. 237, no. 2, pp. 398–409, Sep. 2001.
[141] O. I. Tsukurov, C. J. Kwolek, G. J. L’Italien, A. Benbrahim, B. B. Milinazzo, N. E. Conroy, J. P. Gertler, R. W. Orkin, and W. M. Abbott, “The response of adult human saphenous vein endothelial cells to combined pressurized pulsatile flow and cyclic strain, in vitro,” *Ann. Vasc. Surg.*, vol. 14, no. 3, pp. 260–267, May 2000.
[142] S. Kwei, G. Stavrakis, M. Takahas, G. Taylor, M. J. Folkman, M. A. Gimbrone,

and G. García-Cardeña, “Early Adaptive Responses of the Vascular Wall during Venous Arterialization in Mice,” *Am. J. Pathol.*, vol. 164, no. 1, pp. 81–89, Jan. 2004.
[143] a K. Raap, “Advances in fluorescence in situ hybridization.,” *Mutat. Res.*, vol. 400, no. 1–2, pp. 287–298, May 1998.
[144] Y. Watanabe and M. Buckingham, “The formation of the embryonic mouse heart: heart fields and myocardial cell lineages.,” *Ann. N. Y. Acad. Sci.*, vol. 1188, no. 1, pp. 15–24, Feb. 2010.
[145] J.-D. Drenckhahn, Q. P. Schwarz, S. Gray, A. Laskowski, H. Kiriazis, Z. Ming, R. P. Harvey, X.-J. Du, D. R. Thorburn, and T. C. Cox, “Compensatory growth of healthy cardiac cells in the presence of diseased cells restores tissue homeostasis during heart development.,” *Dev. Cell*, vol. 15, no. 4, pp. 521–33, Oct. 2008.
[146] B. J. Haubner, T. Schuetz, and J. M. Penninger, “A reproducible protocol for neonatal ischemic injury and cardiac regeneration in neonatal mice.,” *Basic Res. Cardiol.*, vol. 111, no. 6, p. 64, Nov. 2016.
[147] L. He, Q. Liu, T. Hu, X. Huang, H. Zhang, X. Tian, Y. Yan, L. Wang, Y. Huang, L. Miquerol, J. D. Wythe, and B. Zhou, “Genetic lineage tracing discloses arteriogenesis as the main mechanism for collateral growth in the mouse heart,” *Cardiovasc. Res.*, vol. 109, no. 3, pp. 419–430, 2016.
[148] P. Ahuja, E. Perriard, J.-C. Perriard, and E. Ehler, “Sequential myofibrillar breakdown accompanies mitotic division of mammalian cardiomyocytes,” *J. Cell Sci.*, vol. 117, no. 15, pp. 3295–3306, Jul. 2004.
[149] P. P. Rumyantsev, “Electron microscope study of the myofibril partial disintegration and recovery in the mitotically dividing cardiac muscle cells,” *Zeitschrift f*[illegible]*r Zellforsch. und mikroskopische Anat.*, vol. 129, no. 4, pp. 471–499, 1972.
[150] M. Ravi, K. Nivedita, and G. M. Pai, “Chromatin condensation dynamics and implications of induced premature chromosome condensation,” *Biochimie*, vol. 95, no. 2. pp. 124–133, Feb-2013.
[151] M. Gemberling, T. J. Bailey, D. R. Hyde, and K. D. Poss, “The zebrafish as a model for complex tissue regeneration,” *Trends in Genetics*, vol. 29, no. 11. Elsevier Current Trends, pp. 611–620, 01-Nov-2013.
[152] B. Zhou, A. von Gise, Q. Ma, Y. Hu, W. Pu, Y. Li, W. Pu, Q. Liu, H. Zhang, X. Tian, H. Zhao, X. Liu, S. Zhang, Y. Nie, S. Hu, X. Miao, Q.-D. Wang, F. Wang, T. Chen, Q. Xu, K. O. Lui, J. D. Molkentin, and B. Zhou, “Preexisting endothelial cells mediate cardiac neovascularization after injury,” *Dev Biol*, vol. 338, no. 2, pp. 251–261, Jun. 2017.

7. ABBREVIATIONS

A	atria
AF	autofluorescence
α-SMA	alpha smooth muscle actin
AVC	atrioventricular canal
BAC	bacterial artificial chromosome
BF	bright field
bp	base pair
C	cytokinesis
CAG	chicken β-actin promoter with CMV enhancer element
CD31	Cluster of differentiation 31
CD45	Cluster of differentiation 45
c-kit	cellular homolog of the feline scarcoma viral oncogene
Chr	Chromosome
COUP	chicken ovalbumin upstream promoter
COUP-TFII	COUP transcription factor 2
Cre	Causes recombination
$CreER^{T2}$	estrogen receptor (T2 mutant) fused Cre recombinase
Cy	Cyanine
DAPI	4',6-diamidino-2-phenylindol
Dll4	Delta-like 4
DMSO	dimethyl sulfoxide

DNA	Deoxyribonucleic acid
DPBS	Dulbecco’s Phosphate-Buffered Saline
dps	day post surgery
DS	donkey serum
E	embryonic day
EC	endothelial cell
EDTA	Ethylenediaminetetraacetic acid
eGFP	enhanced green fluorescent protein
EphB4	Ephrin type-B receptor 4
ER	human estrogen receptor
EtBr	ethidium bromide
FG	foregut
FHF	first heart field
GFP	green fluorescent protein
Hey	Hairy/enhancer-of-split related with YRPW motif protein
HG	hindgut
HRP	horse radish peroxidase
HSC	hematopoietic stem cells
HSP90	heat shock protein 90
H_2O_2	Hydrogen Peroxide
IgG	immunoglobulin G
IP	intraperitoneal injection
IRES	internal ribosome entry site

iVS	intraventricular septum
K	karyokinesis
kb	kilo base pairs
KCl	Potassium Chloride
LA	left atrium
LAD	left anterior descending
LCA	left coronary artery
LoxP	Locus of crossing over in phage P1
LV	left ventricle
MG	midgut
mG	membrane GFP
mT	membrane tdTomato
NaOH	Sodium Hydroxide
Neo	Neomycin
N_2O	nitrous oxide
OT	Outflow Tract
O_2	oxygen
P	postnatal day
PA	pharyngeal arches
pA	polyadenylation
PBS	Phosphate-Buffered Saline
PBST	0.1% (v/v) TritonX-100 in DPBS
PBSST	x% (v/v) Donkey Serum in PBST

PCR	Polymerase chain reaction
PDGFRβ	Beta-type platelet-derived growth factor receptor
PFA	Paraformaldehyde
PM	primary mesoderm
qPCR	quantitative PCR
RA	right atrium
RCA	right coronary artery
RFP	red fluorescence protein
RNA	Ribonucleic acid
RT	Room temperature
RV	right ventricle
SCF	stem cell factor
SDS	Sodium Dodecyl Sulfate
SEC	subepicardial endothelial cell
SHF	secondary heart field
SV	sinus venosus
TAE	Tris-Acetate-EDTA
Tie2	angiopoietin receptor 2
Tg	transgenic line
Tris-HCl	Tris-(Hydroxymethyl)-Aminomethan-Hydrochlorid
TSA	Tyramide signal amplification
UTR	untranslated region
V	ventricle

VEC	vascular endothelial cell
VECad	vascular endothelial cadherin
WT	wild type
2-ME	β-Mercaptoethanol
Ex	exon

LIST OF PUBLICATIONS:

[1] B. Zhou, L. B. Honor, Q. Ma, J.-H. Oh, R.-Z. Lin, J. M. Melero-Martin, A. von Gise, P. Zhou, **T. Hu**, L. He, K. H. Wu, H. Zhang, Y. Zhang, and W. T. Pu, "Thymosin beta 4 treatment after myocardial infarction does not reprogram epicardial cells into cardiomyocytes.," *J. Mol. Cell. Cardiol.*, vol. 52, no. 1, pp. 43–7, 2012.

[2] X. Tian, **T. Hu**, L. He, H. Zhang, X. Huang, R. E. Poelmann, W. Liu, Z. Yang, Y. Yan, W. T. Pu, and B. Zhou, "Peritruncal coronary endothelial cells contribute to proximal coronary artery stems and their aortic orifices in the mouse heart," *PLoS One*, vol. 8, no. 11, pp. 1–9, 2013.

[3] X. Tian, **T. Hu**, H. Zhang, L. He, X. Huang, Q. Liu, W. Yu, L. He, Z. Yang, Y. Yan, X. Yang, T. P. Zhong, W. T. Pu, and B. Zhou, "De novo formation of a distinct coronary vascular population in neonatal heart," *Science (80-.).*, vol. 345, no. 6192, pp. 90–94, 2014.

[4] L. He, X. Tian, H. Zhang, **T. Hu**, X. Huang, L. Zhang, Z. Wang, and B. Zhou, "BAF200 Is Required for Heart Morphogenesis and Coronary Artery Development," *PLoS One*, vol. 9, no. 10, p. e109493, 2014.

[5] X. Tian, **T. Hu**, H. Zhang, L. He, X. Huang, Q. Liu, W. Yu, L. He, Z. Yang, Z. Zhang, T. P. Zhong, X. Yang, Z. Yang, Y. Yan, A. Baldini, Y. Sun, J. Lu, R. J. Schwartz, S. M. Evans, A. C. Gittenberger-de Groot, K. Red-Horse, and B. Zhou, "Subepicardial endothelial cells invade the embryonic ventricle wall to form coronary arteries.," *Cell Res.*, vol. 23, no. 9, pp. 1075–1090, 2013.

[6] H. Zhang, A. Von Gise, Q. Liu, **T. Hu**, X. Tian, L. He, W. Pu, X. Huang, L. He, C. L. Cai, F. D. Camargo, W. T. Pu, and B. Zhou, "Yap1 Is required for endothelial to mesenchymal transition of the atrioventricular cushion," *J. Biol. Chem.*, vol. 289, no. 27, pp. 18681–18692, 2014.

[7] L. He, Q. Liu, **T. Hu**, X. Huang, H. Zhang, X. Tian, Y. Yan, L. Wang, Y. Huang, L. Miquerol, J. D. Wythe, and B. Zhou, "Genetic lineage tracing discloses arteriogenesis as the main mechanism for collateral growth in the mouse heart," *Cardiovasc. Res.*, vol. 109, no. 3, pp. 419–430, 2016.

[8] J. Lu, Y. Zhou, **T. Hu**, H. Zhang, M. Shen, P. Cheng, W. Dai, F. Wang, K. Chen, Y. Zhang, C. Wang, J. Li, Y. Zheng, J. Yang, R. Zhu, J. Wang, W. Lu, H. Zhang, J. Wang, Y. Xia, T. M. De Assuncao, N. Jalan-Sakrikar, R. C. Huebert, Bin Zhou, and C. Guo, "Notch Signaling Coordinates Progenitor Cell-Mediated Biliary Regeneration Following Partial Hepatectomy.," *Sci. Rep.*, vol. 6, no. November 2015, p. 22754, 2016.

[9] J. Lu, Y. Zhou, **T. Hu**, H. Zhang, M. Shen, P. Cheng, W. Dai, F. Wang, K. Chen, Y. Zhang, C. Wang, J. Li, Y. Zheng, J. Yang, R. Zhu, J. Wang, W. Lu, H. Zhang, J. Wang, Y. Xia, T. M. De Assuncao, N. Jalan-Sakrikar, R. C. Huebert, Bin Zhou, and C. Guo, "Notch Signaling Coordinates Progenitor Cell-Mediated Biliary Regeneration Following Partial Hepatectomy," *Sci. Rep.*, vol. 6, no. 1, p. 22754, Sep. 2016.

ACKNOWLEDGEMENTS

I would like to thank Prof. Dr. B. Fleischmann and PD. Dr. M. Hesse for providing me with an exciting topic for my thesis work and for their advice and help during the process. Furthermore, I would also like to thank Prof. Dr. D. Fürst, Prof. Dr. M. Weigend and Prof. Dr. A. Pfeifer for agreeing to join the Examination Board.

I would also like to give my thanks to all our cooperation partners: Prof. Dr. C. Nerlov for providing the mouse lines; Prof. Dr. M. Kotlikoff, Dr. F. Lee, Dr. S. Reining and Dr. J. Lee for providing the mouse lines and performing the mouse surgeries; Prof. Dr. W. Röll and Dr. Annika Ottersbach for performing the mouse surgeries. Furthermore, I would like to thank all my colleagues at the Institute of Physiology I, the staff of the animal core facility at the University Hospital of Bonn and the members of GRK1873 for providing training and assistance.

Last but not least, I would like to thank GRK1873 and Chinese Scholarship Council for funding the project.